9-10-2018

Spectrum- and Energy-Efficient Radio Resource Allocation for Wireless Communications

Shengjie Guo
Louisiana State University and Agricultural and Mechanical College, sguo12@lsu.edu

SPECTRUM- AND ENERGY-EFFICIET RADIO RESOURCE ALLOCATION FOR WIRELESS COMMUNICATIONS

A Dissertation

Submitted to the Graduate Faculty of the
Louisiana State University and
Agricultural and Mechanical College
in partial fulfillment of the
requirements for the degree of
Doctor of Philosophy

in

The Division of Electrical and Computer Engineering

by
Shengjie Guo
B.S., University of Electronics Science and Technology of China, 2012
December 2018

Acknowledgments

First of all, I am very grateful to convey my gratitude to my supervisor Dr. Xiangwei Zhou for his continuous support throughout my Ph.D. study and research. Dr. Zhou's was always able to me the inspiration and guidance when I had trouble with my research. His constant encouragement and expertise have enabled me to accomplish my dissertation.

I also would like to express my sincere thanks to Dr. Amin Kargarian, Dr. Xuebin Liang, Dr. Anas Mahmound, and Dr. Hongchao Zhang for serving on my doctoral committee and for their precious suggestions to concrete this dissertation.

In addition, I am willing to show my thanks to Dr. Sa Xiao, Dr. Yuwen Qian, Mr. Jiaqi Liu, and all other labmates, friends, and my roommates. They always encourage me and show me the warm friendship, without which it is hard for me to be this stage.

At last but not least, I would like to give the greatest gratitude to my dear wife, Peiyun Xie and my parents. I cannot image how could I finish my Ph.D. degree if without their love. Their endless encouragement and understanding make me get through all the difficulties and toughness.

Table of Contents

List of Tables

List of Figures

Abstract

Wireless communications has been evolved significantly over the last decade. During this period, higher *quality of service* (QoS) requirements have been proposed to support various services. In addition, due to the increasing number of wireless devices and transmission, the energy consumption of the wireless networks becomes a burden. Therefore, the energy efficiency is considered as important as spectrum efficiency for future wireless communications networks, and spectrum and energy efficiency have become essential research topics in wireless communications. Moreover, due to the exploding of number mobile devices, the limited radio resources have become more and more scarce. With large numbers of users and various QoS requirements, a lot of wireless communications networks and techniques have emerged and how to effectively manage the limited radio resources become much more important.

In this dissertation, we focus our research on spectrum- and energy-efficient resource allocation schemes in wireless communication networks. Recently, *heterogeneous networks* (HetNets) have been proposed and studied to improve the spectrum efficiency. In a two-tier heterogeneous network, small base stations reuse the same spectrum with macro base stations in order to support more transmission over the limited frequency bands. We design a cascaded precoding scheme considering both interference cancellation and power allocation for the two-tier heterogeneous network. Besides heterogeneous networks, as the fast development of intelligent transportation, we study the spectrum- and energy-efficient resource allocation in vehicular communication networks. The intelligent transportation and vehicular communications both have drawn much attention and are faced special wireless environment, which includes Doppler effects and severe uncertainties in channel estimation. A novel designed spectrum efficiency scheme is studied and verified.With consideration of energy efficiency, the *device-to-device* (D2D) enabled wireless network is an effective network structure to increase the usage of spectrum. From a device's perspective, we design an energy-efficient resource allocation scheme in D2D communication networks. To

improve the energy efficiency of wireless communication networks, energy harvesting technique is a powerful way. Recently, the *simultaneous wireless information and power transfer* (SWIPT) has been proposed as a promising energy harvesting method for wireless communication networks, based on which we derive an energy-efficient resource allocation scheme for SWIPT cooperative networks, which considers both the power and relay allocation.

In addition to the schemes derivation for spectrum- and energy-efficient resource allocation, simulation results and the proofs of the proposed propositions are provided for the completeness of this dissertation.

Chapter 1. Introduction

In the last decade, the explosive demands on wireless transmission have led to the significant evolution of wireless communications. To provide high *quality of service* (QoS) for various wireless services, the most direct way is to exploit and utilize more resources. However, the resources for wireless communications, especially the spectrum resource, are limited and in fact become more and more scarce. In addition to resource scarcity, the energy consumption of wireless communications grows exponentially. The energy efficiency of wireless communications has drawn much attention recently. In such a scenario, improving radio resource allocation efficiency turns out to be an important way to satisfy higher requirements. In this prospectus, we focus on the radio resource allocation in wireless communication networks. We emphasize the spectrum and energy efficiency in wireless communications and derive novel resource allocation algorithms and schemes to improve the performance.

One of important metrics for wireless communications is spectrum efficiency. Improving spectrum efficiency allows higher throughput or supports more transmission links over limited bandwidth. To achiever better spectrum efficiency, the deployment of *small base stations* (SBSs) such as femtocells has emerged recently as a promising technology to extend service coverage, increase network throughput, and improve energy efficiency [1–3]. However, SBSs are usually deployed to overlay with *macro base stations* (MBSs). As a result, cross-tier interference is introduced to limit the performance of two-tier networks. In two-tier *heterogeneous networks* (HetNets), both small cells and macro cells face the cross-tier interference and co-tier interference from the network elements belonging to different and the same tiers, respectively. When SBSs are randomly deployed with high density, the cross-tier interference and co-tier interference dramatically limit the performance of the heterogeneous network [4]. Power allocation is adopted to mitigate both cross-tier and co-tier interference, which allows user coexistence in the same bandwidth [5–8]. In such a way, the spectrum efficiency can be improved.

Energy consumption in wireless networks has experienced a dramatic increase in the last decade. As a result, information and communication technologies have become a major contributor to global greenhouse gas emissions, with a share of more than 2% [9]. Only mobile communication networks by themselves cost 0.5% of the global energy supply, in which the radio access network consumes over 80% of the energy [10, 11]. Driven by environmental concerns, green wireless communications with high energy efficiency has attracted a lot of attention [12–14]. Due to the development of smart devices, the portion of transmission between devices in wireless communications rises up intensively and the improvement of the energy efficiency in *device-to-device* (D2D) communications needs to be explored. Therefore, in addition to the spectrum-efficient resource allocation for D2D communications, the energy-efficient resource allocation is worthy to be studied.

To alleviate energy consumption concerns, there is a new trend that the *radio frequency* (RF) signal is used for transferring power and transmitting information simultaneously [15], which is a more reliable and predictable way to harvest energy. The concept of *simultaneous wireless information and power transfer* (SWIPT) has been proposed in [16]. A SWIPT system transfers the power from the signals to support its own operations and is less dependent on external power supplies. For passive receivers, they can simultaneously receive information and transfer power from the signals to support information processing, which prolongs the usage times of receivers. Although SWIPT can transfer energy from transmitted signals, the transmit power and spectrum allocation still need to be studied to achieve better energy efficiency. Therefore, we will focus on the energy efficient resource allocation in SWIPT networks.

With the fast development of the intelligent transportation and smart vehicles, vehicular communication networks has attracted extensive attention. Obviously, the high-mobility nature of vehicular networks renders more channel estimation errors for *vehicle users* (VUs). With more channel uncertainties in the fast changing vehicular communication environment, it is necessary to consider the imperfect *channel state information* (CSI)

in resource allocation, especially for the reliability of vehicular communications. In [17], resource allocation based on slow fading parameters and fast fading statistical information has been studied. A model of the channel estimation errors caused by delayed CSI feedback rather than the statistical information of the channel has been adopted in [18]. In this dissertation, the reliable and efficient resource allocation for vehicular communications is studied. With the increasing size of vehicular communication networks, vehicles can provide more powerful computations and larger coverage for wireless communications. Therefore, the resource allocation for vehicular communications would improve the spectrum and energy efficiency and satisfy diverse requirements.

The rest of dissertation is organized as follows. The cascaded precoding and power allocation scheme in heterogeneous networks for spectrum efficiency maximization is discussed in Chapter 2. In Chapter 3, resource allocation design in vehicular communications is discussed. An energy-efficient resource allocation scheme in D2D networks is proposed in Chapter 4. In Chapter 5, the resource allocation scheme to improve the energy efficiency of SWIPT networks is developed. Finally, in Chapter 6, conclusions are drawn.

Chapter 2. Cascaded Precoding and Power Allocation in HetNet

To improve the spectrum efficiency in wireless networks, HetNets has been designed recently, which allows different users share the same frequency. However, the coexistence of multi-users in the same channel can cause inevitable interference and limit the performance of users, which reduces the spectrum reuse benefit. With channel state information at the transmitter, precoding and power allocation can be utilized to mitigate the interference and thus improve the spectrum efficiency in HetNets.

In this chapter, with the consideration of both precoding and power allocation, the cascaded precoders in orthogonal frequency-division multiplexing systems are investigated to protect MUEs from the cross-tier interference caused by co-located small cells and at the same time to satisfy the QoS requirement of *small-cell user equipments* (SUEs). An outer precoder ensures that the signals intended for the SUEs are orthogonal to the MUEs thus avoids the cross-tier interference from the second tier. Moreover, optimal power allocation through an inner precoder at each SBS yields better performance of the SUEs and guarantees their QoS requirements. With consideration of the dense deployment of SBSs, an SBS selection algorithm is studied to further reduce the computational complexity. Numerical results demonstrate that the cascaded precoders are effective in mitigating the interference and enhancing the capacity of small cells.

2.1 System Model and Problem Formulation

As shown in Fig. 2.1, the coexistence of one MBS and K SBSs in a downlink HetNet is considered. The MBS serves M single-antenna MUEs and each SBS serves one single-antenna SUE. The MBS adopts *orthogonal frequency-division multiple* (OFDM) based transmission with N subcarriers and a *cyclic prefix* (CP) of length L to avoid the inter-symbol interference. Since the MBS usually covers a large area, the first tier is regarded as primary user and oblivious of the existence of the second tier. The cross-tier interference mitigation strategy is only implemented in the second tier. No cooperation is considered between different tiers or among different SBSs in the same tier. Therefore, the precoders

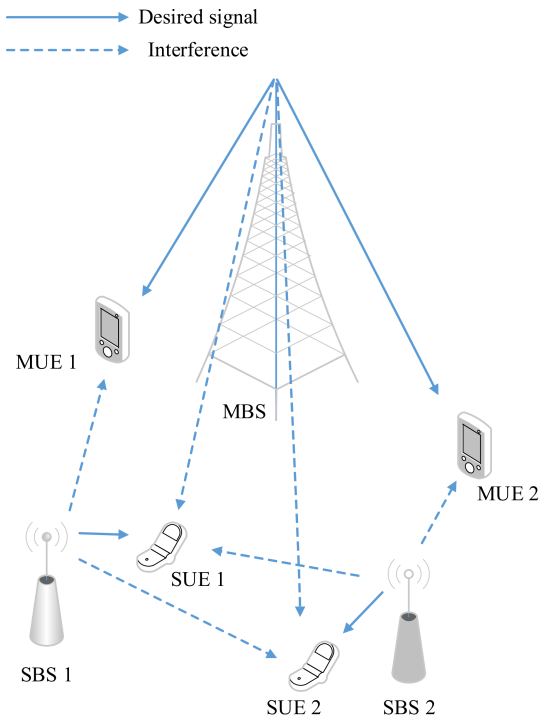

Figure 2.1. A two-tier HetNet.

are designed in a distributed manner. All transmissions are assumed to be synchronized and no radio frequency impairments at the receiver are considered. The knowledge of perfect *channel state information* (CSI) for all links is assumed.

Subscript s denotes the SBSs and m denotes the MBS. $\mathbf{x}_s^{(i)} \in \mathbb{C}^{(N+L)\times 1}$ denotes the precoded signal vector in time domain at the i-th SBS. Then

$$\mathbf{x}_s = [\mathbf{x}_s^{(1)T}, \mathbf{x}_s^{(2)T}, \ldots, \mathbf{x}_s^{(K)T}]^T \in \mathbb{C}^{K(N+L)\times 1} \tag{2.1}$$

is the equivalent aggregate signal vector of the SBSs. $\mathbf{H}_{sm}^{(i,j)}$ denotes the channel matrix from the i-th SBS to the j-th MUE. Then

$$\mathbf{H}_{sm}^{(j)} = [\mathbf{H}_{sm}^{(1,j)}, \mathbf{H}_{sm}^{(2,j)}, \ldots, \mathbf{H}_{sm}^{(K,j)}] \in \mathbb{C}^{N\times K(N+L)} \tag{2.2}$$

is the aggregate channel matrix from the SBSs to the j-th MUE and expressed as

$$\mathbf{H}_{sm}^{(i,j)} = \begin{bmatrix} h_{sm}^{(i,j)}(L) & \cdots & h_{sm}^{(i,j)}(0) & 0 & \cdots & 0 \\ 0 & \ddots & & \ddots & \ddots & \vdots \\ \vdots & \ddots & \ddots & & \ddots & 0 \\ 0 & \cdots & 0 & h_{sm}^{(i,j)}(L) & \cdots & h_{sm}^{(i,j)}(0) \end{bmatrix}, \tag{2.3}$$

where $h_{sm}^{(i,j)}(L)$, $h_{sm}^{(i,j)}(L-1)$, ..., and $h_{sm}^{(i,j)}(0)$ represent the channel taps from the i-th SBS to the j-th MUE.

The received signal vectors of length N in frequency domain at the j-th MUE and i-th SUE are expressed as

$$\mathbf{y}_m^{(j)} = \mathbf{F}(\mathbf{H}_{mm}^{(j)}\mathbf{A}\mathbf{F}^{-1}\mathbf{s}_m^{(j)} + \mathbf{H}_{sm}^{(j)}\mathbf{x}_s + \mathbf{n}_m^{(j)}) \tag{2.4}$$

and

$$\mathbf{y}_s^{(i)} = \mathbf{F}(\mathbf{H}_{ss}^{(i,i)}\mathbf{x}_s^{(i)} + \sum_{\substack{u=1 \\ u\neq i}}^{K} \mathbf{H}_{ss}^{(u,i)}\mathbf{x}_s^{(u)} + \mathbf{H}_{ms}^{(1,i)}\mathbf{A}\mathbf{F}^{-1}\mathbf{s}_m^{(j)} + \mathbf{n}_s^{(i)}), \tag{2.5}$$

respectively, where $\mathbf{s}_m^{(j)} \in \mathbb{C}^{(N+L)\times 1}$ is the input signal vector in time domain at the MBS for the j-th MUE, $\mathbf{n}_m^{(j)}$ and $\mathbf{n}_s^{(i)}$ are the corresponding equivalent noise vectors for the MUEs and SUEs, respectively, $\mathbf{F}$ is an $N \times N$ unitary discrete Fourier transform matrix with the entry in the $(k+1)$-th row and $(l+1)$-th column $[\mathbf{F}]_{(k+1),(l+1)} = \frac{1}{\sqrt{N}} e^{-i2\pi\frac{kl}{N}}$ for $k, l = \{0, \ldots, N-1\}$, $\mathbf{A}$ is an $(N+L) \times N$ CP insertion matrix given by

$$\mathbf{A} = \begin{bmatrix} \mathbf{0_{L,N-L}}, & \mathbf{I_L} \\ & \mathbf{I_N} \end{bmatrix}, \tag{2.6}$$

where $\mathbf{0_{N,L}}$ and $\mathbf{I_N}$ denote an $N \times L$ zero matrix and an $N \times N$ identity matrix, respectively,

$\mathbf{H}_{mm}^{(j)} \in \mathbb{C}^{N\times(N+L)}$ is the channel matrix from the MBS to the j-th MUE, which is

$$\mathbf{H}_{mm}^{(1,j)} = \begin{bmatrix} h_{mm}^{(1,j)}(L) & \cdots & h_{mm}^{(1,j)}(0) & 0 & \cdots & 0 \\ 0 & \ddots & & \ddots & \ddots & \vdots \\ \vdots & \ddots & \ddots & & \ddots & 0 \\ 0 & \cdots & 0 & h_{mm}^{(1,j)}(L) & \cdots & h_{mm}^{(1,j)}(0) \end{bmatrix}, \tag{2.7}$$

where $h_{mm}^{(1,j)}(L)$, $h_{mm}^{(1,j)}(L-1)$, ..., and $h_{mm}^{(1,j)}(0)$ are the channel taps between the MBS and the j-th MUE, $\mathbf{H}_{ss}^{(u,i)}$ and $\mathbf{H}_{ms}^{(1,i)}$ are the channel matrices from the u-th SBS and the MBS to the i-th SUE, respectively, and constructed as

$$\mathbf{H}_{ss}^{(u,i)} = \begin{bmatrix} h_{ss}^{(u,i)}(L) & \cdots & h_{ss}^{(u,i)}(0) & 0 & \cdots & 0 \\ 0 & \ddots & & \ddots & \ddots & \vdots \\ \vdots & \ddots & \ddots & & \ddots & 0 \\ 0 & \cdots & 0 & h_{ss}^{(u,i)}(L) & \cdots & h_{ss}^{(u,i)}(0) \end{bmatrix}, \tag{2.8}$$

and

$$\mathbf{H}_{ms}^{(1,i)} = \begin{bmatrix} h_{ms}^{(1,i)}(L) & \cdots & h_{ms}^{(1,i)}(0) & 0 & \cdots & 0 \\ 0 & \ddots & & \ddots & \ddots & \vdots \\ \vdots & \ddots & \ddots & & \ddots & 0 \\ 0 & \cdots & 0 & h_{ms}^{(1,i)}(L) & \cdots & h_{ms}^{(1,i)}(0) \end{bmatrix}, \tag{2.9}$$

where $h_{ms}^{(1,i)}(L)$, $h_{ms}^{(1,i)}(L-1)$, ..., $h_{ms}^{(1,i)}(0)$ and $h_{ss}^{(u,i)}(L)$, $h_{ss}^{(u,i)}(L-1)$, ..., and $h_{ss}^{(u,i)}(0)$ represent the L channel paths from the MBS to the i-th SUE and from the u-th SBS to the i-th SUE, respectively.

2.2 Proposed Precoding and Power Allocation Scheme

In this section, cascaded precoders are studied. Specifically, the outer precoder and inner precoder are designed and analyzed.

The structure of cascaded precoders is illustrated in Fig. 2.2. The precoded signal

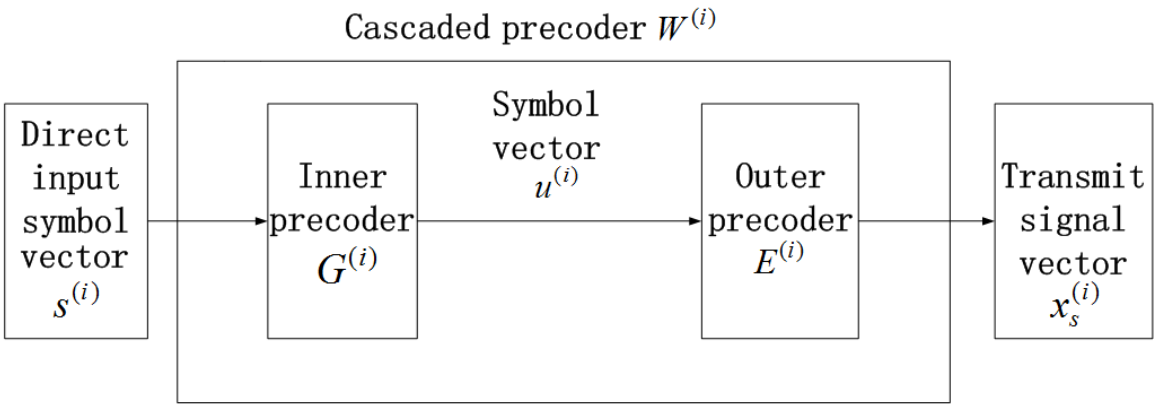

Figure 2.2. Proposed cascaded precoder structure.

vector is obtained from the direct input symbol vector. Specifically,

$$\mathbf{x}_s^{(i)} = \mathbf{W}^{(i)}\mathbf{s}^{(i)}, \tag{2.10}$$

where $\mathbf{s}^{(i)} \in \mathbb{C}^{L\times 1}$ is an *independent identical distributed* (i.i.d.) zero-mean unit-variance direct input symbol vector from the i-th SBS and $\mathbf{W}^{(i)}$ is the overall precoding matrix for the i-th SBS, which is constructed from two cascaded precoders,

$$\mathbf{W}^{(i)} = \mathbf{E}^{(i)}\mathbf{G}^{(i)}, \tag{2.11}$$

where $\mathbf{E}^{(i)}$ is the outer precoder to cancel the cross-tier interference from the SBSs to the MUEs and $\mathbf{G}^{(i)}$ is the inner precoder to mitigate the co-tier interference through power allocation in the second tier.

Outer Precoder Design

The outer precoder is designed to prevent the first tier from the cross-tier interference. To protect the existing MUEs, it is preferred to eliminate the cross-tier interference from the second tier, i.e.,

$$\mathbf{H}_{sm}^{(j)}\mathbf{x}_s = \mathbf{0}, \quad \forall j \in 1, 2, \ldots, M. \tag{2.12}$$

The transmitted signal $\mathbf{x}_s^{(i)}$ from the i-th SBS is designed as

$$\mathbf{x}_s^{(i)} = \mathbf{E}^{(i)}\mathbf{u}^{(i)}, \tag{2.13}$$

where $\mathbf{u}^{(i)} \in \mathbb{C}^{L\times 1}$ is the symbol vector at the i-th SBS and $\mathbf{E}^{(i)} \in \mathbb{C}^{(N+L)\times L}$ is a linear precoder for the i-th SBS to render

$$\mathbf{H}_{sm}^{(i,j)}\mathbf{E}^{(i)} = \mathbf{0}. \tag{2.14}$$

Since $\mathbf{H}_{sm}^{(i,j)}$ is an $(N+L)$ by N matrix with independent elements, the rank of $\mathbf{H}_{sm}^{(i,j)}$ is N and thus the dimension of the null space of $\mathbf{H}_{sm}^{(i,j)}$ is $(N+L)-N = L$. Therefore, the LQ decomposition method [19] can be used to construct an $(N+L)\times L$ precoder $\mathbf{E}^{(i)}$ to transmit L symbols aligned with the null space of $\mathbf{H}_{sm}^{(i,j)}$. The equivalent channel matrix $\mathbf{H}_{sm}^{(i,j)}$, representing the interfering link between the i-th SBS and the j-th MUE, is decomposed as

$$\mathbf{H}_{sm}^{(i,j)} = \mathbf{L}_{sm}^{(i,j)}\mathbf{Q}_{sm}^{(i,j)}, \tag{2.15}$$

where $\mathbf{L}_{sm}^{(i,j)} \in \mathbb{C}^{N\times(N+L)}$ is a lower triangular matrix and $\mathbf{Q}_{sm}^{(i,j)} \in \mathbb{C}^{(N+L)\times(N+L)}$ is a unitary matrix given by

$$\mathbf{Q}_{sm}^{(i,j)} \triangleq [\mathbf{q}_1, \mathbf{q}_2, \cdots, \mathbf{q}_{N+L}]. \tag{2.16}$$

Then the outer precoder $\mathbf{E}^{(i)}$ is constructed as

$$\mathbf{E}^{(i)} \triangleq [\mathbf{q}_{N+1}, \mathbf{q}_{N+2}, \cdots, \mathbf{q}_{N+L}] \tag{2.17}$$

and therefore the equivalent signal model in the first tier is rewritten as

$$\mathbf{y}_m^{(j)} = \mathbf{F}(\mathbf{H}_{mm}^{(j)}\mathbf{A}\mathbf{F}^{-1}\mathbf{s}_m^{(j)} + \mathbf{n}_m^{(j)}), \tag{2.18}$$

which is free of the cross-tier interference from the second tier.

Inner Precoder Design

To reduce the influence of the co-tier interference and achieve higher throughput, an inner precoder is designed to render optimal power allocation.

The inner precoder structure

The inner precoding matrix $\mathbf{G}^{(i)} \in \mathbb{C}^{L\times L}$ is used to generate the SBS symbol vector, i.e.,

$$\mathbf{u}^{(i)} = \mathbf{G}^{(i)}\mathbf{s}^{(i)}. \tag{2.19}$$

The received signal vector at the i-th SUE is

$$\mathbf{y}_s^{(i)} = \mathbf{F}(\mathbf{H}_{ss}^{(i,i)}\mathbf{E}^{(i)}\mathbf{G}^{(i)}\mathbf{s}^{(i)} + \sum_{\substack{u=1\\u\neq i}}^{K}\mathbf{H}_{ss}^{(u,i)}\mathbf{E}^{(u)}\mathbf{G}^{(u)}\mathbf{s}^{(u)} + \mathbf{v}_s^{(i)}), \tag{2.20}$$

where $\mathbf{v}_s^{(i)} = \mathbf{H}_{ms}^{(1,i)}\mathbf{A}\mathbf{F}^{-1}\mathbf{s}_m^{(j)} + \mathbf{n}_s^{(i)}$.

Define matrix $\widetilde{\mathbf{F}}$ such that

$$\widetilde{\mathbf{F}} = \mathbf{F}\widetilde{\mathbf{A}}, \tag{2.21}$$

where $\widetilde{\mathbf{A}}$ denotes the CP removal matrix, which is

$$\widetilde{\mathbf{A}} = \left[\mathbf{0}_{\mathbf{N},\mathbf{L}},\quad \mathbf{I}_{\mathbf{N}}\right]. \tag{2.22}$$

Then the precoded symbol of the i-th SBS in frequency domain, $\mathbf{X}_s^{(i)}$, can be expressed as

$$\mathbf{X}_s^{(i)} = \widetilde{\mathbf{F}}\mathbf{E}^{(i)}\mathbf{G}^{(i)}\mathbf{s}^{(i)}. \tag{2.23}$$

The average transmit power of the i-th SBS over the j-th subcarrier, $P^{(i,j)}$, is given by

$$P^{(i,j)} = \mathbb{E}\{[\mathbf{X}_s^{(i)}]_{(j,1)}^2\}, \tag{2.24}$$

where $\mathbb{E}\{\cdot\}$ denotes the expectation operation. Because $\mathbf{s}^{(i)}$ is i.i.d. with zero-mean and

unit-variance,

$$P^{(i,j)} = [\widetilde{\mathbf{F}}\mathbf{E}^{(i)}\mathbf{G}^{(i)}\mathbf{G}^{(i)T}\mathbf{E}^{(i)T}\widetilde{\mathbf{F}}^{T}]_{(j,j)}. \tag{2.25}$$

Let $\mathbf{B}^{(i)} = \widetilde{\mathbf{F}}\mathbf{E}^{(i)}\mathbf{G}^{(i)}$ and the entry in the m-th row and n-th column be $b^{(i)}_{(m,n)}$. The following N equations are obtained

$$\begin{aligned} b^{(i)2}_{(1,1)} + b^{(i)2}_{(1,2)} + \cdots + b^{(i)2}_{(1,L)} &= P^{(i,1)}, \\ b^{(i)2}_{(2,1)} + b^{(i)2}_{(2,2)} + \cdots + b^{(i)2}_{(2,L)} &= P^{(i,2)}, \\ &\vdots \\ b^{(i)2}_{(N,1)} + b^{(i)2}_{(N,2)} + \cdots + b^{(i)2}_{(N,L)} &= P^{(i,N)}. \end{aligned} \tag{2.26}$$

Define matrix $\mathbf{C}_n$ as

$$\mathbf{C}_n = \begin{bmatrix} \sqrt{P^{*(i,nL+1)}} & \cdots & 0 \\ \vdots & \ddots & \vdots \\ 0 & \cdots & \sqrt{P^{*(i,nL+L)}} \end{bmatrix}. \tag{2.27}$$

To achieve the desired power $P^{*(i,j)}$ for $j = 1, 2, \cdots, N$, $\mathbf{B}^{(i)}$ should be designed as

$$\mathbf{B}^{(i)} = \begin{bmatrix} \mathbf{C}_1 \\ \mathbf{C}_2 \\ \vdots \\ \mathbf{C}_z \\ \mathbf{C}'_{z+1} \end{bmatrix}, \tag{2.28}$$

where z is the largest integer that is smaller than $\frac{N}{L}$ and $\mathbf{C}'_{z+1}$ is constructed with the first $(N - zL)$ rows of $\mathbf{C}_{z+1}$. Then the full rank inner precoding matrix $\mathbf{G}^{(i)}$ can be obtained

through

$$\mathbf{G}^{(i)} = ((\widetilde{\mathbf{F}}\mathbf{E}^{(i)})^H \widetilde{\mathbf{F}}\mathbf{E}^{(i)})^{-1}(\widetilde{\mathbf{F}}\mathbf{E}^{(i)})^H \mathbf{B}^{(i)}, \tag{2.29}$$

where superscript H denotes the Hermitian transpose operation.

The Optimal Power Allocation

Power allocation at each SBS is optimized through the designed inner precoder. Since the power allocation of the MBS is not affected by the second tier, the interference from the first tier is always fixed during the power allocation of the SBSs. Therefore, the interference from the MBS is treated as noise with fixed power during the SBS power optimization and absorbed in the noise expression, $\sigma^2_{(i,j)}$, for simplicity.

Through the precoding matrix $\mathbf{G}^{(i)}$, the transmit power $P^{(i,j)}$ is allocated to maximize the achievable rate $R^{(i)}$ of the i-th SUE. Thus the following optimization problem is formulated

$$\max R^{(i)} = \sum_{j=1}^{N} \log_2 \left(1 + \frac{|g^{(j)}_{i,i}| P^{(i,j)}}{\sum_{u \in \mathcal{S}^{[i]}} |g^{(j)}_{u,i}| P^{(u,j)} + \sigma^2_{(i,j)}}\right),$$

$$\text{subject to } \sum_{j=1}^{N} P^{(i,j)} \leq P^{(i)}_{\max}, \tag{2.30}$$

where $P^{(i)}_{\max}$ is the maximum transmit power of the i-th SBS, $\mathcal{S}^{[i]}$ denotes the set of SBSs excluding the i-th SBS, $\sigma^2_{(i,j)}$ is the noise power for the i-th SUE over the j-th subcarrier, and $|g^{(j)}_{u,i}|$ denotes the channel gain from the u-th SBS to the i-th SUE over the j-th subcarrier, which can be obtained from $\mathbf{H}^{(u,i)}_{ss}$ as

$$|g^{(j)}_{u,i}| = |[\mathbf{F}\mathbf{H}^{(u,i)}_{ss}\mathbf{F}'^H(\widetilde{\mathbf{F}}\widetilde{\mathbf{F}}^H)^{-1}]_{(j,j)}|^2. \tag{2.31}$$

Algorithm 1 QoS guarantee algorithm

Initialize: The total transmit power of the i-th SBS $P^{(i)} = P^{(i)}_{\max}$, $P^{(i,j)} = 0$, i = 1,2,...,K, j = 1,2,...,N.
loop
  loop
    Solve (2.30) for all i = 1, 2, ..., K and j = 1, 2, ..., N. Set $P^{(i,j)}$ and transmit power $P^{(i)}$.
    Set $R^{(i)}$ according to (2.30).
  end loop
  for i = 1 to K,
    if $R^{(i)} > R_{re} + \varepsilon$, set $P^{(i)} = P^{(i)} - \xi$.
    if $R^{(i)} < R_{re}$, set $P^{(i)} = P^{(i)} + \xi$.
    if $P^{(i,j)} > P^{(i)}_{\max}$, $P^{(i,j)} = P^{(i)}_{\max}$.
  end for
  until $R^{(i)} > R_{re}$ for all $i = 1, 2, \ldots, K$. Then set $P^{(i,j)} = P^{*(i,j)}$.
end loop

The Lagrangian function for (2.30) is

$$\begin{aligned}
&\mathcal{L}(P^{(i,j)}, \alpha_i) \\
&= -\sum_{j=1}^{N} \log_2 (1 + \frac{|g^{(j)}_{i,i}| P^{(i,j)}}{\sum_{u \in \mathcal{S}^{[i]}} |g^{(j)}_{u,i}| P^{(u,j)} + \sigma^2_{(i,j)}}) \\
&+ \alpha_i (\sum_{j=1}^{N} P^{(i,j)} - P^{(i)}_{\max}),
\end{aligned} \tag{2.32}$$

where α_i is a Lagrangian multiplier.

By setting the differentiation of (2.32) with respect to $P^{(i,j)}$ to be 0, the power allocated over the j-th subcarrier of the i-th SBS is

$$P^{(i,j)} = [\frac{1}{\alpha_i \ln 2} - \frac{1}{\beta}]^+, \tag{2.33}$$

where $\frac{1}{\alpha_i \ln 2}$ is a constant that ensures the power constraint (2.30) to be satisfied and $\beta = \frac{|g^{(j)}_{i,i}|}{\sum_{u \in \mathcal{S}^{[i]}} |g^{(j)}_{u,i}| P^{(u,j)} + \sigma^2_{(i,j)}}$. Here, $[x]^+ = \max(x, 0)$. Equation (2.33) is a standard form of water-filling power allocation. Given the coupled power allocation in (2.30) for different i's, the iterative water-filling in [20] is effective to optimize the power allocation $P^{(i,j)}$.

To guarantee the QoS of SUEs, Algorithm 1 is adopted to ensure that the achievable rate satisfies the rate requirement R_{re} for each SUE by adjusting the power allocation. Here the parameters ε and ξ are used to reach the desired accuracy. With the optimal power $P^{*(i,j)}$ for the i-th SBS over the j-th subcarrier, the precoding matrix $\mathbf{G}^{(i)}$ can be designed according to (2.27) - (2.29).

2.3 Discussion

Algorithm to Reduce Computational Complexity

Given channel fading and path loss, an SBS may not introduce interference to the other SUEs even with the maximum transmit power. Thus Algorithm 2 is considered to exclude the SBSs from set $\mathcal{S}^{[i]}$ that do not interfere with the i-th SBS, which reduces the computational complexity of the algorithm.

Algorithm 2 SBS selection algorithm

Initialize: Set $P_{\text{cons}}^{(u)}$ for $u = 1, 2, \ldots, K$. Set $\mathcal{S}^{[i]} = \emptyset$, for $i = 1, 2, \ldots, K$.
  for $i = 1$ to K,
    for $u = 1$ to K, $u \neq i$,
      Calculate $P_{arrive}^{(u,i)}$ according to (2.34).
      if $P_{arrive}^{(u,i)} \geq \varepsilon_p$, set $\mathcal{S}^{[i]} = \mathcal{S}^{[i]} + \{u\}$.
      if $P_{arrive}^{(u,i)} < \varepsilon_p$, set $\mathcal{S}^{[i]} = \mathcal{S}^{[i]}$.
  end for
end for

Let $P_I^{(u,i)}$ be the interference power from the u-th SBS at the i-th SUE. If $P_I^{(u,i)}$ does not exceed the threshold ε_p when the u-th SBS uses the maximum power allowed, $P_{\max}^{(u)}$, the u-th SBS will not be considered as an interferer to the i-th SUE.

Given channel fading and path loss, $P_I^{(u,i)}$ can be expressed as

$$P_{I(dBm)}^{(u,i)} = \gamma_{u,i(dB)} + P_{\max(dBm)}^{(u)} - P_{L(dB)}^{(u,i)}, \tag{2.34}$$

where $\gamma_{u,i}$ is the channel fading coefficient from the u-th SBS to the i-th SUE and $P_L^{(u,i)}$ denotes the path loss from the u-th SBS to the i-th SUE.

For a system with K SBSs and N subcarriers, the complexity of the power allocation optimization and inner precoding matrix design increases with the number of SBSs, K.

Through the SBS selection algorithm, the number of SBSs involved in the computation decreases and thus the complexity of optimization reduces.

Imperfect Channel Estimation

In Section 2.2, perfect CSI is assumed to obtain the proposed precoder. However, in practice, it is difficult to obtain perfect CSI. Therefore, the performance of the proposed cascaded precoding scheme under channel estimation is analyzed in this subsection. There has been some discussion regarding the cross-tier interference elimination outer precoder under estimated channel in [21]. As in [22], the estimated channel matrix from the i-th SBS to the j-th SUE $\widehat{\mathbf{H}}_{ss}^{(i,j)}$ can be written as

$$\widehat{\mathbf{H}}_{ss}^{(i,j)} = \mathbf{H}_{ss}^{(i,j)} - \widehat{\mathbf{Er}}, \tag{2.35}$$

where $\widehat{\mathbf{Er}}$ denotes the channel estimation error that is a zero-mean circularly symmetric complex Gaussian matrix, i.e., $\widehat{\mathbf{Er}} \sim (0, \sigma^2_{\widehat{Er}}\mathbf{I})$, with variance $\sigma^2_{\widehat{Er}} = \mathbb{E}(|\mathbf{H}_{ss}^{(i,j)}|^2)$ - $\mathbb{E}(|\widehat{\mathbf{H}}_{ss}^{(i,j)}|^2)$. With the estimated channel matrix, the received signal at the i-th SUE is given by

$$\begin{aligned}
\mathbf{y}_s^{(i)} =& \mathbf{F}(\widehat{\mathbf{H}}_{ss}^{(i,i)}\mathbf{E}^{(i)}\widehat{\mathbf{G}}^{(i)}\mathbf{s}^{(i)} + \sum_{u\in\mathcal{S}^{[i]}} \widehat{\mathbf{H}}_{ss}^{(u,i)}\mathbf{E}^{(u)}\widehat{\mathbf{G}}^{(u)}\mathbf{s}^{(u)} + \mathbf{v}_s^{(i)}) \\
=& \mathbf{F}(\mathbf{H}_{ss}^{(i,i)}\mathbf{E}^{(i)}\widehat{\mathbf{G}}^{(i)}\mathbf{s}^{(i)} + \sum_{u\in\mathcal{S}^{[i]}} \mathbf{H}_{ss}^{(u,i)}\mathbf{E}^{(u)}\widehat{\mathbf{G}}^{(u)}\mathbf{s}^{(u)} + \mathbf{v}_s^{(i)} \\
& \underbrace{- \widehat{\mathbf{Er}}^{(i,i)}\mathbf{E}^{(i)}\widehat{\mathbf{G}}^{(i)}\mathbf{s}^{(i)} - \sum_{u\in\mathcal{S}^{[i]}} \widehat{\mathbf{Er}}^{(u,i)}\mathbf{E}^{(u)}\widehat{\mathbf{G}}^{(u)}\mathbf{s}^{(u)}}_{\text{channel estimation error part}}),
\end{aligned} \tag{2.36}$$

where $\widehat{\mathbf{G}}^{(i)}$ is the inner precoding matrix of the i-th SBS considering channel estimation error. To design the elements of $\widehat{\mathbf{G}}^{(i)}$, the power allocation under channel estimation, $\widehat{P}^{(i,j)}$, is obtained by replacing channel power gain $g_{u,i}^{(j)}$ with $\widehat{g}_{u,i}^{(j)}$ in the optimization problem (2.30).

The data rates with perfect and imperfect CSI, respectively, have a gap introduced by the channel estimation error part, which will be discussed with simulation results.

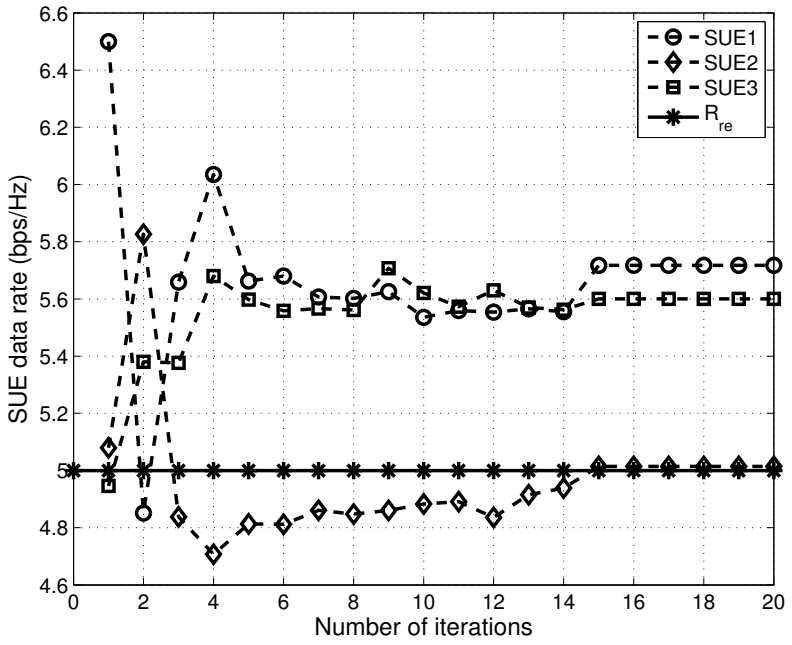

Figure 2.3. SUE data rate versus number of iterations.

2.4 Numerical Results

In this section, simulation results are presented to illustrate the performance with the cascaded precoders. In the simulation, $K = 12$ SBSs are randomly deployed in a circle with radius $R = 50m$ and each SBS serves one SUE. The maximum transmit power is 100 mW for each SBS and 10 W for the MBS. The number of subcarriers and the length of CP are $N = 64$ and $L = 16$, respectively. A path loss model $37 + 32log_{10}(d)$ in decibels for all links is adopted, where d is the distance between a base station and a user.

The average data rates of all the SUEs with perfect CSI and under channel estimation are compared in Fig. 2.4. As shown in the figure, there is a gap between the network performance with perfect CSI and that under channel estimation. It is obvious that the performance is becoming worse when the error variance increases. However, the average data rate under channel estimation is comparable with the perfect case when the error variance is 1, which is large enough in channel estimation according to [22]. Therefore, the cascaded precoders achieve acceptable performance with imperfect CSI.

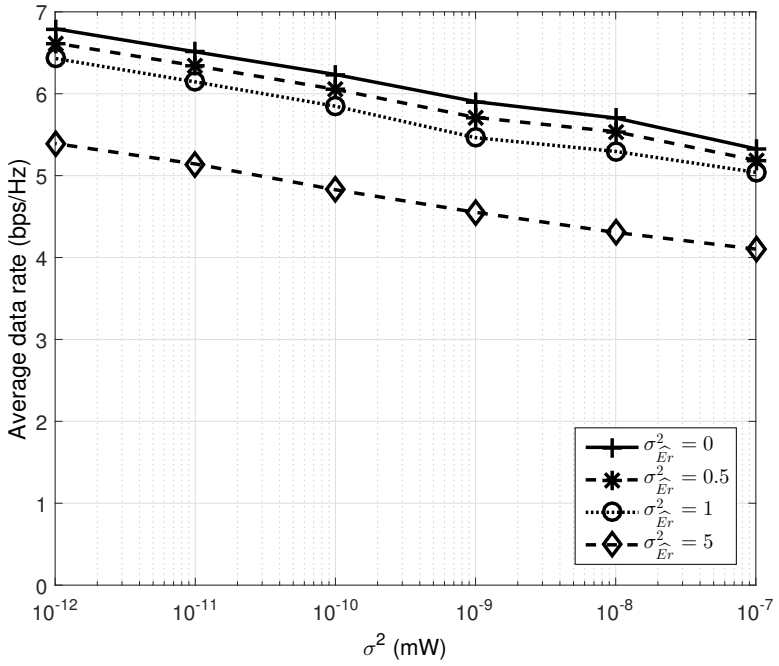

Figure 2.4. Average data rate versus noise power under channel estimation.

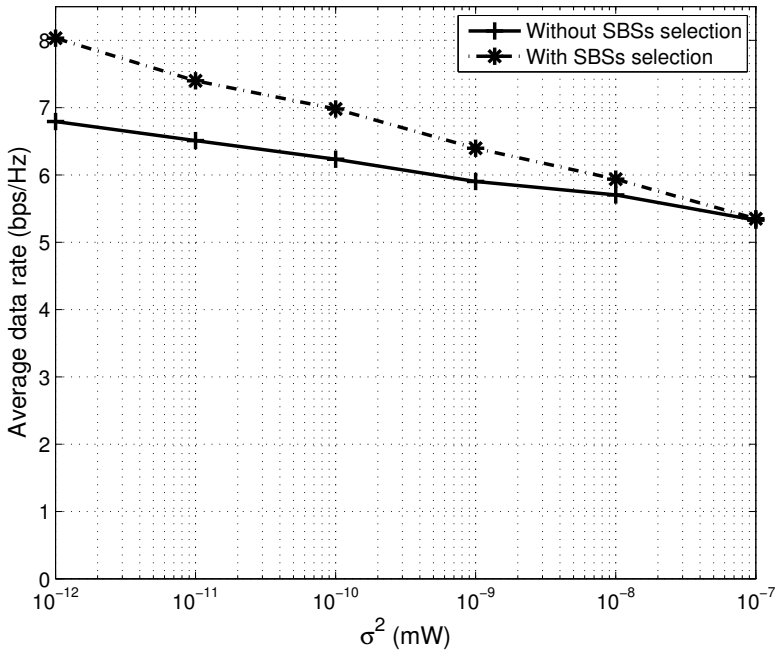

Figure 2.5. Average data rate versus noise power with and without SBS selection algorithm.

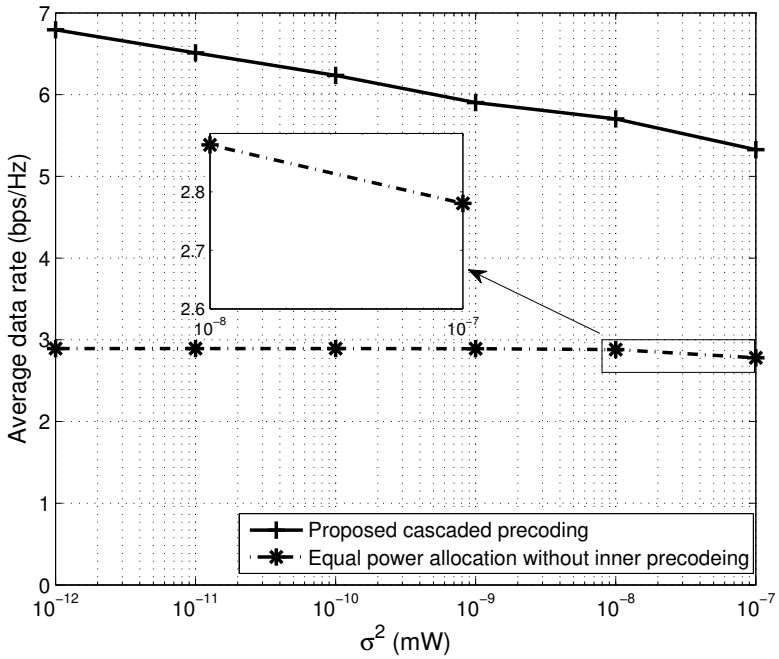

Figure 2.6. Average data rate versus noise power in different schemes.

In Fig. 2.5, the performance of the second tier with and without SBS selection algorithm is illustrated. Because of the random deployment and varying channel conditions, some SBSs do not cause co-tier interference to others even in dense deployment with the maximum power. With the SBS selection algorithm, the SBSs not affecting the i-th SBS will be eliminated from set $\mathcal{S}^{[i]}$. Then each SBS could serve its SUE with a higher power to achieve a better data rate and reduce the computational complexity with a smaller number of SBSs included in the optimization.

In Fig. 2.3, the evolution of SUE data rates is illustrated with the iterations in Algorithm 1. The data rate requirement is $R_{re} = 5$ bps/Hz and the data rates of 3 selected SUEs are shown in Fig. 2.3. The data rate requirement is satisfied for all the SUEs. And the data rates of the SUEs converge fast in a few iterations while the QoS requirements of all the SUEs are met.

The performance of equal power allocation without inner precoder and with cascaded precoders is shown in Fig. 2.6. The cascaded precoders that suppress the co-tier interference render obviously higher data rate than the equal power allocation. Since the fixed co-tier interference in (2.30) dominates in the equal power allocation scheme, the performance gap

increases when the noise power decreases.

Chapter 3. Robust Resource Allocation in NOMA-based Heterogeneous Vehicular Networks

In previous chapters, we discussed the spectrum- and energy-efficient resource allocation in low-mobility wireless networks. With the fast development of intelligent transportation and smart vehicles, high-mobility vehicular communications will play an important role in wireless communications.

With the explosion of information and computer technology, the 5G of wireless communications introduces new technologies and applications, such as small cell communications, vehicular communications, and millimeter wave communications, which comprises an unprecedented ultra-dense and heterogeneous communication environment [23, 24]. Meanwhile, in the fast development of autonomous driving technologies and intelligent vehicles, the reliability and safety of vehicles have gained much attention. Vehicular communications also plays a pivotal role in ensuring the reliability of vehicles through transmission of safety messages among vehicles and between the infrastructures and vehicles. The communication organizations and standardization parties have put efforts in standards and projects of vehicular communications such as IEEE 802.11p and the *European Union Mobile and wireless communications Enablers for Twenty-twenty Information Society* (METIS) project [25].

However, involving massive vehicular communication links into ultra-dense and heterogeneous 5G networks is a challenge. The spectrum resource becomes more scarce in prevailing *orthogonal multiple access* (OMA) networks. To improve spectrum efficiency, *non-orthogonal multiple access* (NOMA) in vehicular communications has been studied recently [26, 27]. Allowing multiple users to share the same channel, NOMA alleviates the spectrum scarcity problem. Furthermore, current vehicles are not only serving as transportation tools but also evolving to infotainment platforms [24]. Therefore, both reliable transmission of safety information and high-speed data rates are required for future vehicular communications.

Obviously, the high mobility of *vehicle users* (VUs) renders different channel models in vehicular communications. The fast changing vehicular communications environment faces

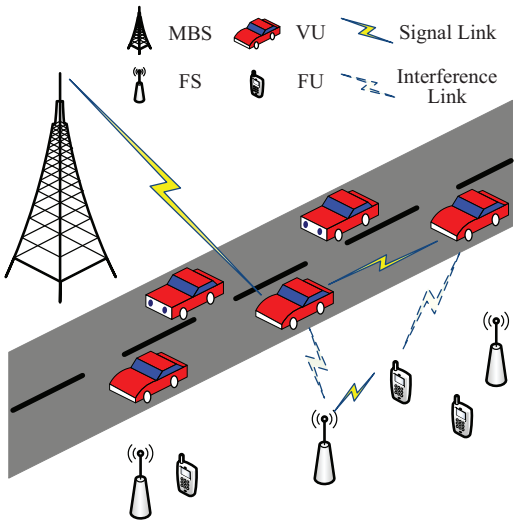

Figure 3.1. A heterogeneous vehicular network.

more channel estimation errors and uncertainties. Therefore, it is necessary in the resource allocation of the vehicular communications to consider the imperfect CSI, especially for the reliability.

Motivated by the above, in this chapter, we will focus on designing robust spectrum- and energy-efficient resource allocation scheme for vehicular communications in 5G heterogeneous vehicular networks to satisfy both V2V and V2I QoS requirements. We will incorporate the chance constraints into the problem formulation to guarantee the strict reliability requirements in vehicular communications and limit the influence of cross-tier interference in heterogeneous networks. Moreover, to improve the spectrum efficiency, NOMA in our formulation will be considered and the optimal power allocation will be derived. In addition, numerical results will be built to demonstrate the desired throughput performance and reliability.

3.1 System Model and Problem Formulation

System Model

A heterogeneous vehicular network is considered and depicted in Fig. 3.1. A *macro base station* (MBS) is used to provide high-speed data stream service for N VUs. *Femto stations* (FSs) coexist with the MBS and serve M *femto users* (FUs) to offload data traffic from the MBS. There are L available channels that are enough for the orthogonal transmission

of the VUs or FUs, i.e., $\max\{N, M\} \leq L$. Each VU adopts NOMA to simultaneously communicate with the MBS for high-speed data service and the corresponding vehicle receivers for safety message exchange. Note that more than two links sharing the same channel is not preferable in NOMA due to the hardware complexity and processing delay [28,29]. Therefore, we assume that each VU transmitter only has one V2V link to its closest VU receiver for safety information transmission. For the other VUs, the information can be obtained from their V2I links. In this case, only one V2V link coexists with the V2I link of each VU transmitter over one channel through NOMA. Furthermore, each channel is reused by one FU to improve spectrum efficiency in the heterogeneous network. Therefore, one VU and one FU share the same channel and form a VU-FU coexisting pair. The entire heterogeneous network may consist of multiple coexisting pairs and different pairs use OMA to avoid interference.

In this chapter, the channel model includes small-scale fast fading, shadowing, and large-scale pathloss. Due to the long distance between the VU transmitter and MBS, the relative position and channel environment changes between the VU transmitter and MBS are limited. Therefore, the channel estimation between the VU transmitters and MBS is assumed error-free. In such a case, the channel power gain between the i-th VU transmitter and MBS over the j-th channel, $g^v_{i,j}$, is

$$g^v_{i,j} = |h^v_{i,j}|^2 \xi_i C d_i^{-\beta} \triangleq |h^v_{i,j}|^2 \alpha_i, \tag{3.1}$$

where $|\cdot|$ is the norm operator, $h^v_{i,j}$ is the fast fading component of the link between the i-th VU transmitter and MBS over the j-th channel, which follows complex Gaussian distribution with zero mean and unit variance, i.e, $h^v_{i,j} \sim \mathcal{CN}(0,1)$, ξ_i is the log-normal shadowing random variable with standard deviation ζ for the link between the i-th VU transmitter and MBS, C is the pathloss constant, d_i is the distance between the i-th VU transmitter and MBS, and β is the pathloss exponent. Since each VU transmitter and

its corresponding receiver have similar speeds and no obstacles in between, we can regard the V2V link channel estimation error-free. Additionally, the FUs are assumed with low mobility, and thus the *FU to FS* (F2FS) link can also be estimated precisely.

However, due to the fast changing environment between the FUs, FSs, and VUs, the fast fading components of cross-tier interference links suffer channel estimation errors. Denote $h^v_{i,m,j}$ and $h^f_{m,i',j}$ as the fast fading components of the interference links from the i-th VU transmitter to the m-th FU's corresponding FS over the j-th channel and from the m-th FU to the i-th corresponding VU receiver, indexed by i', over the j-th channel, respectively. We have

$$h^v_{i,m,j} = \hat{h}^v_{i,m,j} + \epsilon \tag{3.2}$$

and

$$h^f_{m,i',j} = \hat{h}^f_{m,i',j} + \epsilon, \tag{3.3}$$

where $\hat{h}^v_{i,m,j} \sim \mathcal{CN}(0,1)$ and $\hat{h}^f_{m,i',j} \sim \mathcal{CN}(0,1)$ are the estimated fast fading components of the link from the i-th VU transmitter to the m-th FU's corresponding FS over the j-th channel and that from the m-th FU to the i-th corresponding VU receiver over the j-th channel, respectively, and ϵ is the channel estimation error, i.e., $\epsilon \sim \mathcal{CN}(0, \sigma^2_\epsilon)$ [30]. Given the limited transmit powers of FUs, we assume that the interference from the FUs to the MBS is negligible.

The channel power gains between the i-th VU transmitter and its corresponding receiver over the j-th channel, $g^v_{i,i',j}$, and between the m-th FU and its corresponding FS over the j-th channel, $g^f_{m,j}$, and the interference link channel power gains from the i-th VU transmitter to the m-th FU's corresponding FS over the j-th channel, $g^v_{i,m,j}$, and from the m-th FU to the i-th corresponding VU receiver over the j-th channel, $g^f_{m,i',j}$, can be similarly defined as in (3.1).

Problem Formulation

In NOMA, the MBS and VU receivers share the same channel with different link qualities. Due to the short distance between the i-th VU transmitter and its corresponding receiver, $g^v_{i,i',j}$ is larger than $g^v_{i,j}$ and therefore the transmitted messages from the i-th VU transmitter to the MBS can be decoded and subtracted at the i-th corresponding VU receiver via *successive interference cancellation* (SIC). To successfully perform SIC at the VU receiver, a power difference condition needs to be satisfied [31], i.e.,

$$\frac{\sum_{j=1}^{L} a_{i,j}(P^v_i - P^v_{i,i'})g^v_{i,i',j}}{\sigma^2} \geq \delta, \tag{3.4}$$

where $a_{i,j}$ is the channel assignment indicator such that $a_{i,j} = 1$ when the i-th VU transmitter and its corresponding receiver occupy the j-th channel and $a_{i,j} = 0$ otherwise, P^v_i and $P^v_{i,i'}$ are the transmit powers of the i-th VU transmitter for the V2I and V2V links, respectively, σ^2 is the noise power, and δ is the minimum power difference ratio.

With (3.4) satisfied, the *signal to interference noise ratio* (SINR) of the received signal at the MBS from the i-th VU transmitter can be expressed as

$$\gamma^v_i = \frac{\sum_{j=1}^{L} a_{i,j}P^v_i g^v_{i,j}}{\sum_{j=1}^{L} a_{i,j}P^v_{i,i'}g^v_{i,j} + \sigma^2}. \tag{3.5}$$

Due to the limited transmit powers of FUs, the interference from FUs to the MBS is neglected.

Similarly, the SINR of the received signal at the i-th VU receiver from the i-th VU transmitter is

$$\gamma^v_{i,i'} = \frac{\sum_{j=1}^{L} a_{i,j}P^v_{i,i'}g^v_{i,i',j}}{\sum_{m=1}^{M} b_{m,j}P^f_m g^f_{m,i',j} + \sigma^2}, \tag{3.6}$$

and the SINR of the received signal at the FS from the m-th FU is

$$\gamma^f_m = \frac{\sum_{m=1}^{M} b_{m,j}P^f_m g^f_{m,j}}{\sum_{j=1}^{L} a_{i,j}(P^v_i + P^v_{i,i'})g^v_{i,m,j} + \sigma^2}. \tag{3.7}$$

To satisfy various QoS requirements for different types of links, we maximize the overall throughput of V2I links while guaranteeing the reliability of V2V and F2FS links. The power allocation problem is formulated as

$$\max_{\substack{a_{i,j},b_{m,j},\\ P_i^v,P_{i,i'}^v,P_m^f}} \sum_{i=1}^{N} \log_2(1+\gamma_i^v) \tag{3.8}$$

$$s.t.: \quad 0 \leqslant P_i^v, \quad 0 \leqslant P_{i,i'}^v, \quad 0 \leqslant P_i^v + P_{i,i'}^v \leqslant P_{max}^v, \quad \forall i, \tag{3.8a}$$

$$\frac{\sum_{j=1}^{L} a_{i,j}(P_i^v - P_{i,i'}^v) g_{i,i',j}^v}{\sigma^2} \geq \delta, \quad \forall i, \tag{3.8b}$$

$$0 \leqslant P_m^f \leqslant P_{max}^f, \quad \forall m, \tag{3.8c}$$

$$\Pr(\gamma_{i,i'}^v \geqslant \gamma_{th}^v) \geqslant 1 - p_v, \quad \forall i, \tag{3.8d}$$

$$\Pr(\gamma_m^f \geqslant \gamma_{th}^f) \geqslant 1 - p_f, \quad \forall m, \tag{3.8e}$$

$$a_{i,j}, b_{m,j} \in \{0,1\}, \quad \forall i,j,m, \tag{3.8f}$$

$$\sum_{i=1}^{N} a_{i,j} \leqslant 1, \quad \forall j, \quad \sum_{j=1}^{L} a_{i,j} \leqslant 1, \quad \forall i, \tag{3.8g}$$

$$\sum_{m=1}^{M} b_{m,j} \leqslant 1, \quad \forall j, \quad \sum_{j=1}^{L} b_{m,j} \leqslant 1, \quad \forall m, \tag{3.8h}$$

where P_{max}^v and P_{max}^f are the maximum transmit powers of the VU transmitters and FUs, respectively, p_v is the maximum outage probability of the V2V links, p_f is the maximum outage probability of the F2FS links, γ_{th}^v and γ_{th}^f are the SINR thresholds for the V2V and F2FS links, respectively, and $b_{m,j}$ is the channel assignment indicator for each FU such that $b_{m,j} = 1$ if the m-th FU transmits over the j-th channel and $b_{m,j} = 0$ otherwise. (3.8a) ensures that the transmit powers of each VU transmitter for both V2I and V2V links are non-negative and the total transmit power of each VU transmitter is positive and within the maximum VU transmit power. (3.8b) is the aforementioned power difference condition. (3.8c) ensures that the transmit power of each FU is non-negative and within the maximum FU transmit power. (3.8d) and (3.8e) represent the reliability requirements for V2V and

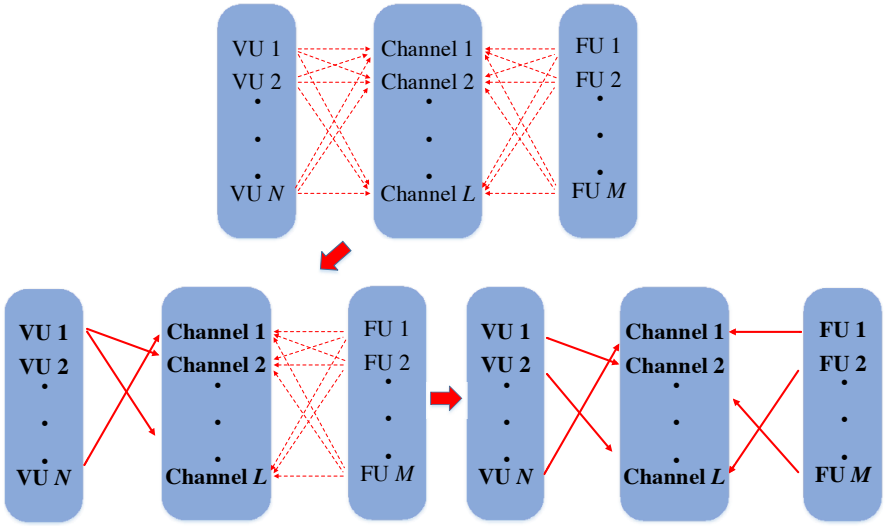

Figure 3.2. Cascaded channel assignment.

F2FS links, respectively. (3.8f) reveals the binary properties of both VU and FU channel assignment indicators. (3.8g) guarantees that each channel can only be assigned by one VU transmitter and each VU transmitter can only occupy one channel. Similarly, (3.8h) ensures that each channel can only be assigned by one FU and each FU can only occupy one channel. Note that, for each channel, one VU transmitter and one FU can coexist.

Obviously, (3.8) is a mixed-integer, non-convex, and chance-constrained problem, which cannot be effectively solved via existing methods. Moreover, the optimal solution requires *exhaustive search* (ES) over combinatorial space of binary variables $a_{i,j}$ and $b_{m,j}$, which results in prohibitive computational complexity in practice. To obtain satisfactory results with low complexity, we will decouple (3.8) into the proposed cascaded channel assignment, through which VUs and FUs are paired, and the power allocation for each VU-FU pair.

3.2 Cascaded Channel Assignment

To relax the binary and combinatorial constraints in (3.8), we propose in this section a cascaded channel assignment algorithm based on the Hungarian algorithm with polynomial complexity [32].

The channel assignment in (3.8) involves two goals. The first one is to assign channels to VUs for the throughput maximization of V2I links while guaranteeing the reliability of

V2V links. The second goal is to share channels with FUs, limit the introduced interference to VUs, and maintain their own reliability. Instead of ES, the Hungarian algorithm is an effective combinatorial optimization algorithm for assignment problems. With the Hungarian algorithm, optimality can be achieved by either maximizing the overall throughput of V2I links or minimizing the total introduced interference to VUs. However, since the channel assignments of VUs and FUs affect each other in our scenario, applying the Hungarian algorithm to the channel assignments of VUs and FUs individually cannot guarantee the two goals to be satisfied at the same time. Therefore, a cascaded channel assignment algorithm is proposed to simultaneously meet the two requirements. The logic of the proposed cascaded channel assignment is illustrated in Fig 3.2.

Cascaded Channel Assignment Algorithm

Given that the reliability of V2V links is more important than that of F2FS links from the safety perspective, we assume that VUs have priorities to access channels. Before the channel assignment is determined, the optimal powers cannot be allocated and the throughput of V2I links and interference from FUs to VUs cannot be calculated at this stage. Therefore, the proposed cascaded channel assignment consists of two phases. Firstly, channels are assigned to VUs according to the Hungarian algorithm to maximize the overall throughput of V2I links based on the *channel to noise ratios* (CNRs). With the channel assignment of VUs, the CNR of the interference link from FUs over each channel is determined through the calculation of the CNR of the interference link from FUs to the VU who occupies that channel. Secondly, the Hungarian algorithm is adopted to assign channels to FUs to minimize the total CNR of the interference links from FUs to VUs and thus to minimize the co-channel interference. Let $\phi_{i,j}^{v}$ denote the V2I link CNR for the i-th VU over the j-th channel and $\phi_{m,j}^{f}$ the interference link CNR for the m-th FU over the j-th channel. The proposed cascaded channel assignment algorithm is detailed in Algorithm 3.

Note that the channel assignment is originally a 3-dimensional assignment problem involving VUs, FUs, and channels. In Algorithm 3, the cascaded channel assignment based

on the outcome of Phase I reduces to 1-dimensional for FU channel assignment, which simplifies the problem. Through the proposed cascaded channel assignment, the binary and combinatorial constraints in (3.8) are relaxed.

Algorithm 3 Cascaded Channel Assignment

Initialization: Initialize VU channel assignment matrix $\mathbf{A_{NxL}}$ with entry $a_{i,j} = 0, \forall i, j$, and FU channel assignment channel matrix $\mathbf{B_{MxL}}$ with entry $b_{m,j} = 0, \forall m, j$.
Phase I: VU channel assignment
  for $i = 1 : N$ **do**
    for $j = 1 : L$ **do**
      Calculate $\phi^v_{i,j} = \frac{g^v_{i,j}}{\sigma^2}$.
    end for
  end for
  Use the Hungarian algorithm to find the channel assignment $\mathbf{A}^*$ based on $\{\phi^v_{i,j}\}$.
Phase II: FU channel assignment
  for $m = 1 : M$ **do**
    for $j = 1 : L$ **do**
      if $\sum_{i=1}^{N} a_{i,j} = 1$
        Find i^* such that $a_{i^*,j} = 1$ according to $\mathbf{A}^*$.
        Calculate $\phi^f_{m,j} = \frac{g^f_{m,i',j}}{\sigma^2}$.
      else
        Set $\phi^f_{m,j} = 0$.
    end for
  end for
  Use the Hungarian algorithm to find the channel assignment $\mathbf{B}^*$ based on $\{\phi^v_{m,i'^*j}\}$.
Return VU and FU channel assignment matrices $\mathbf{A}^*$ and $\mathbf{B}^*$.

Hungarian Algorithm Strategies

As stated in Algorithm 3, the ultimate goal of the Hungarian algorithm is to maximize the throughput of V2I links. Since NOMA is adopted at the VUs, there are three possible strategies for the Hungarian algorithm to assign channels.

- *Based on the V2I link CNRs*: The *Hungarian algorithm based on the V2I link CNRs* (HBV2I) is the most straightforward method to maximize the total CNR of V2I links. The HBV2I scheme directly increases the throughput of V2I links.

- *Based on the V2V link CNRs*: The *Hungarian algorithm based on the V2V link CNRs* (HBV2V) can indirectly improve the throughput of V2I links. Since less transmit

power for the V2V links is needed to satisfy the reliability constraints with better V2V link CNRs, more transmit power becomes available for the V2I links under the total transmit power constraint. Therefore, the overall throughput of V2I links can be increased.

- *Based on the difference between the V2I link CNRs and V2V link CNRs*: In power-domain NOMA, the users with more distinctive channel conditions achieve better throughput performance [33]. Therefore, the *Hungarian algorithm based on the difference of V2I link CNRs and V2V link CNRs* (HBD) can be beneficial to the throughput performance of V2I links.

Since our model mainly focuses on the throughput maximization of V2I links while guaranteeing the reliability of V2V links, the HBV2I is adopted in our paper and obtains the best performance improvement due to the direct relationship between the total CNR and the throughput of V2I links although both the HBV2V and HVD can increase the throughput of V2I links. The comparison of the three schemes is provided in the simulation.

3.3 Power Allocation

Through the proposed cascaded channel assignment algorithm, the VU and FU who share the same channel form a VU-FU pair. Since different VU-FU pairs adopt orthogonal channels, the power allocation in (3.8) can be carried out at each single VU-FU pair. To derive the power allocation for each single VU-FU pair, we first transform the probabilistic constraints into deterministic forms in this section through approximation. Then we derive the feasible power allocation region and the optimal solution to the transformed problem.

After the channel assignment is determined, a channel can be shared within an arbitrary VU-FU pair, e.g., the i-th VU shares the j-th channel with the m-th FU. (3.8) is transformed to

$$\max_{P_i^v, P_{i,i'}^v, P_m^f} \log_2(1+\gamma_i^v) \tag{3.9}$$

$$s.t.: \quad 0 \leqslant P_i^v, \quad 0 \leqslant P_{i,i'}^v, \quad 0 \leqslant P_i^v + P_{i,i'}^v \leqslant P_{max}^v, \quad \forall i, \tag{3.9a}$$

$$\frac{(P_i^v - P_{i,i'}^v) g_{i,i',j}^v}{\sigma^2} \geq \delta, \tag{3.9b}$$

$$0 \leqslant P_m^f \leqslant P_{max}^f, \tag{3.9c}$$

$$\Pr(\gamma_{i,i'}^v \geqslant \gamma_{th}^v) \geqslant 1 - p_v, \tag{3.9d}$$

$$\Pr(\gamma_m^f \geqslant \gamma_{th}^f) \geqslant 1 - p_f. \tag{3.9e}$$

Since channel estimation errors exist in the interference links, we substitute (3.1), (3.2), and (3.3) into (3.9d) and (3.9e) to evaluate the reliability requirements and have

$$\Pr\Big(\frac{P_{i,i'}^v g_{i,i',j}^v}{P_m^f \alpha_{m,i',j}^f |\hat{h}_{m,i',j}^f + \epsilon|^2 + \sigma^2} \geqslant \gamma_{th}^v\Big) \geqslant 1 - p_v \tag{3.10}$$

and

$$\Pr\Big(\frac{P_m^f g_{m,j}^f}{P^v \alpha_{i,m,j}^v |\hat{h}_{i,m,j}^v + \epsilon|^2 + \sigma^2} \geqslant \gamma_{th}^f\Big) \geqslant 1 - p_f, \tag{3.11}$$

where P^v is the total VU transmit power, i.e., $P^v = P_i^v + P_{i,i'}^v$.

Given the estimated fast fading components $\hat{h}_{m,i',j}^f$ and $\hat{h}_{i,m,j}^v$, $\frac{|\hat{h}_{m,i',j}^f + \epsilon|^2}{\sigma_\epsilon^2}$ and $\frac{|\hat{h}_{i,m,j}^v + \epsilon|^2}{\sigma_\epsilon^2}$ are 2-degree non-central Chi-square distributed with non-centrality parameters $\lambda_f = \frac{2|\hat{h}_{m,i',j}^f|^2}{\sigma_\epsilon^2}$ and $\lambda_v = \frac{2|\hat{h}_{i,m,j}^v|^2}{\sigma_\epsilon^2}$, respectively [34]. Define the corresponding 2-degree non-central Chi-square random variables as $\mathcal{X}_{2,nc}^2$ and $\mathcal{Y}_{2,nc}^2$. Then (3.10) and (3.11) can be rearranged as

$$\Pr\Big(\frac{P_{i,i'}^v g_{i,i',j}^v - \sigma^2 \gamma_{th}^v}{\frac{\sigma_\epsilon^2}{2} P_m^f \alpha_{m,i',j}^f \gamma_{th}^v} \geqslant \mathcal{X}_{2,nc}^2\Big) \geqslant 1 - p_v \tag{3.12}$$

and

$$\Pr\Big(\frac{P_m^f g_{m,j}^f - \sigma^2 \gamma_{th}^f}{\frac{\sigma_\epsilon^2}{2} P_v \alpha_{i,m,j}^v \gamma_{th}^f} \geqslant \mathcal{Y}_{2,nc}^2\Big) \geqslant 1 - p_f, \tag{3.13}$$

with *probability density functions* (PDFs)

$$
\begin{aligned}
&f_{\mathcal{X}^2_{2,nc}}(x) \\
=&\frac{1}{\sigma^2_\epsilon}\exp(-\frac{|\hat{h}^f_{m,i',j}|^2+x}{\sigma^2_\epsilon})I_0(\sqrt{x|\hat{h}^f_{m,i',j}|^2}\frac{2}{\sigma^2_\epsilon})
\end{aligned} \tag{3.14}
$$

and

$$
\begin{aligned}
&f_{\mathcal{Y}^2_{2,nc}}(y) \\
=&\frac{1}{\sigma^2_\epsilon}\exp(-\frac{|\hat{h}^v_{i,m,j}|^2+y}{\sigma^2_\epsilon})I_0(\sqrt{y|\hat{h}^v_{i,m,j}|^2}\frac{2}{\sigma^2_\epsilon}),
\end{aligned} \tag{3.15}
$$

where I_0 is the zero-order modified Bessel function of the first kind.

Even with (3.14) and (3.15), it is still difficult to obtain closed-form expressions of reliability requirements (3.12) and (3.13). Therefore, we adopt an approximation of non-central Chi-square distribution to simplify (3.12) and (3.13) [35]. With some manipulation of the rest constraints, the feasible power region of (3.8) is given in 3.3.1 and depicted in Fig. 3.3.

Proposition 3.3.1. *The feasible power allocation region of* (3.8) *is derived in two cases as*

Case I: $\frac{B_2}{A_2} > \frac{B_1}{A_1}$ *and* $\frac{B_2}{A_2}\bar{P}^f_{max} + \frac{C_2}{A_2} \leqslant P^v_{max}$

$$
\begin{aligned}
&\{(P^v_i, P^v_{i,i'}, P^f_m): \\
&0 \leqslant P^f_m \leqslant \bar{P}^f_{max}, P^v_{i,i'} \geqslant \frac{B_1}{A_1}P^f_m + \frac{C_1}{A_1}, \\
&P^v_i + P^v_{i,i'} \leqslant \frac{B_2}{A_2}P^f_m + \frac{C_2}{A_2}, P^v_{i,i'} \leqslant \frac{P^v_{max} - \frac{\delta\sigma^2}{g^v_{i,i',j}}}{2}\};
\end{aligned} \tag{3.16}
$$

Case II: $\frac{B_2}{A_2} > \frac{B1}{A_1}$ *and* $\frac{B_2}{A_2}\bar{P}^f_{max} + \frac{C_2}{A_2} > P^v_{max}$

$$\begin{aligned}
&\{(P^v_i, P^v_{i,i'}, P^f_m) : \\
&0 \leqslant P^f_m \leqslant \bar{P}^f_{max}, P^v_{i,i'} \geqslant \frac{B_1}{A_1}P^f_m + \frac{C_1}{A_1}, \\
&P^v_i + P^v_{i,i'} \leqslant \frac{B_2}{A_2}P^f_m + \frac{C_2}{A_2}, P^v_{i,i'} \leqslant \frac{P^v_{max} - \frac{\delta\sigma^2}{g^v_{i,i',j}}}{2}, \\
&P^v_i + P^v_{i,i'} \leqslant P^v_{max}\},
\end{aligned} \tag{3.17}$$

where $A_1 = \frac{g^v_{i,i',j}}{\gamma^v_{th}}$, $B_1 = \frac{\sigma^2_\epsilon}{2}(1 + \frac{\lambda_f}{2})\alpha^f_{m,i',j}\ln\frac{1}{p^2_v}$, $C_1 = \sigma^2$, $A_2 = \frac{\sigma^2_\epsilon}{2}(1 + \frac{\lambda_v}{2})\alpha^v_{i,m,j}\ln\frac{1}{p^2_f}$, $B_2 = \frac{g^f_{m,j}}{\gamma^f_{th}}$, $C_2 = -\sigma^2$, *and* $\bar{P}^f_{max} = \min\{\frac{A_1(P^v_{max} - \frac{\delta\sigma^2}{g^v_{i,i',j}}) - 2C_1}{2B_1}, P^f_{max}\}$.

Proof. *See Appendix A.1.*

Based on 3.3.1, the optimal power allocation solution to (3.9) is provided in 3.3.2.

Proposition 3.3.2. *The optimal power allocation solution to* (3.9) *is*

$$P^{f*}_m = \begin{cases} \bar{P}^f_{max}, & \textit{Case I}, \\ \frac{A_2}{B_2}P^v_{max} - \frac{C_2}{B_2}, & \textit{Case II}, \end{cases} \tag{3.18}$$

$$\begin{aligned}
&P^{v*}_i \\
&= \begin{cases} (\frac{B_2}{A_2} - \frac{B_1}{A_1})\bar{P}^f_{max} + (\frac{C_2}{A_2} - \frac{C_1}{A_1}), & \textit{Case I}, \\ P^v_{max} - \frac{B_1}{A_1}(\frac{A_2}{B_2}P^v_{max} - \frac{C_2}{B_2}) - \frac{C_1}{A_1}, & \textit{Case II}, \end{cases}
\end{aligned} \tag{3.19}$$

and

$$P^{v*}_{i,i'} = \begin{cases} \frac{B_1}{A_1}\bar{P}^f_{max} + \frac{C_1}{A_1}, & \textit{Case I}, \\ \frac{B_1}{A_1}(\frac{A_2}{B_2}P^v_{max} - \frac{C_2}{B_2}) + \frac{C_1}{A_1}, & \textit{Case II}. \end{cases} \tag{3.20}$$

Proof. *See Appendix A.2.*

3.3.2 gives the optimal power allocation to the transformed throughput optimization problem of V2I links while guaranteeing the reliability of V2V and F2FS links for each VU-FU pair.

For the proposed resource allocation scheme, the cascaded channel assignment requires $\mathcal{O}(NL+ML)$ to calculate link CNRs and $\mathcal{O}(L^3+L^3)$ for the Hungarian algorithm. And the optimal power allocation has a computational complexity of $\mathcal{O}(\max\{N, M\})$. Therefore, the computational complexity of the proposed resource allocation scheme is $\mathcal{O}((M+N)L+L^3+\max\{N, M\})$. In comparison, the computational complexity of the optimal search and power allocation is $\mathcal{O}((\frac{(L!)^2}{(L-M)!(L-N)!})\cdot\max\{N, M\})$. Therefore, the proposed resource allocation scheme significantly reduces the computational complexity.

3.4 Numerical Results

In this section, we present simulation results to illustrate the performance of the proposed resource allocation scheme in a heterogeneous vehicular network. We simulate a two-way urban roadway scenario. The vehicles are covered by a single macrocell and several non-overlapping coexisting femtocells as illustrated in Fig. 3.1. The VUs are dropped according to a spatial Poisson point process with density determined by the vehicle speed. The FUs are generated by a spatial Poisson point process with density 8 per femtocell. Each VU sets up a V2V link to the nearest VU behind and the coexisting FU is randomly selected from the generated FUs. The numbers of selected VUs and FUs, N and M, are both 4. The total number of channels, L, is 4. The major simulation parameters are listed in Table 3.1 [17, 18, 36]. In our simulation, the V2I, V2FS, and F2FS links are modeled as *non-line-of-sight* (NLOS) while the V2V and F2V links are modeled as *line-of-sight* (LOS). The NLOS and LOS pathloss models are $128.1 + 37.6\log_{10} d$ and WINNER + B1 [37], respectively.

In Fig. 3.4, the overall throughput of the V2I links with different schemes and channel estimation errors is shown. In Fig. 3.4(a), the proposed NOMA resource allocation scheme

Table 3.1. Simulation Parameters.

Parameter	**Value**
Carrier frequency	2 GHz
Macrocell radius	500 m
Femtocell radius	50 m
Vehicle speed s	60 km/h
Vehicle density	$2.5s$, s in m/s
FU density	8/2500 /m^2
SINR threshold for V2V link γ_v^{th}	5 dB
SINR threshold for F2FS link γ_f^{th}	5 dB
Reliability for V2V link p_v	10^{-3}
Reliability for F2FS link p_f	10^{-3}
Maximum VU transmit power P_v^{max}	23 dBm
Maximum FU transmit power P_f^{max}	10 dBm
Noise power σ^2	-114 dBm
Required power difference ratio δ	10 dB

is compared with the OMA resource allocation scheme and NOMA power allocation with ES under different channel estimation errors. Although the ES renders the best performance, the complexity is prohibited in practice. Our proposed NOMA resource allocation scheme achieves comparable performance with the ES and outperforms the OMA resource allocation. However, due to the interference from the V2V links to the V2I links, the proposed NOMA resource allocation scheme results in less than double throughput performance of the OMA resource allocation. It can be noticed that larger channel estimation errors degrade the performance with NOMA power allocation, but has little influence on that of OMA power allocation when different links use orthogonal channels. In Fig. 3.4(b), the performance of different Hungarian channel assignment schemes are illustrated. Without consideration of computational complexity, the ES provides the best performance. It is obvious that HBV2I achieves better performance than HBV2V and HBD due to the direct relationship between the V2I link CNRs and throughput. Since HBV2V only considers the V2V link CNRs, the overall throughput of the V2I links with HBV2V is the lowest.

In Fig. 3.5, the SINRs of the V2V links with different schemes and $\sigma_e^2 = 0.01$ are illustrated. Fig. 3.5(a) shows the SINRs of the V2V links for all 4 VUs in NOMA and OMA. It is obvious that both NOMA and OMA can satisfy the minimum SINR requirement, i.e., 5 dB. Since the channel estimation error in NOMA from the V2I link to the V2V link is considered in (3.8d), there are some margins for SINRs in NOMA to guarantee the outage probability constraint. In contrast, no interference exists in OMA and thus no protection margins are needed. Therefore, the power allocation in OMA assigns the V2V transmit power to maintain the minimum SINR requirement. In Fig. 3.5(b), VU1's V2V link SINRs with different channel allocation schemes are illustrated. The ES for channel allocation has the minimum SINR margin to guarantee the outage probability constraint. The HBV2I outperforms the HBV2V and HBD schemes with less V2V link SINR margin, which can allocate more transmit power to V2I links while satisfying the reliability requirements.

In Fig. 3.6, the SINRs of the F2FS links with different schemes and $\sigma_e^2 = 0.01$ are shown. The required SINR for F2FS links is also 5 dB. As shown in Fig. 3.6(a), the SINRs of the F2FS links with our proposed NOMA scheme still have larger SINR margins than those with OMA scheme to guarantee the reliability constraint in our formulated problem, which is the same for the V2V links. However, the SINRs of the F2FS links with OMA scheme also have SINR margins due to the fact that in OMA scheme, FUs still coexist with VUs and have to consider the interference and channel estimation errors. In Fig. 3.6(b), different channel assignment schemes render similar SINRs of F2FS links. This is because in NOMA, the F2FS links share the channel with both the V2I and V2V links, no matter how different VU transmit powers are allocated to V2I and V2V links. The interference from the VU to FU depends on the total VU transmit power, which equals the maximum VU transmit power in order to maximize the throughput of V2I links as long as the outage probability constraint of F2FS links can be satisfied.

Fig. 3.7 shows the *cumulative distribution functions* (CDFs) of the V2V and F2FS links with respect to the SINR for VU1 and its co-existing FU. It can be seen that the V2V link

achieves the reliability requirement with our proposed resource allocation scheme. However, since P_i^v exists in (3.7), the approximation error of non-central Chi-square distribution is amplified in the F2FS link, which renders the SINR of F2FS link slightly larger than the desired threshold, i.e., 5 dB, at the target outage probability. Moreover, due to P_m^f in the numerator of γ_m^f and P_i^v in the denominator, a larger P_m^f allows a larger P_i^v, which increases the throughput of V2I link. Meanwhile, a larger P_m^f may result in a larger SINR of F2FS link, which is reflected in Fig. 3.7 with a larger probability of higher SINR of F2FS link than that of V2V link. Because the V2V link competes for resource with the V2I link, a large percentage of V2V link SINRs stick around the desired threshold, i.e., 5 dB, to maximize the transmit power for the V2I link.

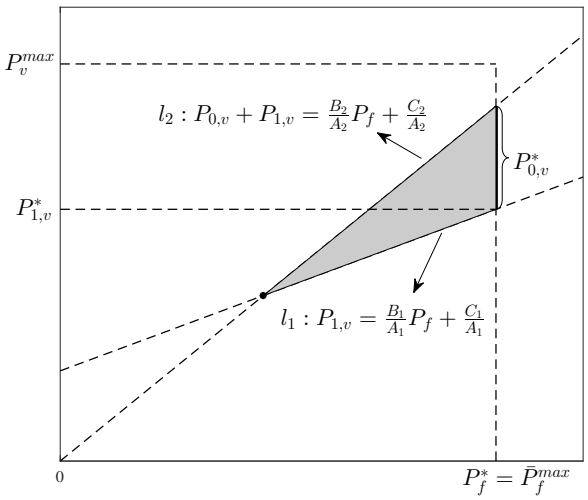

(a) Case I.

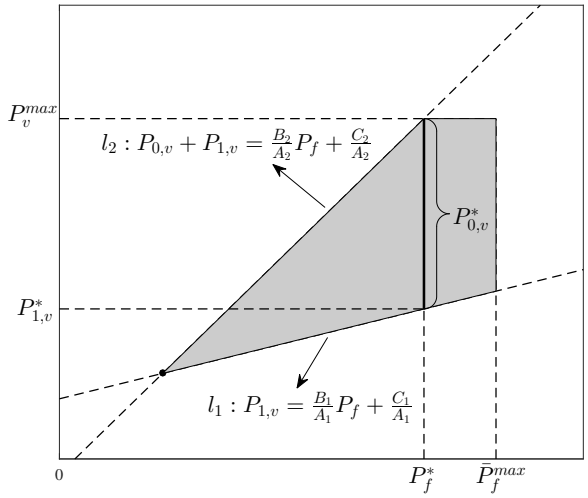

(b) Case II.

Figure 3.3. Feasible power allocation region of (3.9) in two cases.

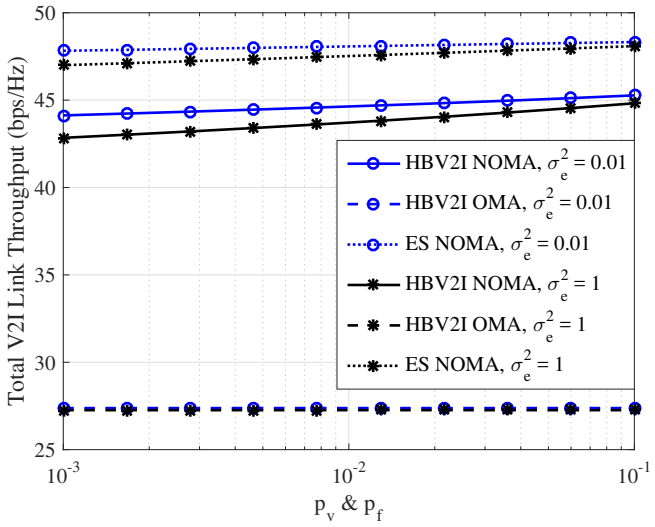

(a) NOMA vs OMA with different channel estimation errors.

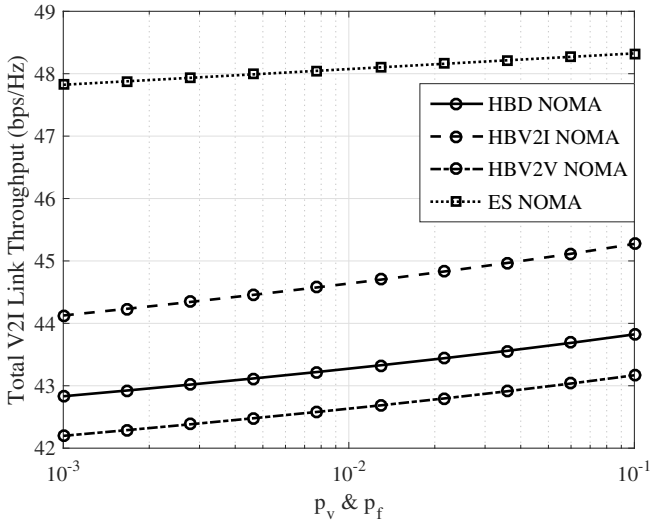

(b) HBV2I vs HBV2V vs HBD with $\sigma_e^2 = 0.01$.

Figure 3.4. Overall throughput of V2I links with different channel estimation errors and schemes.

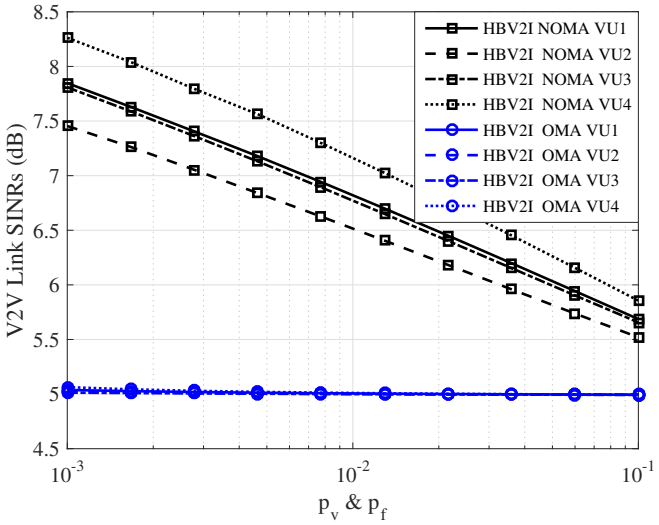

(a) NOMA vs OMA with $\sigma_e^2 = 0.01$ for 4 VUs.

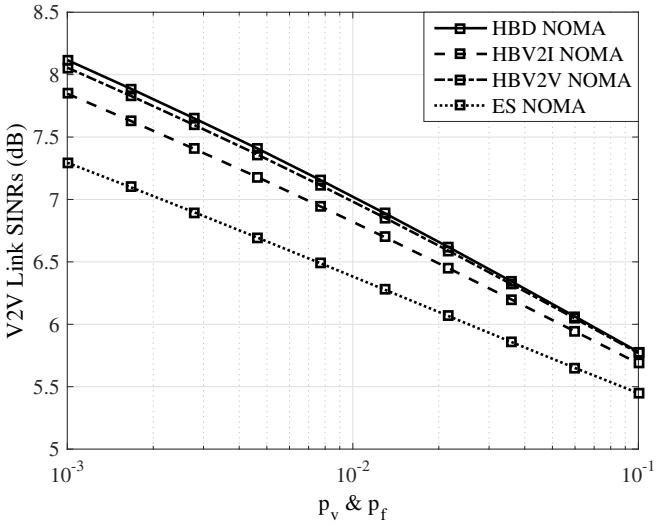

(b) HBV2I vs HBV2V vs HBD with $\sigma_e^2 = 0.01$ for VU1.

Figure 3.5. SINRs of V2V links with different schemes and $\sigma_e^2 = 0.01$.

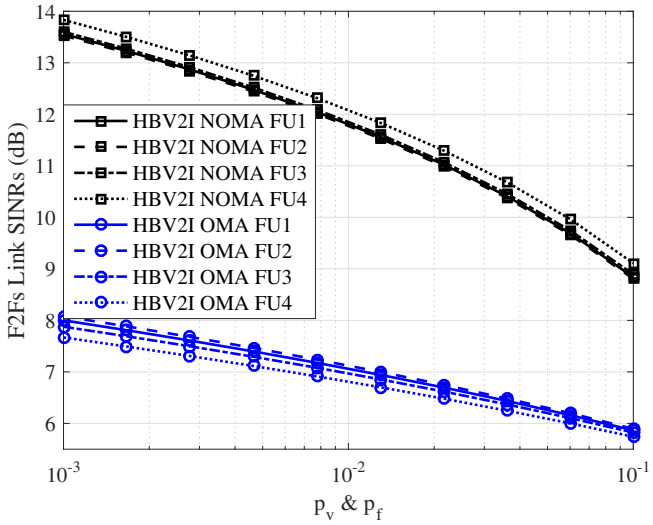

(a) NOMA vs OMA with $\sigma_e^2 = 0.01$ for 4 FUs.

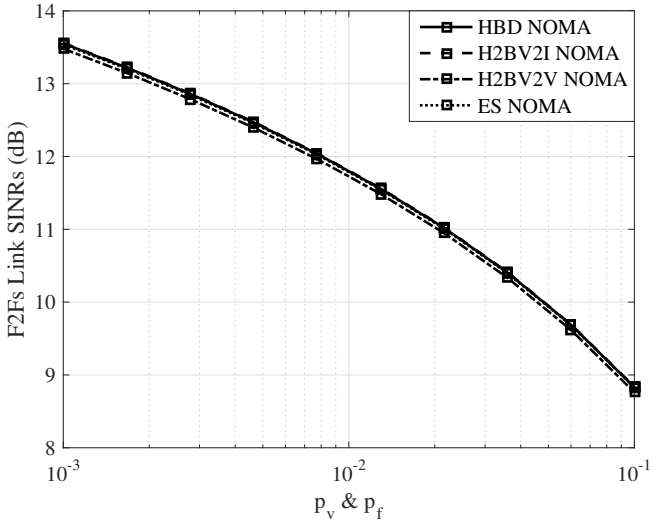

(b) HBV2I vs HBV2V vs HBD with $\sigma_e^2 = 0.01$ for FU1.

Figure 3.6. The SINRs of F2FS links with different schemes and $\sigma_e^2 = 0.01$.

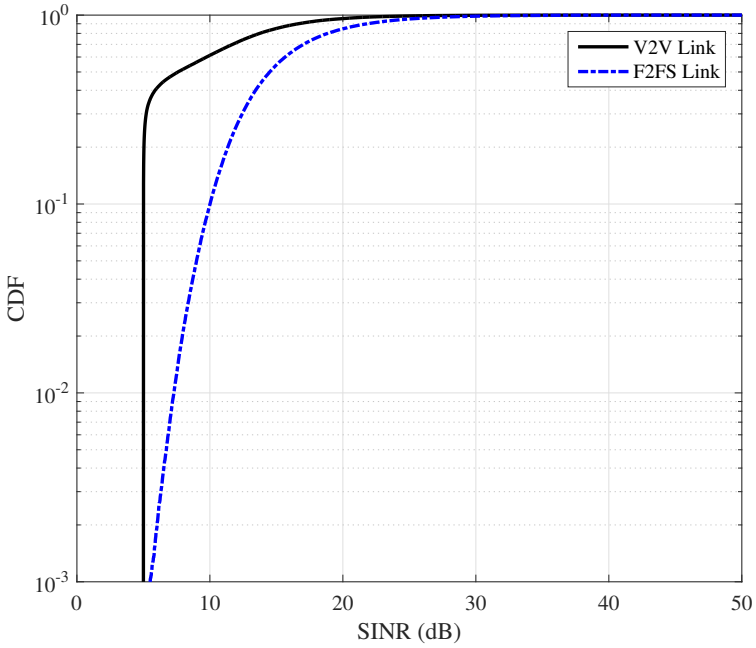

Figure 3.7. CDFs of V2V and F2FS links versus SINR with $p_v = p_f = 10^{-3}$ and $\gamma_v^{th} = \gamma_f^{th} = 5$ dB for VU1 and its co-existing FU.

Chapter 4. Energy-Efficient Resource Allocation in D2D Communications

Aside from spectrum efficiency, energy efficiency becomes more important for wireless communications. Due to the explosive number of devices in wireless communications, D2D communications has been included in 5G standard. Unfortunately, millions of devices consume huge amount of energy for data collection and transmission. To this point, energy-efficient D2D communications design becomes one of the most important pieces in 5G blueprint.

In this chapter, the energy efficiency in a cellular network with D2D communications is studied from user fairness perspective. A mixed-integer max-min resource allocation problem is formulated, in which both mode selection and resource allocation are considered. Since the optimal solution requires an exhaustive search, which is NP-hard, two sub-optimal methods are derived. First, a *Lagrangian decomposition based* (LDB) method is proposed to jointly solve subcarrier assignment and power allocation with integer constraint relaxation under different modes. To further reduce the computational complexity, a *low-complexity decomposition* (LCD) method is derived. A novel mode selection scheme, a subcarrier assignment scheme, a power allocation scheme, and a mode switching scheme are introduced and analyzed. The LCD method is scalable and suitable for a large number of devices and subcarriers. Numerical results demonstrate that our proposed sub-optimal methods achieve satisfactory energy efficiency performance and promote the fairness among individual users.

4.1 System Model and Problem Formulation

We consider a cellular network with one base station, K users, and N orthogonal subcarriers. As shown in Fig. 4.1, we classify K users into K_c cellular users and K_d D2D users. A cellular user connects to the core network via the base station, so cellular users cannot be in D2D mode. Therefore, we focus on the mode selection of D2D users that can be in either D2D or cellular mode. However, the cellular users compete for subcarriers with the D2D users. As a result, we consider the resource allocation among cellular and D2D users.

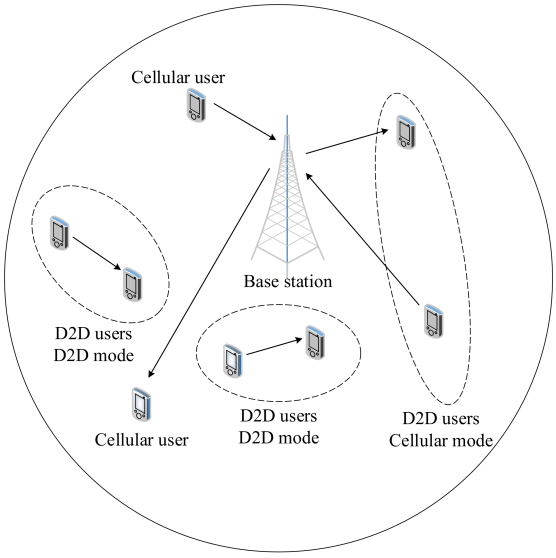

Figure 4.1. A D2D enabled cellular network.

Note that we can view a cellular user as a special D2D user in D2D mode, where the other user of the pair is the base station. Denote $\mathcal{K}$ as the user set with a size of K. Let $\mathcal{K}_1$ be the set of the D2D users in D2D mode and the cellular users. Denote $\mathcal{K}_2$ as the set of the D2D users in cellular mode. Each user can only be in one set, so $\mathcal{K}_1 \bigcap \mathcal{K}_2 = \emptyset$ and $\mathcal{K}_1 \bigcup \mathcal{K}_2 = \mathcal{K}$. Assume that the total bandwidth is B and thus the bandwidth of each subcarrier, B_0, is B/N. Rayleigh fading is assumed in this paper. To avoid excess interference, one subcarrier cannot be occupied by more than one user pair.

The data rate of the kth user pair in $\mathcal{K}_1$, $R_k^{(1)}$, can be expressed as

$$R_k^{(1)} = \sum_{n=1}^{N} a_{k,n} B_0 \log_2(1 + \frac{P_{k,n} g_{k,n}}{\sigma^2}), \tag{4.1}$$

where $P_{k,n}$ is the transmit power of the transmitter of the kth user pair over subcarrier n, $g_{k,n}$ is the channel power gain of subcarrier n from the transmitter to the receiver of the kth user pair, σ^2 is the noise power, and $a_{k,n}$ is the subcarrier indicator that $a_{k,n} = 1$ if the kth user pair occupies subcarrier n and $a_{k,n} = 0$ otherwise. Note that the transmitter and receiver of the kth user pair can be the base station for cellular users in $\mathcal{K}_1$ in the downlink and uplink, respectively.

Since the base station works as a relay for D2D users in cellular mode, the average data rate of the kth user pair in $\mathcal{K}_2$, $R_k^{(2)}$, is [38]

$$R_k^{(2)} = \frac{1}{2}\sum_{n=1}^{N} a_{k,n} B_0 \log_2 \left(1 + \min\{\frac{P_{k,n}\hat{g}_{k,n}}{\sigma^2}, \frac{P_{0,n}\check{g}_{k,n}}{\sigma^2}\}\right), \tag{4.2}$$

where $\hat{g}_{k,n}$ and $\check{g}_{k,n}$ are the channel power gains over subcarrier n from the transmitter of user pair k to the base station and from the base station to the receiver of user pair k, respectively, $P_{0,n}$ is the transmit power of the base station over subcarrier n. Note that $R_k^{(2)}$ depends on the smaller term of $\frac{P_{k,n}\hat{g}_{k,n}}{\sigma^2}$ and $\frac{P_{0,n}\check{g}_{k,n}}{\sigma^2}$. Given that the base station can usually provide a wider range of power than devices, we assume that the base station can always adjust $P_{0,n}$ to ensure that $\frac{P_{k,n}\hat{g}_{k,n}}{\sigma^2} = \frac{P_{0,n}\check{g}_{k,n}}{\sigma^2}$ [39–42], which can be guaranteed by admission control strategy [43]. Then $R_k^{(2)}$ can be rewritten as

$$R_k^{(2)} = \frac{1}{2}\sum_{n=1}^{N} a_{k,n} B_0 \log_2(1 + \frac{P_{k,n}\hat{g}_{k,n}}{\sigma^2}). \tag{4.3}$$

For the kth user pair in $\mathcal{K}_1$, its power consumption is given by

$$P_{con,k}^{(1)} = \sum_{n=1}^{N} a_{k,n} P_{k,n} + P_{cir,k}, \tag{4.4}$$

where $P_{cir,k}$ is the static circuit power of the kth user pair. The average power consumption for the kth user pair in $\mathcal{K}_2$ is

$$P_{con,k}^{(2)} = \frac{1}{2}(\sum_{n=1}^{N} a_{k,n} P_{k,n} + \sum_{n=1}^{N} a_{k,n} P_{0,n}) + P_{cir,0} + P_{cir,k}, \tag{4.5}$$

where $P_{cir,0}$ is the base station static circuit power and $P_{0,n} = P_{k,n}\frac{\hat{g}_{k,n}}{\check{g}_{k,n}}$.

Because users may dynamically select D2D or cellular mode to improve their performance, we define m_k as the mode indicator that $m_k = 0$ if user pair k belongs to set $\mathcal{K}_1$ and $m_k = 1$ if user pair k belongs to set $\mathcal{K}_2$. Since each user pair can only belong to one

set at one time, the data rate and power consumption for user pair k are given by

$$R_k(\mathbf{a_k}, \mathbf{P_k}, m_k) = (1 - m_k)R_k^{(1)} + m_k R_k^{(2)} \tag{4.6}$$

and

$$P_{con,k}(\mathbf{a_k}, \mathbf{P_k}, m_k) = (1 - m_k)P_{con,k}^{(1)} + m_k P_{con,k}^{(2)}, \tag{4.7}$$

respectively, where $\mathbf{a_k}$ is the subcarrier indicator vector of user pair k that $\mathbf{a_k} = [a_{k,1}, \ldots, a_{k,N}]$ and $\mathbf{P_k}$ is the transmit power vector of user pair k that $\mathbf{P_k} = [P_{k,1}, \ldots, P_{k,N}]$.

Unlike the base station that can adjust the transmit power for each cellular user in the downlink of cellular networks, the D2D user pairs communicate with their own energy sources that cannot be compensated by the others in the network. Moreover, the battery-limited D2D networks emphasis more on energy efficiency for each user pair. To improve the energy efficiency performance of individual user pairs rather than the entire network in D2D communications, we adopt max-min fairness criterion and formulate a max-min problem. The problem maximizes the energy efficiency of the worst-case user in the network and improves the fairness among individual user pairs. Specifically, we have

$$\max_{\mathbf{a_k}, \mathbf{P_k}, m_k} \min_{k \in \mathcal{K}_1, \mathcal{K}_2} \frac{R_k(\mathbf{a_k}, \mathbf{P_k}, m_k)}{P_{con,k}(\mathbf{a_k}, \mathbf{P_k}, m_k)} \tag{4.8}$$

$$s.t.: \quad \text{C1:} \quad a_{k,n} = \{0, 1\}, \forall n, \forall k, \tag{4.8a}$$

$$\text{C2:} \quad \sum_{k=1}^{K} a_{k,n} \leq 1, \forall n, \tag{4.8b}$$

$$\text{C3:} \quad m_k = \{0, 1\}, \forall k, \tag{4.8c}$$

$$\text{C4:} \quad \sum_{n=1}^{N} a_{k,n} P_{k,n} \leq P_{k,max}, \forall k, \tag{4.8d}$$

$$\text{C5:} \quad a_{k,n} P_{k,n} \geq 0, \forall n, \forall k, \tag{4.8e}$$

$$\text{C6:} \quad R_k(\mathbf{a_k}, \mathbf{P_k}, m_k) \geq R_{k,req}, \forall k, \tag{4.8f}$$

where $P_{k,max}$ and $R_{k,req}$ are the maximum transmit power and the minimum data rate requirement for user pair k, respectively. (4.8a) and (4.8b) indicate that each subcarrier can be used by at most one user pair. (4.8c) indicates that each user can only work in a certain mode at a time. In different time slots, the users can switch modes. (4.8d) and (4.8e) guarantee that the transmit power is within the maximum power constraint and always non-negative. (4.8f) is the data rate requirement constraint to guarantee the QoS.

Since the subcarrier and mode indicators are binary variables, (4.8) is a *mixed-integer non-linear programming* (MINLP) problem and the optimal solution can be achieved with an exhaustive search, whose complexity is $O(2^{K_d} \cdot \frac{N!}{(N-K)!})$, which approaches $O(2^{K_d} \cdot N^K)$ when N becomes larger and is exponentially complicated. In the following, we propose two sub-optimal methods that can achieve satisfactory performance with low computational complexity.

4.2 Proposed Resource Allocation

LDB Method

In the inner loop, the mode indicator for user pair k, m_k, is treated as constant, the optimization problem (4.8) can be viewed as a generalized fractional programming with a max-min function in terms of $\mathbf{a_k}$ and $\mathbf{P_k}$. Based on the max-min function and **Proposition 2.1** regarding fractional optimization in [44], we give the following proposition.

Proposition 4.2.1. *Given m_k, the optimal solution, $\{\mathbf{a_k}^*, \mathbf{P_k}^*\}$, and the optimal energy efficiency, ϵ^*, of problem* (4.8) *are achieved if and only if*

$$\min_k \{R_k(\mathbf{a_k^*}, \mathbf{P_k^*}) - \epsilon^* P_{con,k}(\mathbf{a_k^*}, \mathbf{P_k^*})\} = 0. \tag{4.9}$$

Proof. *See Appendix B.1.*

According to Proposition 4.2.1, (4.8) is equivalent to (4.9). The algorithm in [44, 45] can be adopted to obtain the solution to (4.9), based on which we derive Algorithm 4. The convergence of Algorithm 4 has also been proved in [44].

Algorithm 4 Dinkelbach's Method

1: **Initialization**: Set $P_{k,max}$ and $R_{k,req}$ for $\forall k$. Set the maximum number of iterations I and tolerance ε. Initialize index $i = 0$ and energy efficiency of user pair k in the ith iteration $\epsilon_k^i = 0$.
2: **For** $k = 1 : K$
3: **While** $i < I$
4: Solve the problem

$$\max_{\mathbf{a_k},\mathbf{P_k}\in\mathcal{S}} [R_k(\mathbf{a_k},\mathbf{P_k}) - \epsilon_k^i P_{con,k}(\mathbf{a_k},\mathbf{P_k})] \quad (4.10)$$
$$s.t.: \quad \text{(4.8a)-(4.8b), (4.8d)-(4.8f)}$$

5: to obtain the solution $\{\mathbf{a_k^i},\mathbf{P_k^i}\}$.
6: **If** $|R_k(\mathbf{a_k^i},\mathbf{P_k^i}) - \epsilon_k^i P_{con,k}(\mathbf{a_k^i},\mathbf{P_k^i})| < \varepsilon$
7: $\{\mathbf{a_k}^*,\mathbf{P_k}^*\} = \{\mathbf{a_k^i},\mathbf{P_k^i}\}$ and $\epsilon_k^* = R_k(\mathbf{a_k^i},\mathbf{P_k^i})/P_{con,k}(\mathbf{a_k^i},\mathbf{P_k^i})$.
8: Break.
9: **Else**
10: $\epsilon_k^{i+1} = R_k(\mathbf{a_k^i},\mathbf{P_k^i})/P_{con,k}(\mathbf{a_k^i},\mathbf{P_k^i})$ and $i = i + 1$.
11: **End while**
12: **End for**
13: $\epsilon^* = \min_{1\le k\le K} \epsilon_k^*$.

In Algorithm 4, the most important step is to solve the max-min problem (4.10) with a given ϵ_k^i. To tackle the max-min problem, we introduce an auxiliary variable ξ and rewrite (4.10) as

$$\max_{\mathbf{a_k},\mathbf{P_{t,k}},\xi} \xi \quad (4.11)$$
$$s.t.: \quad \text{(4.8a)-(4.8b), (4.8d)-(4.8f),}$$
$$\text{C7:} \quad R_k(\mathbf{a_k},\mathbf{P_{t,k}}) - \epsilon_k^i P_{con,k}(\mathbf{a_k},\mathbf{P_{t,k}}) \ge \xi, \forall k.$$

Problem (4.11) involves both binary and continuous variables with non-linear constraint (4.8f) and is still an MINLP problem. The optimal solution requires to search over all K^N possible cases, which is impractical. To reduce the complexity and make the problem more trackable, we relax the binary variables $a_{k,n}$ into continuous variables [46–48]. As indicated in [47], as long as the number of subcarriers N is large enough, the relaxation is acceptable. We also introduce a new variable $u_{k,n} = a_{k,n}P_{k,n}$ and vector $\mathbf{u_k} = [u_{k,1},\ldots,u_{k,N}]$. Then

the problem becomes

$$\max_{\mathbf{a_k},\mathbf{u_k},\xi} \xi \tag{4.12}$$

$$s.t.: \quad \text{C1:} \quad 0 \leq a_{k,n} \leq 1, \forall n, \forall k, \tag{4.12a}$$

$$\text{C2:} \quad \sum_{k=1}^{K} a_{k,n} \leq 1, \forall n, \tag{4.12b}$$

$$\text{C3:} \quad \sum_{n=1}^{N} u_{k,n} \leq P_{k,max}, \forall k, \tag{4.12c}$$

$$\text{C4:} \quad u_{k,n} \geq 0, \forall n, \forall k, \tag{4.12d}$$

$$\text{C5:} \quad R_k(\mathbf{a_k}, \mathbf{u_k}) \geq R_{k,req}, \forall k, \tag{4.12e}$$

$$\text{C6:} \quad R_k(\mathbf{a_k}, \mathbf{u_k}) - \epsilon_k^i P_{con,k}(\mathbf{u_k}) \geq \xi, \forall k. \tag{4.12f}$$

In reality, $a_{k,n} = 0$ means channel n is not used by user k, we set $a_{k,n} B_0 \log_2(1 + \frac{u_{k,n} g_{k,n}}{a_{k,n}\sigma^2})$ and $a_{k,n} B_0 \log_2(1 + \frac{u_{k,n} \hat{g}_{k,n}}{a_{k,n}\sigma^2})$ to be 0 when $a_{k,n} = 0$. To further explore the problem (4.12), we give the following proposition.

Proposition 4.2.2. *The optimization problem* (4.12) *given* m_k *is convex with respect to* $\mathbf{a_k}, \mathbf{u_k}$*, and* ξ*.*

Proof. *See Appendix B.2.*

With Proposition 4.2.2, the Lagrangian decomposition can be adopted and we have

$$
\begin{aligned}
&\mathcal{L}(\mathbf{a_k}, \mathbf{u_k}, \xi, \boldsymbol{\lambda}, \boldsymbol{\beta}, \boldsymbol{\gamma}, \boldsymbol{\nu}) \\
=&\xi + \sum_{n=1}^{N} \lambda_n (1 - \sum_{k=1}^{K} a_{k,n}) + \sum_{k=1}^{K} \beta_k (P_{k,max} - \sum_{n=1}^{N} u_{k,n}) \\
&+ \sum_{k=1}^{K} \gamma_k \big[R_k(\mathbf{a_k}, \mathbf{u_k}) - R_{k,req} \big] + \sum_{k=1}^{K} \nu_k \Big\{ R_k(\mathbf{a_k}, \mathbf{u_k}) \\
&- \epsilon_k^i P_{con,k}(\mathbf{u_k}) - \xi \Big\},
\end{aligned} \tag{4.13}
$$

where $\boldsymbol{\lambda}$, $\boldsymbol{\beta}$, $\boldsymbol{\gamma}$, $\boldsymbol{\nu}$ are the Lagrange multiplier vectors that $\boldsymbol{\lambda} = [\lambda_1, \ldots, \lambda_N]$, $\boldsymbol{\beta} = [\beta_1, \ldots, \beta_K]$, $\boldsymbol{\gamma} = [\gamma_1, \ldots, \gamma_K]$, and $\boldsymbol{\nu} = [\nu_1, \ldots, \nu_K]$ associated with constraints (4.12b), (4.12c), (4.12e), and (4.12f). The Lagrangian dual problem of (4.12) is accordingly

$$
\begin{aligned}
&\min_{\{\boldsymbol{\lambda}, \boldsymbol{\beta}, \boldsymbol{\gamma}, \boldsymbol{\nu}\}} \max_{\{\mathbf{a_k}, \mathbf{u_k}, \xi\}} \mathcal{L}(\mathbf{a_k}, \mathbf{u_k}, \xi, \boldsymbol{\lambda}, \boldsymbol{\beta}, \boldsymbol{\gamma}, \boldsymbol{\nu}) \\
&\quad s.t.: \quad \text{(4.12a), (4.12d),} \\
&\qquad\quad \text{C8:} \quad \boldsymbol{\lambda}, \boldsymbol{\beta}, \boldsymbol{\gamma}, \boldsymbol{\nu} \succeq 0.
\end{aligned} \tag{4.14}
$$

For the Lagrangian dual problem (4.14), we first solve primal resource allocation problem given fixed Lagrangian multipliers and then adopt the sub-gradient method to update Lagrangian multipliers.

Given the fixed Lagrangian multipliers, the concavity of (4.13) on $\{\mathbf{a_k}, \mathbf{u_k}\}$, constraint (4.12d), and *Karush-Kuhn-Tucker* (KKT) conditions, we differentiate (4.13) with respect to $u_{k,n}$ and obtain

$$
\frac{\partial \mathcal{L}(\mathbf{a_k}, \mathbf{u_k}, \xi, \boldsymbol{\lambda}, \boldsymbol{\beta}, \boldsymbol{\gamma}, \boldsymbol{\nu})}{\partial u_{k,n}} \begin{cases} \leq 0, & \text{if } u_{k,n}^* = 0, \forall k, n, \\ = 0, & \text{if } u_{k,n}^* > 0, \forall k, n, \end{cases} \tag{4.15}
$$

where $u^*_{k,n}$ is the optimal value of $u_{k,n}$. By solving (4.15), we obtain the optimal power allocation, $P^*_{k,n}$, as

$$\begin{aligned} P^*_{k,n} &= \frac{u^*_{k,n}}{a_{k,n}} \\ &= \begin{cases} \left[\frac{B_0(\gamma_k+\nu_k)}{\ln 2(\beta_k+\nu_k\epsilon^i_k)} - \frac{\sigma^2}{g_{k,n}}\right]^+, & \text{if } m_k = 0, \\ \left[\frac{B_0(\gamma_k+\nu_k)}{2\ln 2(\beta_k+\frac{1}{2}\nu_k\epsilon^i_k+\frac{1}{2}\nu_k\epsilon^i_k\frac{\hat{g}_{k,n}}{\bar{g}_{k,n}})} - \frac{\sigma^2}{\hat{g}_{k,n}}\right]^+, & \text{if } m_k = 1, \end{cases} \end{aligned} \tag{4.16}$$

where $[x]^+ = \max\{0, x\}$. Similarly, considering the concavity of (4.13), constraint (4.12a), and KKT conditions, we have

$$\frac{\partial \mathcal{L}(\mathbf{a_k}, \mathbf{u_k}, \xi, \boldsymbol{\lambda}, \boldsymbol{\beta}, \boldsymbol{\gamma}, \boldsymbol{\nu})}{\partial a_{k,n}} \begin{cases} < 0, & \text{if } a^*_{k,n} = 0, \forall k, n, \\ = 0, & \text{if } 0 < a^*_{k,n} < 1, \forall k, n, \\ > 0, & \text{if } a^*_{k,n} = 1, \forall k, n, \end{cases} \tag{4.17}$$

where $a^*_{k,n}$ is the optimal value of $a_{k,n}$.

By solving (4.17), we obtain $a^*_{k,n}$ as

$$a^*_{k,n} = \begin{cases} 0, & \text{if } A_{k,n} < \lambda_n, \forall k, n, \\ 1, & \text{if } A_{k,n} > \lambda_n, \forall k, n, \end{cases} \tag{4.18}$$

where

$$A_{k,n} = \begin{cases} B_0(\gamma_k+\nu_k)\log_2\left(1+\frac{P^*_{k,n}g_{k,n}}{\sigma^2}\right) & \\ -(\beta_k+\nu_k\epsilon^i_k)P^*_{k,n}, & \text{if } m_k=0, \\ \frac{B_0(\gamma_k+\nu_k)}{2}\log_2\left(1+\frac{P^*_{k,n}\hat{g}_{k,n}}{\sigma^2}\right) & \\ -\left[\beta_k P^*_{k,n}+\frac{\nu_k\epsilon^i_k}{2}(P^*_{k,n}+P_{0,n})\right], & \text{if } m_k=1. \end{cases}$$

According to (4.19), as long as $A_{k,n}$ is larger than the Lagrangian multiplier λ_n for user pair k over subcarrier n, subcarrier n will be assigned to user pair k. Therefore, it is necessary to carefully choose a suitable value of λ_n to make sure that at most one user can access subcarrier n. However, since λ_n is predefined and $A_{k,n}$ varies in every update, it is difficult to set λ_n to be always smaller than only the largest $A_{k,n}$. Observing that λ_n is not related to the power allocation and mode selection, we assign positive constant values to $\boldsymbol{\lambda}$ and allocate subcarrier n to user pair k^* such that $k^* = \arg\max_{k\in\{\mathcal{K}_1,\mathcal{K}_2\}} A_{k,n}$ to guarantee that one subcarrier will not be occupied by multiple user pairs.

Given (4.13), $\mathbf{a}^*_\mathbf{k}$, and $\mathbf{u}^*_\mathbf{k}$, we have

$$\max\left(1-\sum_{k=1}^{K}\nu_k\right)\xi \tag{4.19}$$
$$s.t.: \quad 0 \le \xi \le R_k(\mathbf{a}^*_\mathbf{k},\mathbf{u}^*_\mathbf{k}) - \epsilon^i_k P_{con,k}(\mathbf{u}^*_\mathbf{k}), \forall k.$$

The optimal ξ^* is

$$\xi^* = \begin{cases} 0, & \text{if } \sum_{k=1}^{K}\nu_k > 1, \\ \min_k\{R_k(\mathbf{a}^*_\mathbf{k},\mathbf{u}^*_\mathbf{k}) - \epsilon^i_k P_{con,k}(\mathbf{u}^*_\mathbf{k})\}, & \text{if } \sum_{k=1}^{K}\nu_k \le 1. \end{cases}$$

Once we have the solution with fixed Lagrangian multipliers, we can use sub-gradient

method to iteratively update the Lagrangian multipliers.

According to [49], the sub-gradients of $\boldsymbol{\beta}$,$\boldsymbol{\gamma}$,$\boldsymbol{\nu}$ are

$$\nabla\beta_k = P_{k,max} - \sum_{n=1}^{N} u_{k,n}^*, \tag{4.20}$$

$$\nabla\gamma_k = R_k(\mathbf{a_k^*}, \mathbf{u_k^*}, m_k) - R_{k,req}, \tag{4.21}$$

$$\nabla\nu_k = \left(R_k(\mathbf{a_k^*}, \mathbf{u_k^*}) - \epsilon_k^i P_{con,k}(\mathbf{u_k^*})\right) - \xi. \tag{4.22}$$

With the sub-gradients in (4.20), (4.21), and (4.22), we can update the Lagrangian multipliers by

$$\beta_k(i+1) = [\beta_k(i) - \triangle\beta(i)\nabla\beta_k(i)]^+, \tag{4.23}$$

$$\gamma_k(i+1) = [\gamma_k(i) - \triangle\gamma(i)\nabla\gamma_k(i)]^+, \tag{4.24}$$

$$\nu_k(i+1) = [\nu_k(i) - \triangle\nu(i)\nabla\nu_k(i)]^+, \tag{4.25}$$

where i is the iteration index and $\triangle\beta(i), \triangle\gamma(i), \triangle\nu(i)$ are small steps for the update.

Mode Selection for LDB Method

In the outer loop, the mode is determined for each individual user pair. The most straightforward way to find out the optimal modes is that we directly search over all possible cases. In Algorithm 5, we set a mode selection pattern, Ψ, which determines all the values of m_k at the controller. For example, we first initialize $\Psi^{(0)}$ that $m_k = 0$, $\forall k$. Then we switch to another mode selection pattern, i.e., $\Psi^{(1)}$ that $m_k = 1$ for a certain D2D user and $m_k = 0$ for the rest $K_d - 1$ users. Note that, for K_c cellular users, m_k is always 0. By searching over 2^{K_d} patterns, we can obtain the final solution to problem (4.10). The entire procedure of the LDB method is summarized in Algorithm 5.

In the proposed LDB method, it is necessary to search over all 2^{K_d} cases to obtain the solution to the max-min problem. The computational complexity increases exponentially with the number of the user pairs in D2D mode. Besides, the subcarrier allocation requires

Algorithm 5 LDB Method

Initialization: Set initial values for $\{\boldsymbol{\lambda}, \boldsymbol{\beta}, \boldsymbol{\gamma}, \boldsymbol{\nu}\}$, maximum number of iterations i_{max}, $\triangle\boldsymbol{\beta}$, $\triangle\gamma$, $\triangle\nu$, and tolerance ε'. Set $i = 0$.
For all Ψ
  While$(i < i_{max})$
    Solve for optimal power, $\mathbf{P}^*_{\mathbf{k}}$, for each user according to (4.16).
    Calculate $A_{k,n}$ according to (4.19) for each subcarrier and each user. Assign subcarrier n to user k^* that $k^* = \arg \max_{k \in \{\mathcal{K}_1, \mathcal{K}_2\}} A_{k,n}, \forall n$ and record corresponding optimal allocation $\mathbf{a}^*_{\mathbf{k}}$.
    Update $\boldsymbol{\beta}$, $\boldsymbol{\gamma}$, and $\boldsymbol{\nu}$ from (4.23), (4.24), and (4.25), respectively.
    $i = i + 1$.
    If $\|\boldsymbol{\beta}(i) - \boldsymbol{\beta}(i-1)\|_2 < \varepsilon'$, $\|\boldsymbol{\gamma}(i) - \boldsymbol{\gamma}(i-1)\|_2 < \varepsilon'$, and $\|\boldsymbol{\nu}(i) - \boldsymbol{\nu}(i-1)\|_2 < \varepsilon'$
      Break.
  End while
  Record $k_\Psi = \arg\min_k \{R_k(\mathbf{a}^*_{\mathbf{k}}, \mathbf{P}^*_{\mathbf{k}}, m^*_k) - \epsilon^i_k P_{con,k}(\mathbf{a}^*_{\mathbf{k}}, \mathbf{P}^*_{\mathbf{k}}, m^*_k)\}$ and $\{\mathbf{a}^*_{\mathbf{k}_\Psi}, \mathbf{P}^*_{\mathbf{k}_\Psi}, m^*_{k_\Psi}\}$.
End for
Choose the best mode selection pattern Ψ^* that $\Psi^* = \arg\max_\Psi \{R_{k_\Psi}(\mathbf{a}^*_{\mathbf{k}_\Psi}, \mathbf{P}^*_{\mathbf{k}_\Psi}, m^*_{k_\Psi}) - \epsilon^i_{k_\Psi} P_{con,k_\Psi}(\mathbf{a}^*_{\mathbf{k}_\Psi}, \mathbf{P}^*_{\mathbf{k}_\Psi}, m^*_{k_\Psi})\}$ and $\mathbf{a}^*_{\mathbf{k}_{\Psi^*}}, \mathbf{P}^*_{\mathbf{k}_{\Psi^*}}, m^*_{k_{\Psi^*}}$.
End

that the base station, as a central controller, knows each user pair's channel state information over all subcarriers. Since the user pairs in D2D mode have no direct links to the base station, the channel state information between the user pairs in D2D mode has to be frequently reported to the base station, which can cause delays and overhead. Therefore, for large-scale networks and practical implementation, the computational complexity and the overhead for information exchange need to be reduced.

LCD Method

Mode Selection for LCD Method

Since the D2D mode provides the reuse gain, hop gain, and proximity gain [50], every D2D user pair chooses the D2D mode to communicate if possible in mode selection. Different from the distance-based criterion [42], we derive a criterion based on the *channel to noise ratio* (CNR).

Because mode selection occurs before subcarrier assignment, we adopt the average CNR, which describes the overall channel quality. Specifically, $\tau_k = \frac{\sum_{n=1}^{N} g_{k,n}}{N\sigma^2}$ is the average CNR of D2D user pair k. The user pair selects D2D mode if $\tau_k \geq \tau_{th}$ and cellular mode

otherwise, where τ_{th} is the minimum average CNR required for D2D mode.

Subcarrier Assignment for LCD Method

In the proposed subcarrier assignment scheme, the base station, as a controller, assigns subcarriers to user pairs according to their selected modes. Equal power allocation to every subcarrier is assumed.

Define $\bar{R}_{k,n}$ and $\bar{P}_{k,n}$ as

$$\bar{R}_{k,n} = B_0 \log_2(1 + \frac{\hat{g}_{k,n} P_{k,max}}{N\sigma^2}) \tag{4.26}$$

and

$$\bar{P}_{k,n} = (1 + \frac{\hat{g}_{k,n}}{\check{g}_{k,n}}) \frac{P_{k,max}}{N}. \tag{4.27}$$

The energy efficiency achieved by equal power allocation over subcarrier n for user pair k is $\bar{\epsilon}_{k,n} = \frac{\bar{R}_{k,n}}{\bar{P}_{k,n}}$.

Since the user pairs in D2D mode have shorter distance between their transmitters and receivers than the user pairs in cellular mode, the user pairs in D2D mode are very likely to suffer less path loss. Denote d_{dm} as the distance between the transmitter and receiver of a user pair in D2D mode and d_{cm} as the distance between the transmitter and receiver of a user pair in cellular mode. Let α be the path loss exponent. We have the following proposition.

Proposition 4.2.3. *The probability of the channel gain of a user pair in D2D mode being larger than the channel gain of a user pair in cellular mode is greater than q when $d_{cm} > (\frac{q}{1-q})^{\frac{1}{\alpha}} d_{dm}$.*

Proof. *See Appendix B.3.*

Assuming a practical parameter $\alpha = 4$, we have the channel gain of the user pair in D2D mode larger than that of the user pair in cellular mode with a probability 98.8% when $d_{cm} > 3dm$. In practice, d_{cm} is usually a few hundred meters while d_{dm} is less than 100

meters. The ratio between d_{cm} and d_{dm} is larger than 3 and thus the probability is larger than 98.8%. Therefore, priority is given to the user pairs in cellular mode in the proposed subcarrier assignment to achieve a probabilistic fairness.

Algorithm 6 Subcarrier Assignment

Initialization: $\mathcal{N} = \{1,2,\ldots,\mathrm{N}\}$, $\mathcal{N}_{req} = \emptyset$, $\mathcal{N}_k = \emptyset$, $\mathcal{N}_u = \mathcal{N}$, $\mathcal{K}_1$, $\mathcal{K}_2$, $R_{req,k}$, and P_k^{max}.
Repeat (QoS-guarantee subcarrier assignment)
  Find $k^* = \arg\min_{k\in\mathcal{K}_2} R_k^*$.
  If $R_k^* \geq R_{req,k^*}$
    Break.
  Else
    Find $n_{k^*}^* = \arg\max_{n\in\mathcal{N}_u} \check{g}_{k,n}$. $\mathcal{N}_{k^*} = \mathcal{N}_{k^*} \bigcup \{n_{k^*}^*\}$, $\mathcal{N}_{req} = \mathcal{N}_{req} \bigcup \{n_{k^*}^*\}$, and $\mathcal{N}_u = \mathcal{N}_u \setminus \{n_{k^*}^*\}$.
Until $|\mathcal{N}_u| = |\mathcal{K}_1|$
Repeat (Energy-efficient subcarrier assignment)
  Find $\hat{k} = \arg\min_{k\in\mathcal{K}_2} R_k / P_{con,k}$.
  Find $n_{\hat{k}}^* = \arg\max_{n\in\mathcal{N}_u} \bar{R}_{\hat{k},n} / \bar{P}_{\hat{k},n}$.
  If $(R_{\hat{k}} + \frac{1}{2}\bar{R}_{\hat{k},n_{\hat{k}}^*}) / (P_{con,\hat{k}} + \frac{1}{2}\bar{P}_{\hat{k},n_{\hat{k}}^*}) > R_{\hat{k}} / P_{con,\hat{k}}$.
    $\mathcal{N}_u = \mathcal{N}_u \setminus \{n_{\hat{k}}^*\}, \mathcal{N}_{\hat{k}} = \mathcal{N}_{\hat{k}} \bigcup \{n_{\hat{k}}^*\}$.
  Else
    Break.
Until $|\mathcal{N}_u| = |\mathcal{K}_1|$
Randomly divide $\mathcal{N}_u$ into $|\mathcal{K}_1|$ sets and assign to each user in $\mathcal{K}_1$.
End

The subcarriers are firstly assigned to the user pairs in cellular mode to satisfy the QoS requirements. To ensure that each user pair in D2D mode is assigned one or more subcarriers, the minimum number of unassigned subcarriers is equal to the number of the user pairs in D2D mode. After QoS-guarantee subcarrier assignment, the subcarriers are assigned to achieve better energy efficiency. Different from the algorithm in [49] that assigns the subcarrier to the worst-case user pair with the best channel gain, $\hat{g}_{k,n}$, our algorithm then assigns the subcarrier that has the largest energy efficiency, $\bar{\epsilon}_{k,n}$, to the worst-case user pair in cellular mode. This is because for user pair k in cellular mode, not only $\hat{g}_{k,n}$ but also the ratio between $\hat{g}_{k,n}$ and $\check{g}_{k,n}$ affects the energy efficiency. Finally, the base station assigns the rest of the subcarriers to the user pairs in D2D mode in a random manner.

Since there is no links set up for data transmission between the base station and user pairs in D2D mode, the random manner can avoid huge information exchange between the base station and user pairs in D2D mode for D2D direct links.

Denote $\mathcal{N}, \mathcal{N}_{req}, \mathcal{N}_k$, and $\mathcal{N}_u$ as the entire subcarrier set, the set of subcarriers assigned to satisfy the QoS requirement of the user pairs in cellular mode, the subcarrier set of the k-th user, and the unassigned subcarrier set, respectively. The subcarrier assignment procedure is described in Algorithm 6.

Power Allocation with QoS Constraint for LCD Method

Once mode selection and subcarrier assignment are determined, problem (4.8) can be simplified as

$$\max_{\mathbf{P_k}} \quad \frac{\sum_{n\in\mathcal{N}_k} B_0 \log_2(1+\frac{P_{k,n}g_{k,n}}{\sigma^2})}{\sum_{n\in\mathcal{N}_k} P_{k,n} + P_{cir,k}} \tag{4.28}$$

$$s.t.: \quad \hat{C}1: \quad P_{k,n} \geq 0, \forall n \in \mathcal{N}_k, \tag{4.28a}$$

$$\hat{C}2: \quad \sum_{n\in\mathcal{N}_k} P_{k,n} \leq P_{k,max}, \tag{4.28b}$$

$$\hat{C}3: \quad \sum_{n\in\mathcal{N}_k} B_0 \log_2(1+\frac{P_{k,n}g_{k,n}}{\sigma^2}) \geq R_{k,req} \tag{4.28c}$$

for $k \in \mathcal{K}_1$, and

$$\max_{\mathbf{P_k}} \quad \frac{\frac{1}{2}\sum_{n\in\mathcal{N}_k} B_0 \log_2(1+\frac{P_{k,n}\hat{g}_{k,n}}{\sigma^2})}{\frac{1}{2}\sum_{n\in\mathcal{N}_k}(1+\frac{\hat{g}_{k,n}}{\check{g}_{k,n}})P_{k,n} + P_{cir,0} + P_{cir,k}} \tag{4.29}$$

$$s.t.: \quad (4.28a), \quad (4.28b),$$

$$\hat{C}4: \quad \frac{1}{2}\sum_{n\in\mathcal{N}_k} B_0 \log_2(1+\frac{P_{k,n}\hat{g}_{k,n}}{\sigma^2}) \geq R_{k,req}$$

for $k \in \mathcal{K}_2$. Since (4.29) can be solved by the same methodology as (4.28), we only discuss our proposed power allocation scheme for (4.28).

Denote $P_{k,tot}$ as the total transmit power of user pair k, i.e., $P_{k,tot} = \sum_{n\in\mathcal{N}_k} P_{k,n}$.

Given $P_{k,tot}$ in (4.28), the denominator of the objective function in problem (4.28) is fixed. Moreover, $\max_{\mathbf{P_k}} \sum_{n\in\mathcal{N}_k} B_0 \log_2(1+\frac{P_{k,n}g_{k,n}}{\sigma^2})$ in (4.28) can be uniquely maximized by the waterfilling algorithm with given $P_{k,tot}$. Therefore, problem (4.28) is equivalent to an energy efficiency problem with respect to $P_{k,tot}$, which is

$$\epsilon_k(P_{k,tot}) = \max_{P_{k,tot}} \quad \frac{\hat{R}_k(P_{k,tot})}{P_{k,tot}+P_{cir,k}} \tag{4.30}$$

$$s.t.: \quad P_{k,tot} \le P_{k,max}, \tag{4.30a}$$

$$\hat{R}_k(P_{k,tot}) \ge R_{k,req}, \tag{4.30b}$$

where $\hat{R}_k(P_{k,tot})$ is the maximum data rate with respect to $P_{k,tot}$, which is

$$\hat{R}_k(P_{k,tot}) = \max_{\mathbf{P_k}} B_0 \log_2(1+\frac{g_{k,n}P_{k,n}}{\sigma^2}) \tag{4.31}$$

$$s.t.: \quad P_{k,n} \ge 0, \forall n,$$

$$\sum_{n\in\mathcal{N}_k} P_{k,n} = P_{k,tot}.$$

Denote $P^*_{k,tot}$ as the optimal total transmit power of user pair k for the objective function of problem (4.30), which can be obtained with Dinkelbach's method. We have the following proposition regarding $\epsilon_k(P_{k,tot})$ and $P_{k,tot}$.

Proposition 4.2.4. *When $P_{k,tot} < P^*_{k,tot}$, $\epsilon_k(P_{k,tot})$ is increasing as $P_{k,tot}$ increases. When $P_{k,tot} > P^*_{k,tot}$, $\epsilon_k(P_{k,tot})$ is decreasing as $P_{k,tot}$ increases.*

Proof. *See Appendix B.4.*

According to Proposition 4.2.4, we can classify the optimal solution to (4.30) into 4 cases that are illustrated in Fig. 4.2.

With different channel gains, $P^*_{k,tot}$ for optimal energy efficiency could be within $P_{k,max}$ and out of $P_{k,max}$ represented by energy efficiency scenario 1 and scenario 2, respectively. When $P^*_{k,tot} < P_{k,max}$, the data rate at $P^*_{k,tot}$ could satisfy QoS requirement or not, which are

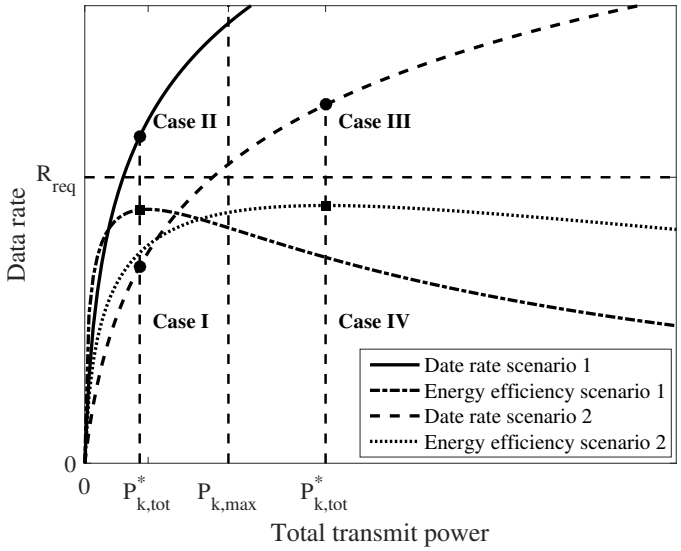

Figure 4.2. Illustration of throughput and energy efficiency versus user total transmit power.

represented by data rate scenario 1 and scenario 2. Note that the data rate at $P_{k,tot}^*$ must satisfy the QoS requirement when $P_{k,tot}^* \geq P_{k,max}$; otherwise there is no feasible solution. According to different combinations of energy efficiency and data rate scenarios, we have 4 different cases. The solutions are analyzed as follows.

We assume that with the maximum transmit power, $P_{k,max}$, the QoS requirement can be satisfied. Otherwise, there is no feasible solution. The solutions are analyzed as follows.

- **Case I:**

When $P_{k,tot}^* < P_{k,max}$ and $\hat{R}_k(P_{k,tot}^*) < R_{k,req}$, which considers data rate scenario 2 and energy efficiency scenario 1 in Fig. 4.2, the data rate does not satisfy the QoS requirement when the optimal energy efficiency is achieved. To satisfy the QoS requirement, we need to increase $P_{k,tot}$. According to Proposition 4.2.4, with $P_{k,tot}$ increasing, the energy efficiency will decrease. Therefore, $P_{k,tot}$ should decrease as little as possible. Then the problem can

be simplified as

$$\min_{\mathbf{P_k}} \sum_{n\in\mathcal{N}_k} P_{k,n} \tag{4.32}$$
$$s.t.: \quad \sum_{n\in\mathcal{N}_k} B_0 \log_2(1+\frac{P_{k,n}g_{k,n}}{\sigma^2}) = R_{k,req}.$$

- **Case II:**

When $P^*_{k,tot} < P_{k,max}$ and $\hat{R}_k(P^*_{k,tot}) \geq R_{k,req}$, which considers data rate scenario 1 and energy efficiency scenario 1 in Fig. 4.2, both power and QoS constraints are satisfied with $\mathbf{P^*_k}$. Therefore, $\mathbf{P^*_k}$ is the solution.

- **Case III:**

When $P^*_{k,tot} > P_{k,max}$ and $\hat{R}_k(P^*_{k,tot}) \geq R_{k,req}$, which considers data rate scenario 2 and energy efficiency scenario 2 in Fig. 4.2, the optimal energy efficiency cannot be reached. Note that data rate scenario 1 and 2 are equivalent in this case since both have $\hat{R}_k(P^*_{k,tot}) \geq R_{k,req}$. To limit total transmit power within $P_{k,max}$ and consider Proposition 4.2.4, we can simplify the problem as

$$\max_{\mathbf{P_k}} \sum_{n\in\mathcal{N}_k} B_0 \log_2(1+\frac{P_{k,n}g_{k,n}}{\sigma^2}) \tag{4.33}$$
$$s.t.: \quad \sum_{n\in\mathcal{N}_k} P_{k,n} = P_{k,max}.$$

- **Case IV:**

When $P^*_{k,tot} > P_{k,max}$ and $\hat{R}_k(P^*_{k,tot}) < R_{k,req}$, there is no feasible solution since neither constraints can be guaranteed.

Therefore, the power allocation problem is transformed into three simple subproblems (4.30)-(4.33) that can be solved via standard convex optimization method.

Mode Switching for LCD Method

In mode selection, each user pair selects D2D mode if possible. Then resource allocation is calculated based on the result of mode selection. However, depending on channel conditions, cellular mode may benefit D2D user pairs more. Therefore, we consider a mode switching procedure.

In mode switching, we only consider the worst-case user pair because our objective is to maximize the minimum energy efficiency among all user pairs to guarantee the max-min fairness. Only when the worst-case user pair pre-selects D2D mode, mode switching will be executed. Otherwise, no mode switching is needed as the minimum average CNR required for D2D mode is not met. Therefore, in mode switching, the base station calculates the subcarrier and power allocation assuming that the worst-case user pair is in cellular mode. If the minimum energy efficiency increases, the user pair switches to cellular mode. Otherwise, it remains in D2D mode.

To avoid unnecessary recalculation of subcarrier and power allocation of the entire system, we derive a mode switching condition so that only the user pairs who satisfy the condition are allowed to switch mode. Denote $P_{k,tot}$ to be the total transmit power of user pair k. For user pair k with equal power allocation to every subcarrier, we have the following proposition.

Proposition 4.2.5. *A necessary condition for cellular mode to outperform D2D mode is*

$$\prod_{n=1}^{N}(1+\frac{P_{k,tot}}{N\sigma^2}\hat{g}_{k,n}) > \prod_{n=1}^{N}(1+\frac{P_{k,tot}}{N\sigma^2}g_{k,n}). \tag{4.34}$$

Proof. *See Appendix B.5.*

Note that the mode switching condition is based on equal power allocation and the average ratio between the channel gains, because both the subcarrier assignment and power allocation in the other mode is unknown when calculating the mode switching condition. The entire mode selection procedure is summarized in Algorithm 7.

Algorithm 7 Mode Switching

Initialization: Set $\mathcal{K}_1$ and $\mathcal{K}_2$ according to mode selection and ϱ_{th}.
Repeat
  Find $k^* = \arg\min_{k\in\mathcal{K}} \frac{R_k}{P_{con,k}}$ and record $\varepsilon_{min} = \frac{R_{k^*}}{P_{con,k^*}}$.
  If $k^* \in \mathcal{K}_1$
    Calculate $\prod_{n=1}^{N}(1 + \frac{P_{k^*,tot}}{N\sigma^2}\hat{g}_{k^*,n}), \prod_{n=1}^{N}(1 + \frac{P_{k^*,tot}}{N\sigma^2}g_{k^*,n})$, and ϱ_{k^*}.
    If (4.34) is satisfied
      Consider $k^* \in \mathcal{K}_2$.
      Do subcarrier assignment and power allocation.
      Find $\hat{k} = \arg\min_{k\in\mathcal{K}} \frac{R_k}{P_{con,k}}$.
      If $\frac{R_{\hat{k}}}{P_{con,\hat{k}}} \geq \varepsilon_{min}$
        $\mathcal{K}_1 = \mathcal{K}_1 \setminus \{k^*\}, \mathcal{K}_2 = \mathcal{K}_2 \bigcup \{k^*\}$.
      End if
    End if
  End if
Until no user switches mode

4.3 Numerical Results

In this section, we provide simulation results to evaluate the performance of our proposed methods. In our simulation, MATLAB is used to simulate the performance of our proposed methods. In our simulation setup, the locations of cellular users and D2D users' transmitters follow a Poisson point process, with a density of 16 users per cell [51]. Among the generated users, we randomly select K_c cellular users and K_d D2D users.

For each D2D user's transmitter, its corresponding receiver is randomly located with a probability of 50% within the direct D2D communications range and a probability of 50% out of the direct D2D communications range but within the AP coverage. The direct D2D communications range is 70 m and the radius of the AP coverage is 150 m [52]. The one-shot system topology for $K_c = 2, K_d = 6$ is shown in Fig. 4.3.

The total bandwidth is 1 MHz, the QoS data rate requirement for each user pair is 1 bit/s/Hz, the noise power density is -139 dBm/Hz, the path loss exponent of each D2D direct link is 4, and the path loss exponent of each link between a device and the AP is 3.76 [42]. The user static power consumption is 50 mW. We set the tolerance with

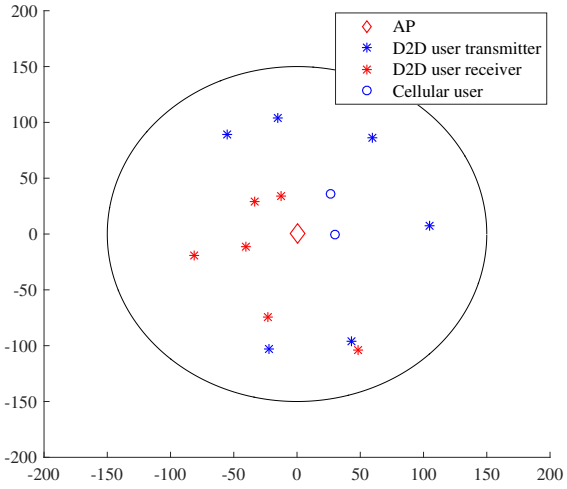

Figure 4.3. The one-shot system topology.

Table 4.1. Minimum User Energy Efficiency (bits/Hz/Joule) of Exhaustive Search and Proposed Sub-optimal Methods.

Scenario	ES	LDB	LCD
$K_d = 2,\ K_c = 2,\ \mathrm{N} = 4$	12.2531	10.4423	8.9564
$K_d = 1,\ K_c = 1,\ \mathrm{N} = 4$	23.8811	21.5656	19.2995

Dinkelbach's and Lagrangian methods to be 10^{-3} and 10^{-2}, respectively, and the step sizes $\triangle\beta(i), \triangle\gamma(i)$, and $\triangle\nu(i)$ to be $\frac{1}{i}$.

In Table 4.1, we illustrate the gaps of the minimum user energy efficiency between *exhaustive search* (ES) and two proposed sub-optimal methods. Since the complexity of exhaustive search increases exponentially with K and N, we set $K_d = 2, K_c = 2, N = 4$ and $K_d = 1, K_c = 1, N = 4$. The minimum user energy efficiency gap between the LDB method and exhaustive search is 1.8108 bits/Hz/Joule for $K_d = 2, K_c = 2$ and 2.3155 bits/Hz/Joule for $K_d = 1, K_c = 1$. The gap between exhaustive search and our LCD method is 3.2967 bits/Hz/Joule for $K_d = 2, K_c = 2$ and 4.5816 bits/Hz/Joule for $K_d = 1, K_c = 1$. However, the computational complexity reduces with the degradation of the energy efficiency performance.

In Fig. 4.4, we take two user pairs as examples to show the convergence of the proposed LDB method. It is obvious that all multipliers converge within 20 iterations. The fast

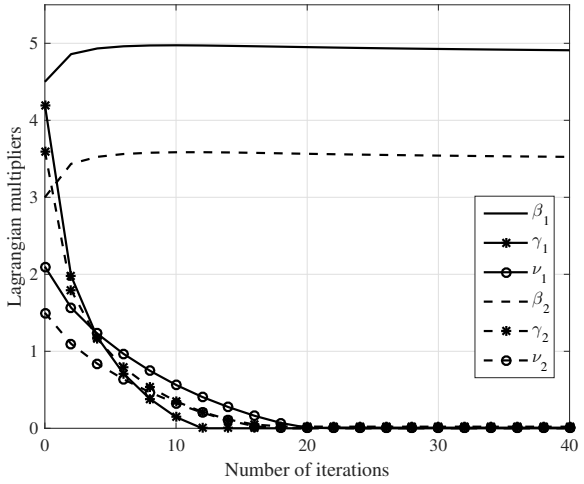

Figure 4.4. Convergence of the proposed LDB method for two different users when $P_{cir,0} = 0.5$ W and $P_{k,max} = 0.2$ W.

convergence illustrates the significant computational efficiency of the LDB in terms of subcarrier assignment in comparison with exhaustive search.

In Fig. 4.5, we consider two D2D pairs and two cellular users to illustrate the performance of different mode selection schemes. Without mode selection, no D2D mode is considered and D2D pairs use the AP as the relay in cellular mode. In this case, the energy efficiency is low due to the power consumption at the AP. In the distance-based mode selection scheme [42], a D2D pair selects D2D mode as long as the distance between the transmitter and receiver is within the discovery range. However, it is possible that the direct D2D links suffer blocking and shadowing and thus mode selection in our proposed LCD method improves the performance as shown in Fig. 4.5. If the user pair with the minimum energy efficiency selects D2D mode, the mode switching provides a chance for the user pair to switch to cellular mode with priority to improve its performance. Once the mode switching succeeds, the minimum user energy efficiency improves. When the number of subcarriers increases, more subcarriers are available for the user pairs with priority to choose, which improves the chance that the mode switching procedure succeeds. Note that the modes of user pairs are fixed once they are determined in the distance-based mode selection. Therefore, the more subcarriers, the better performance the proposed LCD method

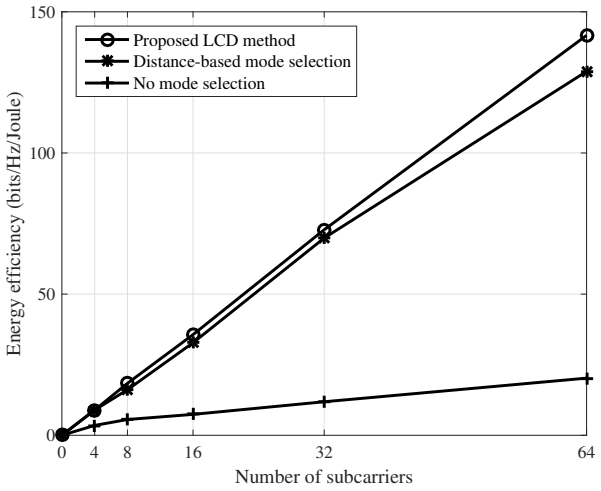

Figure 4.5. Comparison of the minimum user energy efficiency with different mode selection schemes when $P_{cir,0} = 0.5$ W, $P_{k,max} = 0.2$ W, and K = 4.

achieves in comparison with the distance-based mode selection.

In Fig. 4.6, we compare the performance of different subcarrier assignment algorithms. The proposed subcarrier assignment outperforms the max channel gain subcarrier assignment [49]. When the number of subcarriers increases, the minimum user energy efficiency increases for both algorithms. When the number of user pairs increases, the subcarriers for each user pair becomes scarce and thus the minimum user energy efficiency decreases.

In Fig. 4.7, the energy efficiency of the worst-case user, the best-case user, and the network is illustrated under four different methods. Among these methods, the *max-min energy efficiency* (MME) method [49] only considers the subcarrier and power allocation, the *iterative subcarrier and power allocation* (ISP) method [53] adopts an iterative way to allocate subcarriers and powers to guarantee the fairness, the *ascending ordered mode selection* (AOMS) method [52] sorts D2D users according to CSI in ascending order and provides higher priorities to the D2D users with worse channel conditions in selecting better modes to achieve fairness. Although all these methods focus on improving the fairness in energy efficiency, the proposed LCD method has the best worst-case user performance. This is mainly because the proposed LCD method jointly considers the mode selection, subcarrier assignment, and power allocation, while no mode selection is considered in MME

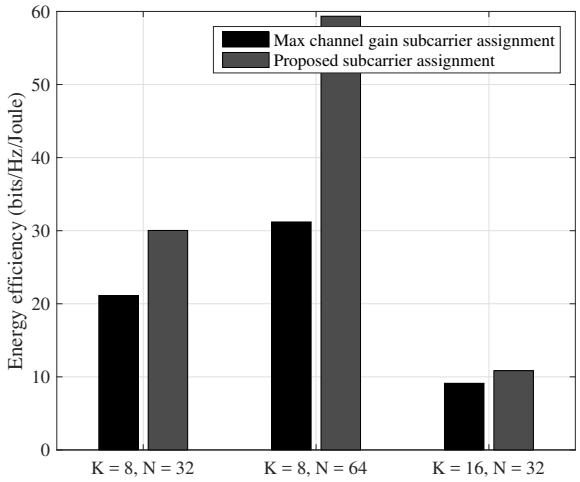

Figure 4.6. Comparison of the minimum user energy efficiency with different subcarrier assignment schemes when $P_{cir,0} = 0.5$ W and $P_{k,max} = 0.2$ W.

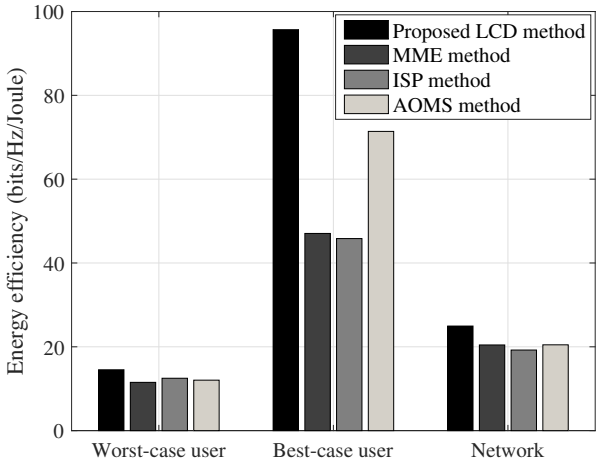

Figure 4.7. Comparison of energy efficiency performance with different methods when $P_{cir,0} = 0.5$ W and $P_{k,max} = 0.2$ W.

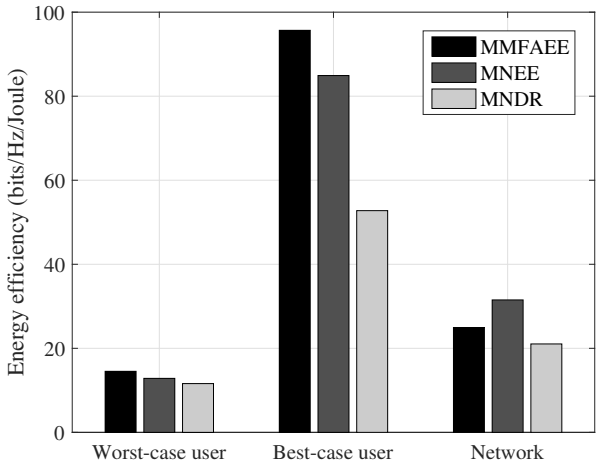

Figure 4.8. Comparison of energy efficiency performance under different metrics when $P_{cir,0} = 0.5$ W and $P_{k,max} = 0.2$ W.

and ISP methods and no subcarrier assignment is adopted in AOMS method.

In Fig. 4.8, the energy efficiency of the worst-case user, the best-case user, and the network is illustrated under three different optimization metrics, *max-min fairness-awareness energy efficiency* (MMFAEE), *max network energy efficiency* (MNEE) [54, 55], and *max network data rate* (MNDR). The MNEE method focuses on maximizing the energy efficiency of the entire system rather than that of each individual user. It can be seen that the proposed LCD method achieves the highest worst-case user energy efficiency for fairness. The MNEE method renders the best network energy efficiency performance by sacrificing the worst-case user energy efficiency. Since the MNDR method does not focus on improving energy efficiency, the user and network energy efficiency performance is sacrificed for higher data rates.

Chapter 5. Energy-Efficient Resource Allocation in SWIPT Cooperative Networks

Cooperative networks is an another effective way to improve the system performance in terms of energy efficiency and system reliability. However, the performance of cooperative networks is usually constrained by the limitations of conventional relay power supplies such as their locations. Recently, an emerging technique, SWIPT, enables receivers recycle parts of transmission power for their operations. SWIPT cooperative networks conquers the constraints for typical cooperative networks and developing an energy efficient resource allocation scheme in SWIPT networks can further improve energy efficiency.

In this chapter, energy-efficient resource allocation in SWIPT cooperative networks is studied. Two typical relay structures, *decode-and-forward* (DF) and *amplify-and-forward* (AF), are exploited for optimal relay selection and power allocation in cooperative networks with a power splitting SWIPT architecture. Non-convex energy efficiency optimization problems are formulated for both DF and AF relays. A decomposed relay selection and power allocation scheme is proposed without loss of optimality. Based on the *signal-to-noise ratios* (SNRs) at the destination, closed-form expressions of the optimal power splitting ratios are provided for DF and AF relays, respectively. With the optimal power splitting ratio and selected relay, a novel power allocation scheme is then proposed and illustrated based on the property of the simplified optimization problem with power and quality of service constraints. Numerical results demonstrate that the proposed resource allocation scheme achieves the maximum energy efficiency with low computational complexity, in which our relay selection outperforms typical relay selection schemes in terms of energy efficiency.

5.1 System Model and Problem Formulation

In this section, we present the adopted cooperative wireless network and power splitting SWIPT architecture, based on which we formulate the energy efficiency optimization problems for both the DF and AF relay types.

As shown in Figure 5.1, a cooperative wireless network with one source node, one

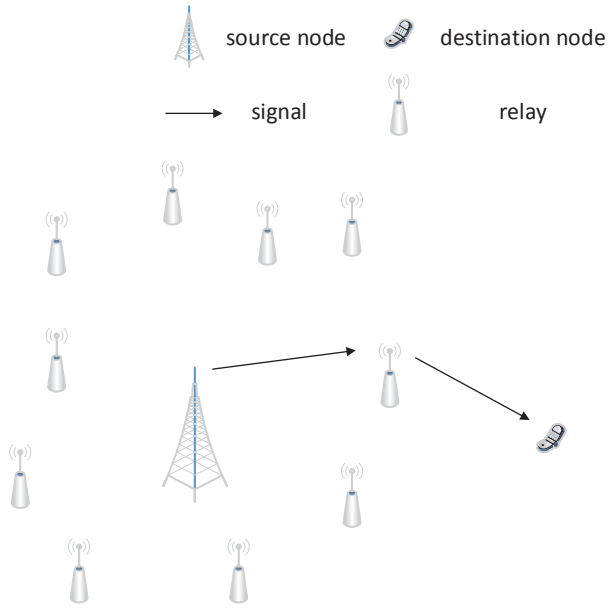

Figure 5.1. System model.

destination node, and M SWIPT relays is considered. All nodes and relays are each equipped with one antenna. We assume that no batteries are equipped to accumulate the transferred power, which provides more flexibility for the deployment of relays [56]. The super-capacitor is used for temporary power holding. We assume that the direct link between the source and destination nodes is blocked. The CSI of each link can be estimated through training symbols without error. For the links from the source node to the relays, called the first links, the energy transfer unit is activated when the training signals are transmitted from the source and the transferred power is used to process them, after which the obtained CSI is sent back to the source node. For the links from the relays to the destination node, the relays forward the training signals to the destination node, collect the CSIs from the destination node, and then report them back to the source node.

As illustrated in Figure 5.2, the SWIPT architecture adopts a power splitting structure, which provides a better tradeoff between the information rate and the amount of transferred power [57, 58]. With the power splitting structure, the i-th relay splits the received signal into two streams with a power splitting ratio ρ_i. Specifically, ρ_i of the received signal

power is used for power transfer and $(1-\rho_i)$ of the received signal power is used for information processing. An efficiency of η, $0 \leq \eta \leq 1$, for ρ_i of the transferred power is considered, which is determined by the SWIPT circuit. At the SWIPT relay, due to the power amplifier inefficiency, α of the effectively transferred power is used to forward the signal. Since SWIPT relays only work when signals are received and transferred, no static circuit power consumption at SWIPT relays is considered. At the source node, the power amplifier efficiency factor is ξ. Because the source node is always processing and exchanging data with the core network, a static power consumption P_c is taken into account.

We assume that the nodes and relays operate in a half-duplex manner, in which the source node transmits its signal in the first half slot and the selected SWIPT relay forwards the signal in the second half slot. We consider a strict delay constraint, under which the SWIPT relay has to receive and forward the signal to the destination node in the same slot. The duration of a slot is T. We assume that the transmission only occupies one frequency band during each time slot, which can avoid interference effectively. Subscripts s, r_i, and d denote the source node, the i-th relay, and the destination node, respectively.

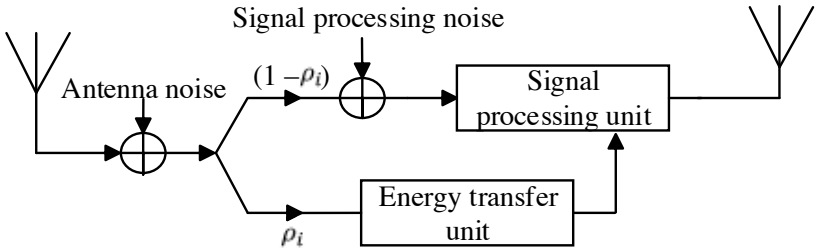

Figure 5.2. SWIPT relay architecture.

Let P_s and P_{r_i} be the transmit powers of the source node and the i-th relay, respectively. Denote l_{sr_i} and l_{r_id} as the distances between the source node to the i-th relay and between the i-th relay to the destination node, respectively. Let g_{s,r_i} be the channel coefficient from the source node to the i-th relay and $g_{r_i,d}$ be the channel coefficient from the i-th relay to the destination node, both of which are assumed Rayleigh fading. Antenna and signal

processing noises are modeled as *additive white Gaussian noise* (AWGN) with zero mean.

Signal Model and Problem Formulation for DF Relay

We first consider the DF relay type where the selected relay decodes the received signal then forwards the signal to the destination node. The received signal at the i-th DF relay, $y_{r_i}^{DF}$, is given by

$$y_{r_i}^{DF} = \sqrt{(1-\rho_i)P_s}\bar{g}_{sr_i}x_s + \sqrt{1-\rho_i}n_{r_i}^{[a]} + n_{r_i}^{[s]}, \tag{5.1}$$

where x_s is the transmitted signal from the source node, $n_{r_i}^{[a]}$ and $n_{r_i}^{[s]}$ are the antenna and signal processing noises at the i-th DF relay, respectively, and $\bar{g}_{sr_i} = \frac{g_{sr_i}}{\sqrt{l_{sr_i}^{\beta}}}$ denotes the equivalent channel coefficient from the source node to the i-th relay, where β is the path loss coefficient. Similarly, the received signal at the destination node in the DF relay case with the i-th relay, $y_{d_i}^{DF}$, is given by

$$y_{d_i}^{DF} = \sqrt{P_{r_i}}\bar{g}_{r_id}x_s + n_d^{[a]} + n_d^{[s]}, \tag{5.2}$$

where $\bar{g}_{r_id} = \frac{g_{r_id}}{\sqrt{l_{r_id}^{\beta}}}$ denotes the equivalent channel coefficient from the i-th DF relay to the destination node, $n_d^{[a]}$ is the antenna noise at the destination node, and $n_d^{[s]}$ is the signal processing noise at the destination node.

Since the antenna noise power is negligible in comparison with the signal processing noise power in practice [59, 60], we set both the signal processing noise powers at the i-th relay and destination node to be σ^2 and the antenna noise powers to be 0. Therefore, the SNR at the i-th relay, $\gamma_{r_i}^{DF}$, can be expressed as

$$\gamma_{r_i}^{DF} = \frac{(1-\rho_i)P_s|\bar{g}_{sr_i}|^2}{\sigma^2}, \tag{5.3}$$

where $|\cdot|$ is the absolute value operator, and the SNR at the destination node with the i-th relay, $\gamma_{d_i}^{DF}$, is

$$\gamma_{d_i}^{DF} = \frac{P_{r_i}|\bar{g}_{r_id}|^2}{\sigma^2}. \tag{5.4}$$

During the first half slot, the effectively transferred energy at the i-th relay, E_{r_i}, is

$$E_{r_i} = \eta \rho_i |\bar{g}_{sr_i}|^2 P_s \cdot \frac{T}{2}. \tag{5.5}$$

Because only α of the effectively transferred energy is used to transmit the signal in the second half slot, the transmit power of the i-th relay is

$$P_{r_i} = \frac{\alpha E_{r_i}}{T/2} = \alpha \eta \rho_i |\bar{g}_{sr_i}|^2 P_s. \tag{5.6}$$

After we substitute (5.6) into (5.4), the SNR at the destination node is expressed in terms of P_s as

$$\gamma_{d_i}^{DF} = \frac{\alpha \eta \rho_i |\bar{g}_{sr_i}|^2 P_s |\bar{g}_{r_i d}|^2}{\sigma^2}. \tag{5.7}$$

In DF relay networks, the achievable transmit rate with the i-th relay, R_i^{DF}, is [61]

$$R_i^{DF} = \frac{1}{2} \log_2 \left(1 + \min \left\{\gamma_{r_i}^{DF}, \gamma_{d_i}^{DF}\right\}\right). \tag{5.8}$$

Accordingly, the energy efficiency for DF relay networks with the i-th relay, ε_i^{DF}, is given by

$$\varepsilon_i^{DF} = \frac{R_i^{DF}}{\frac{1}{\xi} P_s + P_c}, \tag{5.9}$$

where $\frac{1}{\xi} P_s$ is the power consumption for signal transmission and P_c is the power consumption for the static circuit at the source node. Note that all the power consumption at the relay for cooperative transmission is compensated from the transferred power.

The energy efficiency optimization problem for DF relay networks can be formulated

as

$$\max_{i,P_s,\rho_i} \varepsilon_i^{DF} \tag{5.10}$$

$$s.t. \ : \quad \min\{\gamma_{r_i}^{DF}, \gamma_{d_i}^{DF}\} \geq \gamma_{th}, \forall i, \tag{5.10a}$$

$$0 \leq P_s \leq P_{max}, \tag{5.10b}$$

$$0 \leq \rho_i \leq 1, \forall i, \tag{5.10c}$$

where γ_{th} is the minimum SNR requirement to guarantee the *quality of service* (QoS) and P_{max} is the maximum transmit power of the source node.

Signal Model and Problem Formulation for AF Relay

In the AF relay case, the selected relay directly amplifies the received signal then forwards the signal to the destination node. The received signal at the i-th AF relay, $y_{r_i}^{AF}$, is given by

$$y_{r_i}^{AF} = \sqrt{(1-\rho_i)P_s}\bar{g}_{sr_i}x_s + \sqrt{1-\rho_i}n_{r_i}^{[a]} + n_{r_i}^{[s]}, \tag{5.11}$$

which is the same as in the DF relay case. The received signal at the destination node through the i-th relay, $y_{d_i}^{AF}$, is given by

$$y_{d_i}^{AF} = \sqrt{P_{r_i}}\bar{g}_{r_id}\frac{y_{r_i}^{AF}}{\sqrt{(1-\rho_i)P_s|\bar{g}_{sr_i}|^2+\sigma^2}} + n_d^{[a]} + n_d^{[s]}, \tag{5.12}$$

where $\sqrt{(1-\rho_i)P_s|\bar{g}_{sr_i}|^2+\sigma^2}$ is the normalizing factor to guarantee that the relay transmit power satisfies the power constraint. With the antenna noise neglected and some mathematical manipulation, $y_{d_i}^{AF}$ can be expressed as

$$y_{d_i}^{AF} = \frac{\sqrt{(1-\rho_i)P_sP_{r_i}}\bar{g}_{sr_i}\bar{g}_{r_id}x_s}{\sqrt{(1-\rho_i)P_s|\bar{g}_{sr_i}|^2+\sigma^2}} + \frac{\sqrt{P_{r_i}}\bar{g}_{r_id}n_{r_i}^{[s]}}{\sqrt{(1-\rho_i)P_s|\bar{g}_{sr_i}|^2+\sigma^2}} + n_d^{[s]}. \tag{5.13}$$

The first term in (5.13) is the desired signal and the rest two are noises. With (5.6), the SNR at the destination node in the AF relay case with the i-th relay, $\gamma_{d_i}^{AF}$, is

$$\begin{aligned}\gamma_{d_i}^{AF} &= \frac{\frac{(1-\rho_i)P_s P_{r_i}|\bar{g}_{sr_i}|^2|\bar{g}_{r_i d}|^2}{(1-\rho_i)P_s|\bar{g}_{sr_i}|^2+\sigma^2}}{\frac{P_{r_i}|\bar{g}_{r_i d}|^2\sigma^2}{(1-\rho_i)P_s|\bar{g}_{sr_i}|^2+\sigma^2}+\sigma^2} \\ &= \frac{\alpha\eta\rho_i(1-\rho_i)|\bar{g}_{sr_i}|^4|\bar{g}_{r_i d}|^2 P_s^2}{\alpha\eta\rho_i|\bar{g}_{sr_i}|^2|\bar{g}_{r_i d}|^2 P_s\sigma^2+(1-\rho_i)|\bar{g}_{sr_i}|^2 P_s\sigma^2+\sigma^4}. \end{aligned} \tag{5.14}$$

In AF relay networks, the achievable transmit rate with the i-th relay, R_i^{AF}, is

$$R_i^{AF} = \frac{1}{2}\log_2\left(1+\gamma_{d_i}^{AF}\right). \tag{5.15}$$

The energy efficiency for AF relay networks with the i-th relay, ε_i^{AF}, is expressed as

$$\varepsilon_i^{AF} = \frac{R_i^{AF}}{\frac{1}{\xi}P_s+P_c} \tag{5.16}$$

and the energy efficiency optimization problem for AF relay networks is formulated as

$$\max_{i,P_s,\rho_i} \varepsilon_i^{AF} \tag{5.17}$$

$$s.t.\ :\quad \gamma_{d_i}^{AF} \geq \gamma_{th}, \forall i, \tag{5.17a}$$

$$0 \leq P_s \leq P_{max}, \tag{5.17b}$$

$$0 \leq \rho_i \leq 1, \forall i. \tag{5.17c}$$

It is obvious that the energy efficiency optimization problems (5.10) and (5.17) are multi-variable and non-convex. Although the optimal solutions can be obtained through the computation of energy-efficient power allocation at each relay, the complexity is prohibitive in practice. Therefore, we analyze the problems and propose individual relay selection schemes and power allocation to simplify the problems. We first derive the optimal power splitting ratios. With different levels of CSI knowledge, we propose different relay selection

schemes for the DF and AF cases. Moreover, we efficiently solve the power allocation problems without iterative algorithms.

5.2 Proposed Resource Allocation

Resource Allocation for DF Relay

In this section, the energy efficiency optimization problem is simplified into relay selection and energy-efficient power allocation in the DF relay case. The corresponding relay selection scheme and power allocation method are derived and discussed.

To simplify the joint relay selection and power allocation problems, we have the following theorem in DF relay case.

Proposition 5.2.1. *or the joint SWIPT DF relay selection and power allocation problem* (5.10)*, the relay selection can be decoupled from the power allocation without loss of optimality. The maximum energy efficiency, ε^{DF*}, can be obtained at the i-th DF relay with the highest equivalent channel-to-noise ratio (CNR), $\zeta_i = \min\left\{\frac{(1-\rho_i)|\bar{g}_{sr_i}|^2}{\sigma^2}, \frac{\alpha\eta\rho_i|\bar{g}_{sr_i}|^2|\bar{g}_{r_id}|^2}{\sigma^2}\right\}$.*

Proof. *See Appendix C.1.*

With Proposition 5.2.1, the DF relay selection can be carried out without consideration of the power allocation, which simplifies the original problem (5.10). Designing the relay selection scheme based on the CNR is called the best CNR principle in this paper.

DF Relay Selection

In DF relay networks, according to (5.8) and the best equivalent CNR principle, the index of the selected relay is

$$i^* = \arg\max_i \{\zeta_i\} = \arg\max_i \{\min\{\zeta_{r_i}^{DF}, \zeta_d^{DF}\}\}, \tag{5.18}$$

where $\zeta_{r_i}^{DF} = \frac{(1-\rho_i)|\bar{g}_{sr_i}|^2}{\sigma^2}$ is the CNR at the i-th DF relay and $\zeta_{d_i}^{DF} = \frac{\alpha\eta\rho_i|\bar{g}_{sr_i}|^2|\bar{g}_{r_id}|^2}{\sigma^2}$ is the CNR at the destination through the i-th DF relay. Since the splitting ratio ρ_i influences the values of $\zeta_{r_i}^{DF}$ and $\zeta_{d_i}^{DF}$, the optimal splitting ratio ρ_i^* is determined according to the following proposition.

Proposition 5.2.2. *The optimal splitting ratio ρ_i^* for DF relay selection is obtained when $\zeta_{r_i}^{DF} = \zeta_{d_i}^{DF}$, which is $\rho_i^* = \frac{1}{1+\alpha\eta|\bar{g}_{r_i d}|^2}$.*

Proof. *See Appendix C.2.*

According to Proposition 5.2.2, the CNR at the i-th relay can be rewritten as

$$\zeta_{r_i}^{DF} = \frac{\alpha\eta}{\sigma^2} \frac{|\bar{g}_{sr_i}|^2 |\bar{g}_{r_i d}|^2}{1 + \alpha\eta|\bar{g}_{r_i d}|^2} \tag{5.19}$$

and the index of the selected DF relay is

$$i^* = \arg\max_i \{ \frac{|\bar{g}_{sr_i}|^2 |\bar{g}_{r_i d}|^2}{1 + \alpha\eta|\bar{g}_{r_i d}|^2} \}. \tag{5.20}$$

With full knowledge of CSI, the selected DF relay based on (5.20) is optimal, which is called *full CSI relay selection* (FRS).

Relay Selection with First Link CSI

Note that obtaining full knowledge of CSI involves huge overhead for periodic reporting, especially for the CSI of the second link. Therefore, we consider the DF relay selection with partial knowledge of CSI in the following to reduce overhead. Since there are direct links between the source node and relays, the first link CSI is easy to be collected at the source node. In such a case, only the first link CSI, i.e., $|g_{sr_i}|^2, \forall i$, with distance information is assumed to be known.

In practice, relays are commonly deployed and selected between the source and destination nodes. The distance l_{sr_i} and $l_{r_i d}$ are usually negatively correlated, which results in the negative correlation between $|g_{sr_i}|^2$ and $|g_{r_i d}|^2$. According to (5.19), the CNR, $\zeta_{r_i}^{DF}$, increases with the increasing $|g_{sr_i}|^2$ and $|g_{r_i d}|^2$. Therefore, when only $|g_{sr_i}|^2, \forall i$ is known, larger $|g_{sr_i}|^2$ or smaller $|g_{sr_i}|^2$ may both improve $\zeta_{r_i}^{DF}$. In such a case, how to select the best relay with only the information of $|g_{sr_i}|^2, \forall i$ needs to be analyzed.

Considering the distributions of $|g_{sr_i}|^2$, we analyze the expectation of CNR, based on which we derive the relay selection scheme for the case with partial knowledge of CSI.

In the Rayleigh fading channel model, when distance information is known, $|\bar{g}_{r_i d}|^2$ follows the exponential distribution with rate parameter $\lambda_1 = l_{sr_i}^{\beta}$. With the known $|\bar{g}_{sr_i}|^2$, we have the following proposition.

Proposition 5.2.3. *The expectation of the CNR at the i-th relay approximates*

$$\mathbb{E}[\zeta_{r_i}^{DF}] = \frac{\lambda_1 |\bar{g}_{sr_i}|^2}{(\lambda_1 + \alpha\eta)^2} + \frac{\alpha^2 \eta^2 |\bar{g}_{sr_i}|^2}{(\lambda_1 + \alpha\eta)^3}. \tag{5.21}$$

Proof. *See Appendix C.3.*

In (5.21), $\mathbb{E}[\cdot]$ is the expectation operator. Since $\mathbb{E}[\zeta_{r_i}^{DF}]$ is an increasing function of $|\bar{g}_{sr_i}|^2$. The maximum $|\bar{g}_{sr_i}|^2$ renders the best performance. Therefore, when $|\bar{g}_{sr_i}|^2$ is known, the index of the selected DF relay is

$$i^* = \arg\max_i \{|\bar{g}_{sr_i}|^2\}, \tag{5.22}$$

which is called the *first link relay selection* (FLRS).

Energy-efficient Power Allocation for DF Relay

With the selected DF relay i and corresponding optimal power splitting ratio, ρ_i^*, the energy efficiency optimization problem (5.10) is simplified as

$$\max_{P_s} \quad \varepsilon_i^{DF} = \frac{\frac{1}{2}\log_2(1 + \zeta_{r_i}^{DF} P_s)}{P_s + P_c} \tag{5.23}$$

$$s.t. \ : \quad \zeta_{r_i}^{DF} P_s \geq \gamma_{th}, \tag{5.23a}$$

$$0 \leq P_s \leq P_{max}. \tag{5.23b}$$

From (5.23), it is obvious that the problem is a fractional non-convex optimization problem. Even though the Dinkelbach's method [45] can be used to transform the fractional problem into a linear form, the number of iterations in the Dinkelbach's method can be large. Therefore, we derive a more straightforward *One-step Power Allocation* (OPA) method by analyzing the property of the problem.

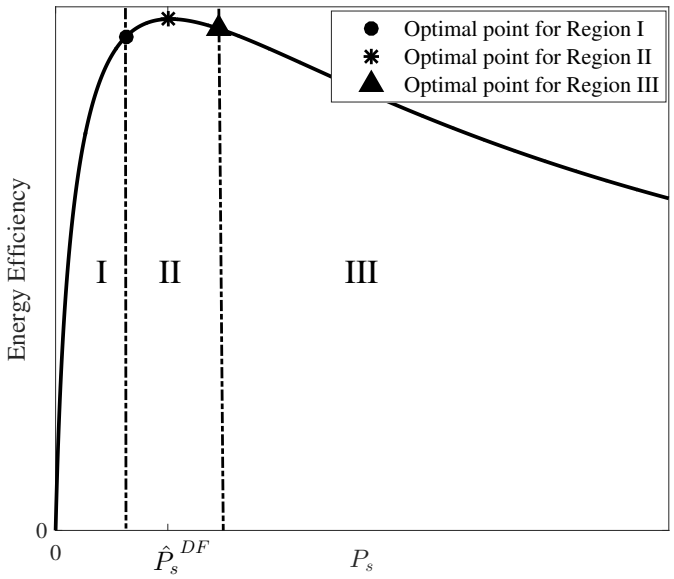

Figure 5.3. Energy efficiency versus transmit power within feasible regions I, II, and III.

We define P_{min} as the minimum transmit power to guarantee the QoS constraint in (5.23a), which is $P_{min} = \frac{\gamma_{th}}{\zeta_{r_i}^{DF}}$ in the DF relay case. Then we have the following proposition regarding the optimal solution to (5.23).

Proposition 5.2.4. *The objective function, ε_i^{DF}, with respect to (w.r.t.) the transmit power P_s^{DF}, is a unimodal function and there exists a unique global maximizer $\hat{P}_s^{DF}$, which is the solution to the following equation*

$$\frac{\zeta_{r_i}^{DF}(P_c + \hat{P}_s^{DF})}{1 + \zeta_{r_i}^{DF}\hat{P}_s^{DF}} = \ln\left(1 + \zeta_{r_i}^{DF}\hat{P}_s^{DF}\right). \tag{5.24}$$

Proof. *See Appendix C.4.*

Since P_{min} and P_{max} are the minimum and maximum allocated powers to satisfy the QoS requirement and transmit power constraint, respectively, the optimal transmit power in the feasible region $[P_{min}, P_{max}]$ is

$$P_s^* = \max\left\{P_{min}, \min\left\{P_{max}, \hat{P}_s^{DF}\right\}\right\}. \tag{5.25}$$

All possible cases are illustrated in Figure 4.4, in which $\hat{P}_s^{DF}$ is the solution to (5.24). If $P_{max} \leq \hat{P}_s^{DF}$, the feasible transmit power falls in Region I, in which ε_i^{DF} is strictly increasing and $P_s^* = P_{max}$ renders the maximum ε_i^{DF*}. If $P_{min} < \hat{P}_s^{DF} < P_{max}$, the feasible transmit power falls in Region II and the optimal transmit power P_s^* is equal to $\hat{P}_s^{DF}$ that renders the maximum ε_i^{DF*}. If $\hat{P}_s^{DF} \leq P_{min} < P_{max}$, the feasible transmit power falls in Region III, in which ε_i^{DF} is strictly decreasing and $P_s^* = P_{min}$ renders the maximum ε_i^{DF*}. Therefore, through OPA method, the optimal transmit power is obtained by (5.25).

Resource Allocation for AF Relay

In this section, the AF relay energy-efficient resource allocation problem is decomposed into relay selection and energy-efficient power allocation. The relay selection scheme and energy-efficient OPA method are derived and discussed.

According to Proposition 5.2.1, we similarly have Lemma 5.2.1 for the AF relay case as follows.

Lemma 5.2.1. *For the joint SWIPT AF relay selection and power allocation problem* (5.17)*, the relay selection can be decoupled from the power allocation without loss of optimality. The maximum energy efficiency, ε^{AF*}, can be obtained at the AF relay with the highest CNR.*

With Lemma 5.2.1, the AF relay selection can be carried out without consideration of the power allocation, which decomposes the original problem (5.17).

AF Relay Selection

Similar to the DF relay case, the AF relay selection scheme is also based on the best CNR principle. With no signal decoding process at the AF relay, the AF relay selection scheme is only based on the CNR at the destination, i.e.,

$$i^* = \arg\max_i \{\zeta_{d_i}^{AF}\}, \tag{5.26}$$

where $\zeta_{d_i}^{AF}$ is the CNR at the destination through the i-th AF relay, which is

$$\zeta_{d_i}^{AF} = \frac{\alpha\eta\rho_i(1-\rho_i)|\bar{g}_{sr_i}|^4|\bar{g}_{r_id}|^2P_s}{\alpha\eta\rho_i|\bar{g}_{sr_i}|^2|\bar{g}_{r_id}|^2P_s\sigma^2 + (1-\rho_i)|\bar{g}_{sr_i}|^2P_s\sigma^2 + \sigma^4}. \tag{5.27}$$

Given that $\sigma^2 \ll P_s$ in practice, (5.27) can be rewritten as

$$\zeta_{d_i}^{AF} = \frac{\alpha\eta\rho_i(1-\rho_i)|\bar{g}_{sr_i}|^2|\bar{g}_{r_id}|^2}{\alpha\eta\rho_i|\bar{g}_{r_id}|^2\sigma^2 + (1-\rho_i)\sigma^2}. \tag{5.28}$$

For (5.28), we have the following proposition.

Proposition 5.2.5. *The optimal splitting ratio ρ_i^* for AF relay selection is*

$$\rho_i^* = \frac{1}{1+\sqrt{\alpha\eta}|\bar{g}_{r_id}|}. \tag{5.29}$$

Proof. *See Appendix C.5.*

Substituting (5.29) into (5.28), we obtain the index of the selected AF relay as

$$i^* = \arg\max_i \{\frac{|\bar{g}_{sr_i}|^2|\bar{g}_{r_id}|^2}{(1+\sqrt{\alpha\eta}|\bar{g}_{r_id}|)^2}\}. \tag{5.30}$$

With full knowledge of CSI, the FRS of the AF relay case is optimal based on (5.30).

With partial knowledge of CSI, similar to the DF relay case, the FLRS of the AF relay case is

$$i^* = \arg\max_i \{|\bar{g}_{sr_i}|^2\} \tag{5.31}$$

when only $|\bar{g}_{sr_i}|^2$ is known.

Energy-efficient Power Allocation for AF Relay

With the selected AF relay i and corresponding optimal power splitting ratio ρ_i^*, the energy efficiency optimization problem for the AF relay case, similar to that of the DF

relay case, can be simplified as

$$\max_{P_s} \quad \varepsilon_i^{AF} = \frac{\frac{1}{2}\log_2(1+\zeta_{d_i}^{AF}P_s)}{P_s+P_c} \tag{5.32}$$

$$s.t. \; : \quad \zeta_{d_i}^{AF}P_s \geq \gamma_{th}, \forall i, \tag{5.23a}$$

$$0 \leq P_s \leq P_{max}. \tag{5.23b}$$

Therefore, the same methodology can be adopted to obtain the optimal transmit power, P_s^*, that is

$$P_s^* = \max\{P_{min}, \min\{P_{max}, \hat{P_s}^{AF}\}\}. \tag{5.33}$$

where $P_{min} = \frac{\gamma_{th}}{\zeta_{d_i}^{AF}}$ is the minimum transmit power in the AF relay case and $\hat{P_s}^{AF}$ is the solution to

$$\frac{\zeta_{d_i}^{AF}(P_c+\hat{P_s}^{AF})}{1+\zeta_{d_i}^{AF}\hat{P_s}^{AF}} = \ln(1+\zeta_{d_i}^{AF}\hat{P_s}^{AF}). \tag{5.34}$$

With the proposed AF relay selection scheme and energy-efficient OPA method, the optimal relay and transmit power for the best energy efficiency in AF relay networks can be obtained with low computational complexity.

5.3 Performance Analysis

In this section, we analyze and compare the performance of the SWIPT cooperative wireless networks with DF and AF relays. Besides, we extend the SWIPT cooperative wireless networks with DF or AF relays to a hybrid SWIPT cooperative wireless network with both DF and AF relays.

Performance Comparison

According to the derived closed-form expressions of the optimal power splitting ratios in Theorems 2 and 4 for DF and AF relays, respectively, the corresponding CNR expressions for DF and AF relays are

$$\zeta_{d_i}^{DF} = \frac{\alpha\eta}{\sigma^2}\frac{|\bar{g}_{sr_i}|^2|\bar{g}_{r_id}|^2}{1+\alpha\eta|\bar{g}_{r_id}|^2} \tag{5.35}$$

and

$$\zeta_{d_i}^{AF} = \frac{\alpha\eta}{\sigma^2} \frac{|\bar{g}_{sr_i}|^2 |\bar{g}_{r_i d}|^2}{(1 + \sqrt{\alpha\eta}|\bar{g}_{r_i d}|)^2}, \tag{5.36}$$

respectively.

From (5.35) and (5.36), it is obvious that the denominator of (5.36) is larger than that of (5.35), which is introduced by the amplified noise from the source node to the AF relay. Therefore, with the same power allocation, the AF relay renders lower energy efficiency performance than the DF relay. Besides, since only the transferred power is used for cooperative transmission at the selected relay in the proposed SWIPT cooperative wireless networks, the transferred power to forward the information is limited, which implies that the amplification of noise is also limited. Therefore, the performance difference between DF and AF relays is small. In comparison with DF relays, AF relays are preferred in SWIPT wireless networks because the performance difference of AF and DF relays is small but the structure of AF relays are much simpler than DF relays from practical perspective.

Hybrid SWIPT Cooperative Wireless Network Extension

In a hybrid SWIPT cooperative wireless network, both DF and AF relays exist. The relay selection between DF and AF relays cannot be determined through directly comparing their CNRs. To avoid calculating and comparing the energy efficiency with each relay, we can separate the SWIPT relays into DF and AF relay groups. In each group, we use the proposed resource allocation schemes to determine the best energy efficiency. Then, the resource allocation resulting in a better energy efficiency among the two is chosen as the optimal solution.

5.4 Numerical Results

In this section, we present simulation results to demonstrate the performance of the proposed schemes in a SWIPT cooperative network. The distance between the source and destination is 60 m. The SWIPT relays are randomly deployed following a homogeneous Poison point process [14] with intensity $\lambda = 0.0005/\text{m}^2$, which implies the average number of relays is 6 with a cell radius of 60 m. Rayleigh fading is used in the simulation. The

Table 5.1. Simulation Parameters.

Parameter	**Value**
Channel bandwitdth	10 kHz
Cell radius	60 m
Average number of relays	6 /cell
Portion coefficient α	0.9
Efficiency coefficient η	1
SINR threshold	0 dB

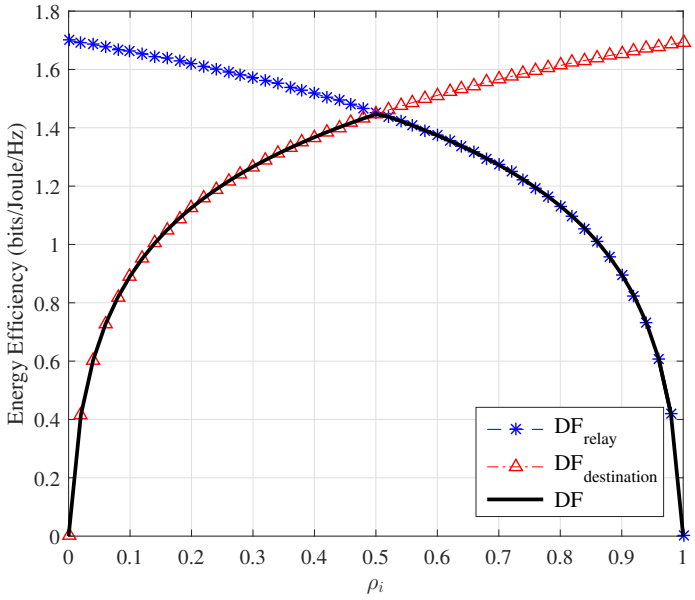

Figure 5.4. Energy efficiency vs. power splitting ratio ρ_i with DF relay case.

path loss model is $38.46 + 20 \log l$ dB [62]. The main simulation parameters are listed in Table 5.1.

In Fig. 5.4 and Fig. 5.5, the energy efficiency performance is illustrated with different power splitting ratios in both the DF and AF relay cases. Similarly to [56], to reveal the relationship between the energy efficiency and power splitting ratio clearly, parameters are normalized in this simulation and only the selected relay i is considered. Only in this simulation, the transmit power P_s is 1 W, the static circuit power P_c is 0.01 W, the distances l_{sr_i} and $l_{r_i d}$ are normalized to 1 m, and the noise power is scaled to be 0.01 W [56].

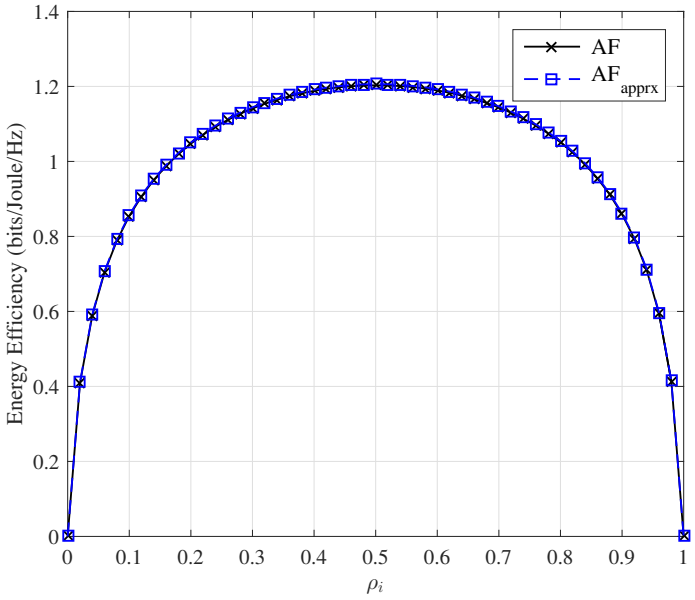

Figure 5.5. Energy efficiency vs. power splitting ratio ρ_i with AF relay case.

In Fig. 5.4, the energy efficiency performance in the DF relay case is determined by the minimum performance of the first link that is from the source node to the relay and the second link that is from the relay to the destination node, which is consistent with (5.8). From Fig. 5.5, it is obvious that the energy efficiency with the approximation of SNR in the proposed relay selection is nearly the same as that with the exact SNR in the AF relay case. Furthermore, since the means of channel fading gain of the first and the second links over 100 runs are 1.1032 and 0.9824, respectively, the optimal splitting ratios of DF and AF relays are 0.5044 and 0.5022, respectively, according to Theorems 2 and 4, which are verified in the figures.

In Fig. 5.6, the relationship between the energy efficiency and the distance between the source node and the selected relay i, l_{sr_i}, is shown. Since no direct link between the source node and the destination node is assumed, the relay is deployed with 15 m $\leq l_{sr_i} \leq$ 45 m in this simulation. As shown in Fig. 4.6, the network achieves the minimum energy efficiency when the selected relay is in the middle of the source node and the destination node. When the selected relay approaches towards the source node or the destination node,

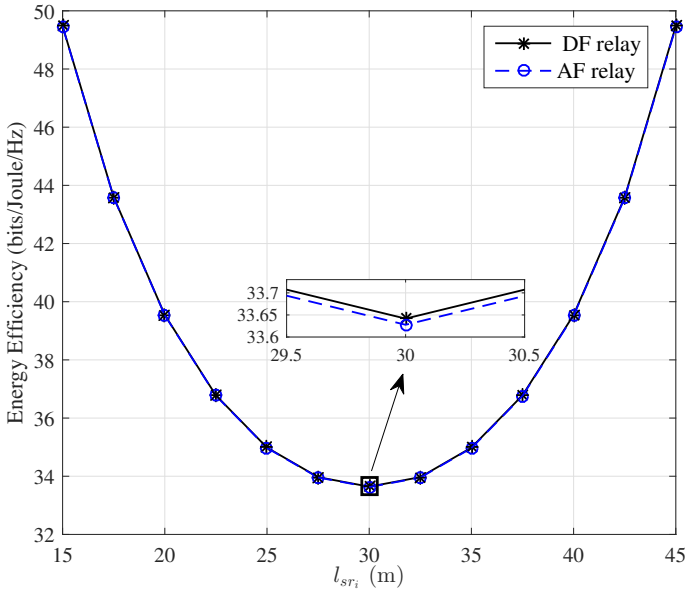

Figure 5.6. Energy efficiency vs. distance between the source node and the relay in both DF and AF relay cases, where P_c = 10 dBm, P_{max} = 46 dBm, and σ^2 = -125 dBm.

the energy efficiency of the network increases gradually. This is because when the selected relay is close to the source node, $|\bar{g}_{sr_i}|$ is larger than $|\bar{g}_{r_id}|$ and thus the CNR of the first link is larger than that of the second link. In this case, the power splitting ratio is adjusted towards 1 to transfer more power for the transmission of the second link. When the selected relay is close to the destination node, $|\bar{g}_{sr_i}|$ and the CNR of the first link are small. The power splitting ratio is adjusted towards 0 to increase the rate of the first link for the DF relay and reduce the power of the amplified noise for the AF relay. This phenomenon is similar to the throughput performance of the time splitting SWIPT relay networks in [63]. In Fig. 4.6, the energy efficiency in the DF relay case is slightly larger than that in the AF relay case, which is consistent with our analysis.

In Figure 5.7, the energy efficiency performance of different relay selection schemes is illustrated in both the DF and AF relay cases. It is obvious that the FRS is better than the FLRS and SLRS schemes in both cases. Before P_{max} reaches 9 dBm with full and partial knowledge of CSI, the energy efficiency remains 0, since the requirement on SNR

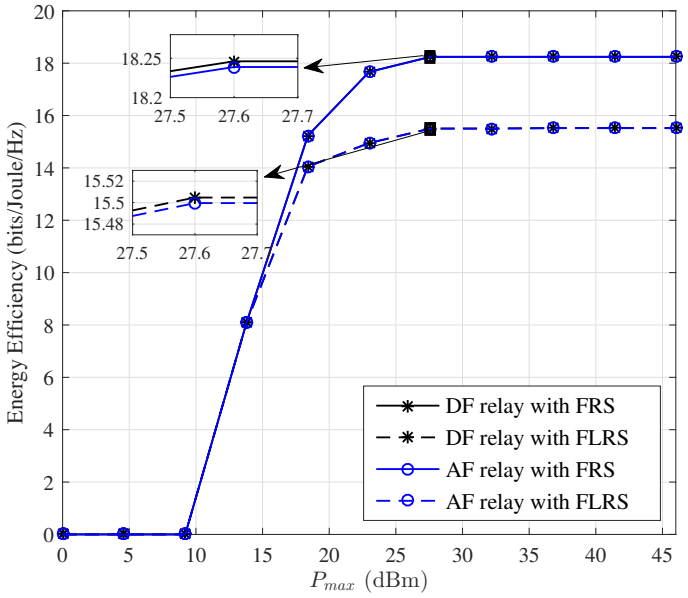

Figure 5.7. The energy efficiency performance of different relay selection schemes with full and partial knowledge of CSI, where P_c = 10 dBm and σ^2 = -125 dBm.

cannot be satisfied within the given P_{max}. After that, the energy efficiency increases with the increase of P_{max}. When P_{max} is larger than 27.6 dBm, the increase of P_{max} no longer provides energy efficiency benefit. As shown in Figure 5.7, the DF relay achieves better performance than the AF relay.

In Fig. 5.8, the energy efficiency of the proposed OPA method is compared with that of the data rate maximization (DRM) method that allocates powers to maximize the data rate and the Dinkelbach's method in the DF and AF relay cases with different relay selection schemes. The tolerance of the Dinkelbach's method is 10^{-3}. In Fig. 5.8, all the methods are shown to achieve the same energy efficiency, data rate, and power consumption when P_{max} is smaller than 15 dBm. In this case, the available power region for the proposed OPA method is Region I illustrated in Fig. 5.3, which results in P_{max} as the optimal power. Meanwhile, the DRM method also assigns P_{max} to achieve the maximum data rate. The Dinkelbach's method obtains the same performance through iterative calculations. When P_{max} keeps increasing, our proposed OPA method and the Dinkelbach's method still achieve the best energy efficiency but the energy efficiency of the DRM method decreases. This

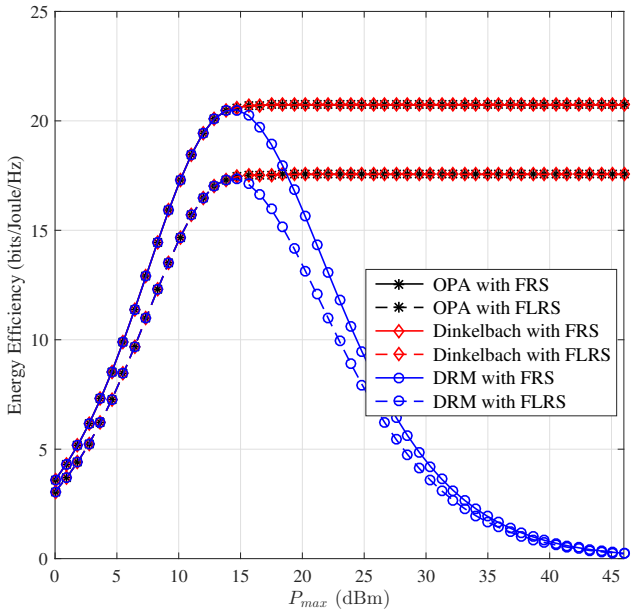

Figure 5.8. Energy efficiency versus maximum transmit power with different power allocation methods and relay selections, where P_c = 10 dBm and σ^2 = -125 dBm.

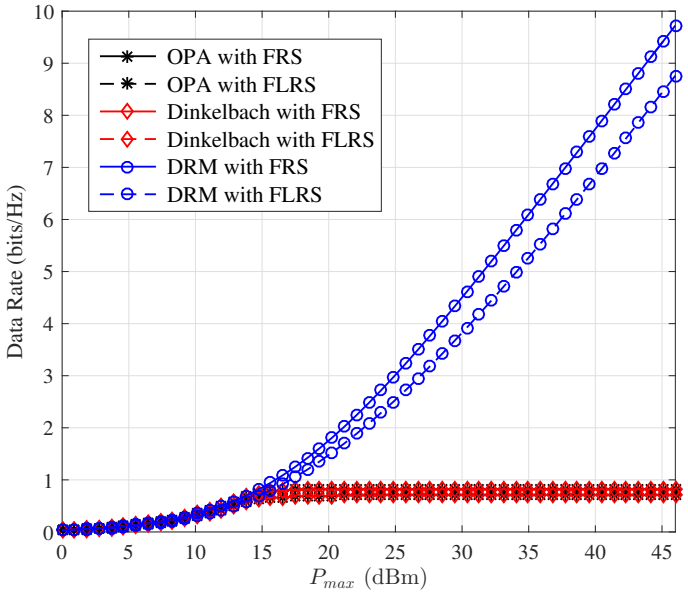

Figure 5.9. Data rate vs. maximum transmit power with different power allocation methods and relay selection schemes, where P_c = 10 dBm and σ^2 = -125 dBm.

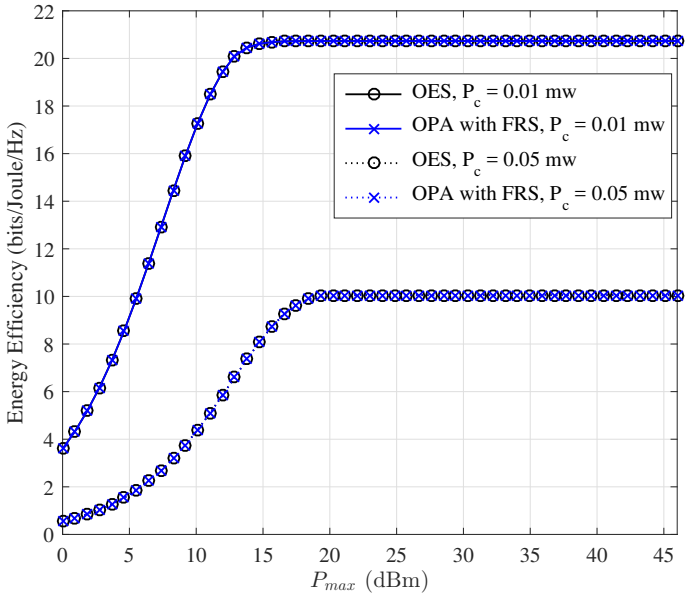

Figure 5.10. Comparison of OES and OPA with FRS, where σ^2 = -125 dBm.

is because that the proposed OPA method and the Dinkelbach's method keep the optimal power but the DRM power allocation method still adopts P_{max} that results in increasing data rate but decreasing energy efficiency, as shown in Fig. 5.8 and 5.9. Therefore, the DRM method deteriorates the energy efficiency of the network. As shown in Fig. 5.8, our proposed OPA method renders the same performance as the Dinkelbach's method without iterative calculations and outperforms DRM method.

In Fig. 5.10, the energy efficiency of the optimal exhaustive search (OES) and that of our proposed decomposed OPA with FRS scheme are compared. The OES scheme exhaustively calculates the energy efficiency with each SWIPT relay and choose the best result, which is the optimal solution to the formulated relay selection and power allocation problem. As shown in Fig. 5.10, when the full CSI is available, our proposed decomposed OPA with FRS scheme achieves the same performance as the optimal solution, which verifies the optimality of our scheme. With the different total static power consumptions of the source and destination nodes, the energy efficiency performance degrades with the increasing static power consumption, but the optimality of our proposed scheme still holds.

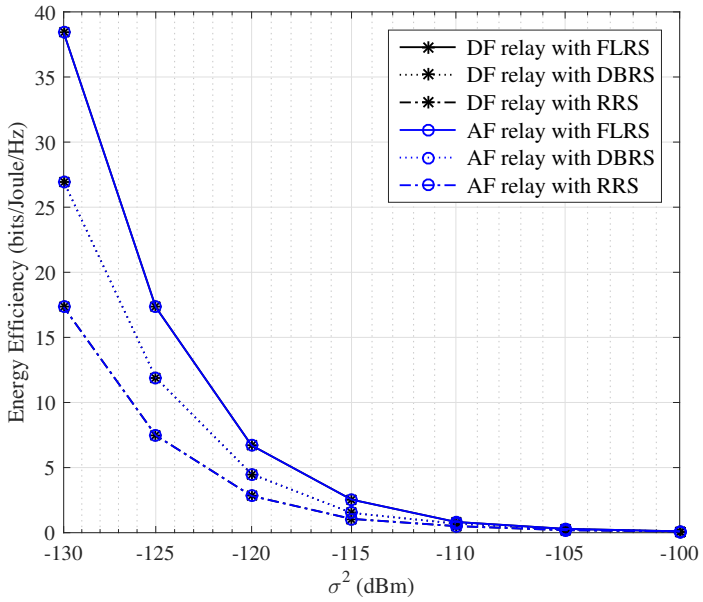

Figure 5.11. Energy efficiency with different relay selection schemes with partial knowledge of CSI, where $P_c = 10$ dBm and $P_{max} = 46$ dBm.

In Fig. 5.11, different relay selection schemes with partial knowledge of CSI are compared in the DF and AF relay cases. As shown in Fig. 5.11, the FLRS scheme renders better energy efficiency than the *distance based relay selection* (DBRS) that selects the relay with the shortest source to relay distance, and the *random relay selection* (RRS) that randomly selects the relay without any further information. The FLRS achieves the best energy efficiency performance and the RRS renders the lowest energy efficiency. Since only distance is considered, DBRS renders worse performance than the proposed FLRS scheme. As the noise power increases, all the relay selection schemes in both the DF and AF relay cases experience degraded energy efficiency performance.

Chapter 6. Conclusions

In this dissertation, we have focused on designing the spectrum- and energy-efficient resource allocation schemes in various modern wireless communication networks.

In Chapter 2, cascaded precoders combining precoding and power allocation are discussed to enhance the throughput of the two-tier heterogeneous networks. With the designed outer precoder, the cross-tier interference from SBSs to MUEs is eliminated. Meanwhile, an inner precoder is derived to improve the performance of the second tier, which allocates the powers of SBSs optimally. Moreover, an SBS selection algorithm is presented to reduce the computational complexity of the proposed scheme. The system performance under channel estimation is also discussed. Simulation results illustrate the effectiveness of the cascaded precoders.

In Chapter 3, mode selection, subcarrier assignment, and power allocation are jointly optimized to improve the individual energy efficiency in a D2D enabled network. Compared with the AP that centrally adjusts transmit powers among different users in traditional cellular networks, D2D pairs are more independent because each user can only use its own battery. Therefore, the individual energy efficiency with D2D communications is emphasized in our paper. For a limited number of users, an LDB method is proposed. To further reduce the computational complexity with a large number of users, an LCD method is derived. Simulation results illustrate the performance of the proposed methods in terms of energy efficiency from user perspective.

In Chapter 4, energy-efficient relay selection and power allocation are studied in SWIPT cooperative wireless networks with DF and AF relays. Non-convex energy efficiency optimization problems are formulated for both DF and AF relay cases. A decomposed relay selection and power allocation scheme is derived without loss of optimality. Given the CNRs at the destination node, the closed-form expressions of the optimal power splitting ratios are derived. With the optimal power splitting ratios, relay selection schemes with full and partial knowledge of CSI are developed, respectively. Based on the property of the

simplified optimization problem, a simple closed-form power allocation scheme is adopted in both DF and AF relay networks. Furthermore, the performance difference between DF and AF relays is discussed. In addition, simulation results verify our analyses and demonstrate the optimality of our proposed resource allocation scheme in terms of the energy efficiency in SWIPT cooperative wireless networks. The proposed scheme achieves better energy efficiency in comparison with typical relay selection schemes and renders the same energy efficiency performance as the optimal exhaustive search scheme but with lower computational complexity.

In Chapter 5, we investigate the robust resource allocation problem for heterogeneous vehicular communications with imperfect channel estimation. NOMA is adopted in the network to increase spectral efficiency. Considering the imperfect channel estimation, we formulate a chance-constrained optimization problem to maximize the throughput of V2I links and retain the reliability requirements of V2V and F2FS links at the same time. To simplify and decouple the joint power and channel assignment problem, we derive a cascaded Hungarian channel assignment algorithm. With the assigned channels, we transform the chance constraints into deterministic ones through the approximation of non-central Chi-square distribution and derive the corresponding feasible region and optimal power allocation. In our simulation, we illustrate the effectiveness and superiority of the proposed resource allocation scheme.

This dissertation is a scientific work to find and design highly efficient resource allocation for wireless communications. The future research would be extended to the more advanced allocation schemes design and wireless networks applications.

References

[1] V. Chandrasekhar, J. Andrews, and A. Gatherer, "Femtocell networks: a survey," *IEEE Commun. Mag.*, vol. 46, no. 9, pp. 59–67, Sep. 2008.

[2] Q. C. Li, R. Q. Hu, Y. Xu, and Y. Qian, "Optimal fractional frequency reuse and power control in the heterogeneous wireless networks," *IEEE Trans. Wireless Commun.*, vol. 12, no. 6, pp. 2658–2668, Jun. 2013.

[3] S. Navaratnarajah, A. Saeed, M. Dianati, and M. A. Imran, "Energy efficiency in heterogeneous wireless access networks," *IEEE Wirelss Commun.*, vol. 20, no. 5, pp. 37–43, Oct. 2013.

[4] A. Damnjanovic, J. Montojo, Y. Wei, T. Ji, T. Luo, M. Vajapeyam, T. Yoo, O. Song, and D. Malladi, "A survey on 3GPP heterogeneous networks," *IEEE Wirelss Commun.*, vol. 18, no. 3, pp. 10–21, Jun. 2011.

[5] X. Kang, R. Zhang, and M. Montani, "Price-based resource allocation for spectrum-sharing femtocell networks: a Stackelberg game approach," *IEEE J. Sel. Areas Commun.*, vol. 30, no. 3, pp. 538–549, Apr. 2012.

[6] S. Shen and T. M. Lok, "Dynamic power allocation for downlink interference management in a two-tier ofdma network," *IEEE Trans. Veh. Technol.*, vol. 62, no. 8, pp. 4120–4125, Oct. 2013.

[7] D. I. Kim, E. H. Shin, and M. S. Jin, "Hierarchical power control with interference allowance for uplink transmission in two-tier heterogeneous networks," *IEEE Wirelss Commun.*, vol. 14, no. 2, pp. 616–627, Feb. 2015.

[8] H. Wang, J. Wang, and Z. Ding, "Distributed power control in a two-tier heterogeneous network," *IEEE Trans. Wireless Commun.*, vol. 14, no. 12, pp. 6509–6523, Dec. 2015.

[9] Z. Hasan, H. Boostanimehr, and V. K. Bhargava, "Green cellular networks: a survey, some research issues and challenges," *IEEE Commun. Surveys Tuts.*, vol. 13, no. 4, pp. 524–540, 4th Quarter, 2011.

[10] B. Wang, Y. Wu, F. Han, Y. H. Yang, and K. J. R. Liu, "Green wireless communications: a time-reversal paradigm," *IEEE J. Sel. Areas Commun.*, vol. 29, no. 8, pp. 1698–1710, Sep. 2011.

[11] A. Fehske, G. Fetweis, J. Malmodin, and G. Biczok, "The global footprint of mobil communications: the ecological and economic perspective," *IEEE Commun. Mag.*, vol. 49, no. 8, pp. 55–62, Aug. 2011.

[12] J. Yang, X. Wu, and J. Wu, "Optimal scheduling of collaborative sensing in evergy harvesting sensor networks," *IEEE J. Sel. Areas Commun.*, vol. 33, no. 3, pp. 512–523, Mar. 2015.

[13] G. Miao, N. Himaya, G. Li, and S. Talwar, "Low-complexity energy-efficient scheduling for uplink OFDMA," *IEEE Trans. Commun.*, vol. 60, no. 1, pp. 112–120, Jan. 2012.

[14] H. S. Dhillon, Y. Li, P. Nuggehalli, Z. Pi, and J. G. Andrews, "Fundamentals of heterogeneous cellular networks with energy harvesting," *IEEE Trans. Wireless Commun.*, vol. 13, no. 5, pp. 2782–2794, May 2014.

[15] L. R. Varshney, "Transporting information and energy simultaneously," in *Proc. IEEE Int. Symp. on Inf. Theory*, Toronto, ON, Canada, Jul. 2008, pp. 1612–1616.

[16] R. Zhang and C. K. Ho, "MIMO broadcasting for simultaneous wireless information and power transfer," *IEEE Trans. Wireless Commun.*, vol. 12, no. 5, pp. 1989–2001, May 2013.

[17] L. Liang, G. Y. Li, and W. Xu, "Resource allocation for D2D-enabled vehicular communications," *IEEE Trans. Commun.*, vol. 65, no. 7, pp. 3186–3197, Jul. 2017.

[18] L. Liang, J. Kim, K. Sivanesan, and G. Y. Li, "Spectrum and power allocation for vehicular communications with delayed CSI feedback," vol. 6, no. 4, pp. 458–461, Aug. 2017.

[19] M. Maso, L. S. Cardoso, M. Debbah, and L. Vangelista, "Cognitive orthogonal precoder for two-tiered networks deployment," *IEEE J. Sel. Areas Commun.*, vol. 31, no. 11, pp. 2338–2348, Nov. 2013.

[20] W. Yu, G. Ginis, and J. M. Cioffi, "Distributed multiuser power control for digital subscriber lines," *IEEE J. Sel. Areas Commun.*, vol. 20, no. 6, pp. 1105–1115, Jun. 2002.

[21] L. S. Cardoso, M. Kobayashi, F. R. P. Cavalcanti, and M. Debbah, "Vandermonde-subspace frequency division multiplexing for two-tiered cognitive radio networks," *IEEE Trans. Commun.*, vol. 61, no. 6, pp. 2212–2220, Jun. 2013.

[22] T. Yoo and A. Goldsmith, "Capacity and power allocation for fading mimo channels with channel estimation error," *IEEE Trans. Inf. Theory*, vol. 52, no. 5, pp. 2203–2214, Apr. 2006.

[23] G. Araniti, C. Campolo, M. Condoluci, A. Iera, and A. Molinaro, "LTE for vehicular networking: A survey," *IEEE Commun. Mag.*, vol. 51, no. 5, pp. 148–157, May 2013.

[24] K. Zheng, Q. Zheng, P. Chatzimisios, W. Xiang, and Y. Zhou, "Heterogeneous vehicular networking: a survey on architecture, challenges, and solutions," *IEEE Commun. Surveys Tuts.*, vol. 17, no. 4, pp. 2377–2396, 4th Quarter, 2015.

[25] (2013, Apr.) Scenarios, requirements and KPIs for 5G mobile and wireless system. METIS ICT-317669-METIS/D1.1, METIS deliverable D1.1. [Online]. Available: https://www.metis2020.com/documents/deliverables/

[26] B. Di, L. Song, Y. Li, and Z. Han, "V2X meets NOMA: Non-orthogonal multiple access for 5G enabled vehicular networks," *IEEE Wireless Commun. Mag.*, vol. 24, no. 6, pp. 14–21, Dec. 2017.

[27] B. Di, L. Song, Y. Li, and G. Y. Li, "Non-orthogonal multiple access for high-reliable and low-latency V2X communications in 5G systems," *IEEE J. Sel. Areas Commun.*, vol. 29, no. 1, pp. 2383–2397, Jul. 2017.

[28] Z. Ding, P. Fan, and H. V. Poor, "User pairnig in non-orthogonal multiple access downlink transmissions," in *Proc. IEEE Global Commun. Conf.*, San Diego, CA, Dec. 2015, pp. 1–5.

[29] Y. Sun, D. W. K. Ng, Z. Ding, and R. Schober, "Optimal joint power and subcarrier allocation for full-duplex multicarrier non-orthogonal multiple access systems," *IEEE Trans. Commun.*, vol. 65, no. 3, pp. 1077–1091, Mar. 2017.

[30] Z. Yang, Z. Ding, P. Fan, and G. K. Karagiannidis, "On the performance of non-orthogonal multiple access systems with partial channel information," *IEEE Trans. Commun.*, vol. 64, no. 2, pp. 654–667, Feb. 2016.

[31] M. S. Ali, E. Hossain, and D. I. Kim, "Non-orthogonal multiple access (NOMA) for downlink multiuser mimo systems: user clustering, beamforming, and power allocation," vol. 5, pp. 565–577, Dec. 2016.

[32] D. B. West, *Introduction to Graph Theory*, 2nd ed. Cambridge, U.K.: Cambridge Univ. Press, 2001.

[33] Z. Ding, P. Fan, and H. V. Poor, "Impact of user paring on 5G nonorthogonal multiple-access downlink transmissions," *IEEE Trans. Veh. Technol.*, vol. 65, no. 8, pp. 6010–6023, Aug. 2016.

[34] N. Y. Soltani, S.-J. Kim, and G. B. Giannakis, "Chance-constrained optimization of OFDMA cognitive radio uplinks," *IEEE Trans. Wireless Commun.*, vol. 12, no. 3, pp. 1098–1107, Mar. 2013.

[35] D. R. Cox and N. Reid, "Approximations to noncentral distributions," *The Canadian Journal of Statistics*, vol. 15, no. 2, pp. 105–114, Jun. 1987.

[36] *3rd Generation Partnership Project; Technical Specification Group Radio Access Network; Study on LTE-based V2X Services*, 3GPP TR 36.885 V2.0.0 (Release 14), 2016.

[37] (2007, Sep.) WINNER II channel models. IST-4-207756 WINNER II D1.1.2V1.2. [Online]. Available: http://projects.celtic-initiative.org/winner+/WINNER2-Deliverables/D1.1.2v1.1.pdf

[38] T. Cover and A. E. Gamal, "Capacity theorems for the relay channel," *IEEE Trans. Inf. Theory*, vol. 25, no. 5, pp. 572–584, Sep. 1979.

[39] C. Chien, Y. Chen, and H. Hsieh, "Exploiting spatial reuse gain through joint mode selection and resource allocation for underlay device-to-device communications," in *Proc. IEEE Wireless Personal Multimedia Commun., 15th Int. Symp. on*, Taipei, Taiwan, Sep. 2012, pp. 80–84.

[40] Y. Li, W. Wang, J. Kong, and M. Peng, "Subcarrier pairing for amplify-and-forward and decode-and-forward OFDM relay links," *IEEE Commun. Lett.*, vol. 13, no. 4, pp. 209–211, Apr. 2009.

[41] D. Wu, J. Wang, R. Q. Hu, Y. Cai, and L. Zhou, "Energy-efficient resource sharing for mobile device-to-device multimedia communications," *IEEE Trans. Veh. Technol.*, vol. 63, no. 5, pp. 2093–2103, Jun. 2014.

[42] G. Yu, L. Xu, D. Feng, R. Yin, G. Y. Li, and Y. Jiang, "Joint mode selection and resource allocation for device-to-device communications," *IEEE Trans. Commun.*, vol. 62, no. 11, pp. 3814–3824, Nov. 2014.

[43] D. Feng, L. Lu, Y. Wu, G. Y. Li, G. Feng, and S. Li, "Device-to-device communications underlaying cellular networks," *IEEE Trans. Commun.*, vol. 61, no. 8, pp. 3541–3551, Aug. 2013.

[44] J. P. Crouzeix, J. A. Ferland, and S. Schaible, "An algorithm for generalized fractional programs," *J. Optim. Theory Appl.*, vol. 47, no. 1, pp. 35–49, Sep. 1985.

[45] W. Dinkelbach, "On nonlinear fractional programming," *Manage. Sic.*, vol. 13, pp. 492–498, Mar. 1967.

[46] R. A. Loodaricheh, S. Mallick, and V. K. Bhargava, "Energy-efficient resource allocation for OFDMA cellular networks with user cooperation and QoS provisioning," *IEEE Trans. Wireless Commun.*, vol. 13, no. 11, pp. 6132–6146, Nov. 2014.

[47] W. Yu and R. Lui, "Dual methods for nonconvex spectrum optimization of multicarrier systems," *IEEE Trans. Wireless Commun.*, vol. 54, no. 7, pp. 1310–1322, Jul. 2006.

[48] Q. Wu, W. Chen, M. Tao, J. Li, H. Tang, and J. Wu, "Resource allocation for joint transmitter and receiver energy efficiency maximization in downlink OFDMA systems," *IEEE Trans. Commun.*, vol. 63, no. 2, pp. 416–430, Feb. 2015.

[49] Y. Li, M. Sheng, C. W. Tan, Y. Zhang, Y. Sun, X. Wang, Y. Shi, and J. Li, "Energy-efficient subcarrier assignment and power allocation in OFDMA systems with max-min fairness guarantees," *IEEE Trans. Commun.*, vol. 63, no. 9, pp. 3183–3194, Sep. 2015.

[50] G. Fodor, E. Dahlman, G. Mildh, S. Parkvall, N. Reider, G. Miklos, and Z. Turanyi, "Design aspects of network assisted device-to-device communications," *IEEE Commun. Mag.*, vol. 50, no. 3, pp. 170–177, Mar. 2012.

[51] Q. Ye, M. Al-Shalash, C. Caramanis, and J. G. Andrews, "Resource optimization in device-to-device cellular systems using time-frequency hopping," *IEEE Trans. Wireless Commun.*, vol. 13, no. 10, pp. 5467–5480, Oct. 2014.

[52] X. Li, L. Ma, R. Shankaran, M. Orgun, and G. Fang, "Joint mode selection and proportional fair scheduling for D2D communication," in *Proc. IEEE Int. Symp. Personal, Indoor, and Mobile Radio Commun.*, Montreal, QC, Oct. 2017, pp. 1–6.

[53] T. D. Hoang, L. B. Le, and T. L. Ngoc, "Resource allocation for D2D communications under proportional fairness," in *Proc. IEEE Global Commun. Conf.*, Austin, TX, Dec. 2014, pp. 1259–1264.

[54] C. Xiong, G. Y. Li, S. Zhang, Y. Chen, and S. Xu, "Energy- and spectral- efficiency tradeoff in downlink ofdma networks," *IEEE Trans. Wireless Commun.*, vol. 10, no. 11, pp. 3874–3886, Nov. 2011.

[55] D. Ng, E. Lo, and R. Schober, "Energy-efficient resource allocation in OFDMA systmes with large numbers of base station antennas," *IEEE Trans. Wireless Commun.*, vol. 11, no. 9, pp. 3292–3304, Sep. 2012.

[56] A. A. Nasir, X. Zhou, S. Durrani, and R. A. Kennedy, "Relaying protocols for wireless energy harvesting and information processing," *IEEE Trans. Wireless Commun.*, vol. 12, no. 7, pp. 3622–3636, Jul. 2013.

[57] D. W. K. Ng, E. S. Lo, and R. Schober, "Wireless information and power transfer: energy efficiency optimization in OFDMA systems," *IEEE Trans. Wireless Commun.*, vol. 12, no. 12, pp. 6352–6370, Dec. 2013.

[58] X. Zhou, R. Zhang, and C. K. Ho, "Wireless information and power transfer: architecture design and rate-energy tradeoff," *IEEE Trans. Commun.*, vol. 61, no. 11, pp. 4757–4767, Nov. 2013.

[59] A. A. Nasir, D. T. Ngo, X. Zhou, R. A. Kennedy, and S. Durrani, "Joint resource optimization for multicell networks with wireless energy harvesting relays," *IEEE Trans. Veh. Technol.*, vol. 68, no. 8, pp. 6168–6183, Aug. 2016.

[60] L. Liu, R. Zhang, and K. C. Chua, "Wireless information and power transfer: a dynamic power splitting approach," *IEEE Trans. Commun.*, vol. 61, no. 9, pp. 3990–4001, Sep. 2013.

[61] T. Cover and A. E. Gamal, "Capacity theorems for the relay channel," *IEEE Trans. Inf. Theory*, vol. 25, no. 5, pp. 572–584, Sep. 1979.

[62] 3GPP, Further advancements for E-UTRA physical layer aspects (Release 9), 3rd Generat. Partnership Project (3GPP) Std. Tech. Rep. 36.814, Mar. 1997.

[63] L. Tang, X. Zhang, P. Zhu, and X. Wang, "Wireless information and energy transfer in fading relay channels," *IEEE J. Sel. Areas Commun.*, vol. 34, no. 12, pp. 3632–3645, Sep. 2016.

[64] S. Boyd and L. Vandenberghe, *Convex Optimization*. Cambridge, U.K.: Cambridge Univ. Press, 2004.

Appendix A. Proofs for Chapter 3

A.1 Proof of Proposition 3.3.1

Rearranging (3.9a) and (3.9b), we obtain

$$P_{i,i'}^{v} \leqslant \frac{P_{max}^{v} - \frac{\delta\sigma^2}{g_{i,i',j}^{v}}}{2}, \tag{A.1}$$

which limits $P_{i,i'}^{v}$ to guarantee successful SIC at the VU receiver. According to [35], the CDF of 2-degree Chi-square distribution, $\mathcal{X}_2^2$, can be used to approximate the CDF of 2-degree non-central Chi-square distribution with non-centrality parameter λ, that is

$$\begin{aligned} & Pr(\mathcal{X}_{2,nc}^2 \leqslant x) \\ \approx & Pr(\mathcal{X}_2^2 \leqslant \frac{x}{1+\lambda^2/2}) \\ = & 1 - e^{(-\frac{\frac{x}{1+\lambda^2/2}}{2})}. \end{aligned} \tag{A.2}$$

With the substitution of (A.2) into (3.12) and (3.13) and some mathematical manipulations, the power allocation should satisfy

$$P_{i,i'}^{v} \geqslant \frac{B_1}{A_1} P_m^f + \frac{C_1}{A_1} \tag{A.3}$$

and

$$P_i^v + P_{i,i'}^{v} \leqslant \frac{B_2}{A_2} P_m^f + \frac{C_2}{A_2}. \tag{A.4}$$

Because $C_1 > 0$, $C_2 < 0$, and $P_i^v + P_{i,i'}^{v} \geqslant P_{i,i'}^{v}$, $\frac{B_2}{A_2} > \frac{B_1}{A_1}$ is necessary to ensure a feasible region. With $\frac{B_1}{A_1} > 0$, (A.1), and (A.3), P_m^f cannot go beyond $\frac{A_1(P_{max}^{v} - \frac{\delta\sigma^2}{g_{i,i',j}^{v}}) - 2C1}{2B1}$. Define $\bar{P}_{max}^{f}$ as $\min\{\frac{A_1(P_{max}^{v} - \frac{\delta\sigma^2}{g_{i,i',j}^{v}}) - 2C1}{2B1}, P_{max}^{f}\}$, we have $P_m^f \leqslant \bar{P}_{max}^{f}$. According to (A.4), $P_i^v + P_{i,i'}^{v} \leqslant \frac{B_2}{A_2}\bar{P}_{max}^{f} + \frac{C_2}{A_2}$ needs to be satisfied.

In consideration of (3.8a), if $\frac{B_2}{A_2}\bar{P}_{max}^{f} + \frac{C_2}{A_2} \leqslant P_{max}^{v}$, we have the feasible power region in Case I; if $\frac{B_2}{A_2}\bar{P}_{max}^{f} + \frac{C_2}{A_2} > P_{max}^{v}$, $P_i^v + P_{i,i'}^{v} \leqslant P_{max}^{v}$ should be considered and we have the

feasible power region in Case II, which completes the proof.

A.2 Proof of Proposition 3.3.2

Observing (3.9), we clearly note that the objective function of (3.9) monotonically increases with increasing P_i^v and decreases with increasing $P_{i,i;}^v$. Therefore, given P_m^f and (A.3), $P_{i,i'}^v$ should reside on the lower boundary for a smaller $P_{i,i'}^v$. Similarly, $P_i^v + P_{i,i'}^v$ must reside on the upper boundary for a larger P_i^v given $P_{i,i'}^v$.

Therefore, we have in Case I

$$P_{i,i'}^v = \frac{B_1}{A_1} P_m^f + \frac{C_1}{A_1} \tag{A.5}$$

and

$$P_i^v + P_{i,i'}^v = \frac{B_2}{A_2} P_m^f + \frac{C_2}{A_2}. \tag{A.6}$$

The objective function of (3.9) can be expressed as

$$R_i^v = \log_2 (1 + \frac{[(\frac{B_2}{A_2} - \frac{B_1}{A_1}) P_m^f + \frac{C_2}{A_2} - \frac{C_1}{A_1}] g_{i,j}^v}{(\frac{B1}{A1} P_m^f + \frac{C_1}{A_1}) g_{i,j}^v + \sigma^2}). \tag{A.7}$$

Because the derivative of R_i^v with respect to P_m^f is greater than 0 in the feasible region, R_i^v increases with increasing P_m^f in the feasible region. Therefore, the optimal P_m^f for Case I is $P_m^{f*} = \bar{P}_{max}^f$. Substituting P_m^{f*} into (A.5) and (A.6), we can obtain $P_{i,i'}^{v*}$ and P_i^{v*} for Case I as

$$P_{i,i'}^{v*} = \frac{B_1}{A_1} \bar{P}_f^{max} + \frac{C_1}{A_1}$$

and

$$P_i^{v*} = (\frac{B_2}{A_2} - \frac{B_1}{A_1}) \bar{P}_{max}^f + (\frac{C_2}{A_2} - \frac{C_1}{A_1}),$$

respectively.

In Case II, when $\frac{B_2}{A_2} P_m^f + \frac{C_2}{A_2} < P_{max}^v$, the objective function of (3.9) is the same as (A.7) and increases with increasing P_m^f. When $\frac{B_2}{A_2} P_m^f + \frac{C_2}{A_2} \geqslant P_{max}^v$, the objective function

of (3.9) can be rewritten as

$$R_i^{'v} = \log_2 (1 + \frac{(P_{max}^v - \frac{B_1}{A_1} P_m^f - \frac{C_1}{A_1}) g_{i,j}^v}{(\frac{B1}{A1} P_m^f + \frac{C_1}{A_1}) g_{i,j}^v + \sigma^2}), \tag{A.8}$$

which decreases with increasing P_m^f. Therefore, the maximum of (3.9) is reached when $\frac{B_2}{A_2} P_m^{f*} + \frac{C_2}{A_2} = P_{max}^v$ is satisfied for Case II. Specifically, $P_m^{f*} = \frac{A_2}{B_2} P_{max}^v - \frac{C_2}{B_2}$. Similar to Case I, $P_{i,i'}^{v*}$ and P_i^{v*} for Case II are

$$P_{i,i'}^{v*} = \frac{B_1}{A_1} (\frac{A_2}{B_2} P_{max}^v - \frac{C_2}{B_2}) + \frac{C_1}{A_1}$$

and

$$P_i^{v*} = P_{max}^v - \frac{B_1}{A_1} (\frac{A_2}{B_2} P_{max}^v - \frac{C_2}{B_2}) - \frac{C_1}{A_1},$$

respectively.

Combining the two cases, we complete the proof.

Appendix B. Proofs for Chapter 4

B.1 Proof of Proposition 4.2.1

To solve a max-min problem, we would like to find out the optimal allocation for the worst-case user k. Therefore, the optimization problem (4.8) can be rewritten as

$$\begin{aligned}\epsilon^* &= \max_{\mathbf{a_k},\mathbf{P_k},m_k\in\mathcal{S}} \min_k \frac{R_k(\mathbf{a_k},\mathbf{P_k},m_k)}{P_{con,k}(\mathbf{a_k},\mathbf{P_k},m_k)} \\ &= \min_k \frac{R_k(\mathbf{a_k}^*,\mathbf{P_k}^*,m_k^*)}{P_{con,k}(\mathbf{a_k}^*,\mathbf{P_k}^*,m_k^*)},\end{aligned} \tag{B.1}$$

where $\mathcal{S}$ denotes the feasible region of (4.8a)-(4.8f), $\{\mathbf{a_k}^*,\mathbf{P_k}^*,m_k^*\}$, and ϵ^* are the optimal solution and energy efficiency of problem (4.8), respectively. According to **Proposition 2.1** [44], the fractional programming problem

$$\epsilon^* = \min_k \frac{R_k(\mathbf{a_k}^*,\mathbf{P_k}^*,m_k^*)}{P_{con,k}(\mathbf{a_k}^*,\mathbf{P_k}^*,m_k^*)}$$

achieves the optimal solution if and only if

$$\min_k\{R_k(\mathbf{a_k^*},\mathbf{P_k^*},m_k^*) - \epsilon^* P_{con,k}(\mathbf{a_k^*},\mathbf{P_k^*},m_k^*)\} = 0. \tag{B.2}$$

Given (B.1), the optimal solution to the original problem (4.8) are achieved if and only if (B.2) holds, which completes the proof.

B.2 Proof of Proposition 4.2.2

In (4.12), the convexity of (4.12) with respect to $\mathbf{a_k}, \mathbf{u_k}$, and ξ can be analyzed with $m_k = 1$ and $m_k = 0$ separately. When $m_k = 1$, D2D user pair k is in D2D mode. Therefore, the data rate and power consumption are simplified to $R_k = \sum_{n=1}^{N} a_{k,n} B_0 \log_2(1 + \frac{u_{k,n} g_{k,n}}{a_{k,n}\sigma^2})$ and $P_{con,k} = \sum_{n=1}^{N} u_{k,n} + P_{cir,k}$, respectively. According to [64], if function $f(u)$ is concave, $af(u/a)$ is concave in (u, a). Since $B_0 \log_2(1 + \frac{u_{k,n} g_{k,n}}{\sigma^2})$ is concave, $a_{k,n} B_0 \log_2(1 + \frac{u_{k,n} g_{k,n}}{a_{k,n}\sigma^2})$ is concave in $(u_{k,n}, a_{k,n})$. The summation $\sum_{n=1}^{N} a_{k,n} B_0 \log_2(1 + \frac{u_{k,n} g_{k,n}}{a_{k,n}\sigma^2})$ is still concave. The power consumption, $P_{con,k} = \sum_{n=1}^{N} u_{k,n} + P_{cir,k}$, is affine with respect to $u_{k,n}$ and

the function $-\epsilon_k^i(\sum_{n=1}^{N} u_{k,n} + P_{cir,k})$ remains affine, and is convex and concave. Therefore, $\sum_{n=1}^{N} a_{k,n} B_0 \log_2(1 + \frac{u_{k,n} g_{k,n}}{a_{k,n}\sigma^2}) - \epsilon_k^i(\sum_{n=1}^{N} u_{k,n} + P_{cir,k})$ is concave. Because the superlevel set of a concave function is convex [64], constraints (4.12e) and (4.12f) are convex for $m = 1$. Similarly, constraints (4.12e) and (4.12f) are also convex, when $m = 0$. Therefore, we conclude that (4.12e), and (4.12f) result in convex set constrains.

Additionally, it is obvious that the objective function is an affine function and constraints (4.12a), (4.12b), (4.12c), and (4.12d) are all linear constraints. The optimization problem (4.12) is therefore a convex problem, which complete the proof.

B.3 Proof of Proposition 4.2.3

Define Rayleigh fading coefficients of the user pair in D2D mode and in cellular mode as h_{dm} and h_{cm}, respectively. Then the channel gains of the user pair in D2D mode and cellular mode are $X = d_{dm}^{-\alpha}|h_{dm}|^2$ and $Y = d_{cm}^{-\alpha}|h_{cm}|^2$, respectively, where $|\cdot|^2$ is the norm operator. Since h_{dm} and h_{cm} follow Rayleigh distribution, X and Y follow exponential distribution with parameters $\omega = d_{dm}^{\alpha}$ and $\upsilon = d_{cm}^{\alpha}$. Let $Z = Y - X$. The probability $\mathbb{P}(Z < 0)$ is

$$\begin{aligned}
&\mathbb{P}(Z < 0) = \mathbb{P}(Y < X) \\
=&\int_0^{\infty} \mathbb{P}(Y < x)\mathbb{P}(X = x)dx \\
=&\int_0^{\infty} (1 - e^{-\upsilon x})\omega e^{-\omega x} dx \\
=&\frac{\upsilon}{\omega + \upsilon}.
\end{aligned}$$

Therefore, $\mathbb{P}(Z < 0) > q$ when

$$d_{cm} > (\frac{q}{1-q}^{\frac{1}{\alpha}}) d_{dm},$$

which completes the proof.

B.4 Proof of Proposition 4.2.4

Define ΔP as a small positive amount of power. We divide the proof into two parts.

(a) $P_{k,tot} > P^*_{k,tot}$

To prove that energy efficiency, ϵ_k, is decreasing when $P_{k,tot} > P^*_{k,tot}$, we show $\epsilon_k(P^*_{k,tot} + 2\Delta P) < \epsilon_k(P^*_{k,tot} + \Delta P)$.

Denote $\Delta R(\Delta P) = \hat{R}_k(P^*_{k,tot} + \Delta P) - \hat{R}_k(P^*_{k,tot})$ and $\Delta\hat{R}(\Delta P) = \hat{R}_k(P^*_{k,tot} + 2\Delta P) - \hat{R}_k(P^*_{k,tot} + \Delta P)$. Define $g_n = \frac{g_{k,n}}{\sigma^2}$ and assume g_n is ordered, i.e., $\log_2(1 + g_1(P^*_{k,1} + \Delta P)) - \log_2(1 + g_1 P^*_{k,1}) \leq \ldots \leq \log_2(1 + g_N(P^*_{k,N} + \Delta P)) - \log_2(1 + g_N P^*_{k,N})$. With ΔP power increase, ΔP should be allocated to subcarrier N to maximize the data rate. In this case, $\hat{R}_k(P^*_{k,tot})$ and $\hat{R}_k(P^*_{k,tot} + \Delta P)$ are

$$\hat{R}_k(P^*_{k,tot}) = \sum_{i=1}^{N} B_0 \log_2(1 + g_i P^*_{k,i})$$

and

$$\begin{aligned} &\hat{R}_k(P^*_{k,tot} + \Delta P) \\ =&\sum_{i=1}^{N-1} B_0 \log_2(1 + g_i P^*_{k,i}) + B_0 \log_2(1 + g_N(P^*_{k,N} + \Delta P)), \end{aligned}$$

respectively. So, we have $\Delta R(\Delta P) = B_0 \log_2(1 + g_N(P^*_{k,N} + \Delta P)) - B_0 \log_2(1 + g_N P^*_{k,N})$.

With $2\Delta P$ of power increase, $2\Delta P$ can be allocated over one subcarrier or two different subcarriers. Therefore, $\Delta\hat{R}(\Delta P)$ can be represented as

$$\begin{aligned} \Delta\hat{R}(\Delta P) = &B_0 \log_2(1 + g_N(P^*_{k,N} + 2\Delta P)) \\ &- B_0 \log_2(1 + g_N(P^*_{k,N} + \Delta P)) \end{aligned} \tag{B.3}$$

or

$$\begin{aligned}
&\Delta\hat{R}(\Delta P)\\
=&B_0\log_2(1+g_N(P^*_{k,N}+\Delta P))+B_0\log_2(1+g_{N-1}(P^*_{k,N-1}+\Delta P))\\
-&B_0\log_2(1+g_N(P^*_{k,N}+\Delta P))-B_0\log_2(1+g_{N-1}P^*_{k,N-1}).
\end{aligned}\tag{B.4}$$

With (B.3), because $f(x)=\log_2(1+g_Nx)$ is a concave function, we have

$$\begin{aligned}
&\Delta\hat{R}(\Delta P)-\Delta R(\Delta P)\\
=&B_0\log_2(1+g_N(P^*_{k,N}+2\Delta P))+B_0\log_2(1+g_NP^*_{k,N})\\
-&2B_0\log_2(1+g_N(P^*_{k,N}+\Delta P))<0.
\end{aligned}\tag{B.5}$$

With (B.4), we have $\Delta\hat{R}(\Delta P)=B_0\log_2(1+g_{N-1}(P^*_{k,N-1}+\Delta P))-B_0\log_2(1+g_{N-1}P^*_{k,N-1})$. Note that $B_0\log_2(1+g_{N-1}(P^*_{k,N-1}+\Delta P))-B_0\log_2(1+g_{N-1}P^*_{k,N-1})\leq B_0\log_2(1+g_N(P^*_{k,N}+\Delta P))-B_0\log_2(1+g_NP^*_{k,N})$, i.e., $\Delta\hat{R}(\Delta P)\leq\Delta R(\Delta P)$. Therefore, we always have $\Delta\hat{R}(\Delta P)\leq\Delta R(\Delta P)$.

Since $P^*_{k,tot}$ is the optimal solution for ϵ^*_k, we have

$$\hat{R}(P^*_{k,tot})/P^*_{k,tot}>\hat{R}(P^*_{k,tot}+\Delta P)/(P^*_{k,tot}+\Delta P).\tag{B.6}$$

Substituting $\hat{R}(P^*_{k,tot}+\Delta P)=\hat{R}(P^*_{k,tot})+\Delta R(\Delta P)$ into (B.6) with mathematical manipulations, we obtain $\hat{R}_k(P^*_{k,tot}+\Delta P)/(P^*_{k,tot}+\Delta P)>\Delta R(\Delta P)/\Delta P$. Because $\Delta\hat{R}(\Delta P)\leq\Delta R(\Delta P)$, we have $\hat{R}_k(P^*_{k,tot}+\Delta P)/(P^*_{k,tot}+\Delta P)>\Delta\hat{R}(\Delta P)/\Delta P$.

Since $\frac{a}{b}>\frac{c}{d}$ results in $\frac{a}{b}>\frac{a+c}{b+d}$, for $a,b,c,d\geq0$, and $\hat{R}_k(P^*_{k,tot}+2\Delta P)=\hat{R}_k(P^*_{k,tot}+\Delta P)+\Delta\hat{R}(\Delta P)$, we obtain $\hat{R}_k(P^*_{k,tot}+\Delta P)/(P^*_{k,tot}+\Delta P)>\hat{R}_k(P^*_{k,tot}+2\Delta P)/(P^*_{k,tot}+2\Delta P)$.

Therefore, ϵ_k is decreasing when $P_{k,tot}>P^*_{k,tot}$.

(b) $P_{k,tot}<P^*_{k,tot}$

Denote $\Delta R(-\Delta P)=\hat{R}_k(P^*_{k,tot})-\hat{R}_k(P^*_{k,tot}-\Delta P)$ and $\Delta\hat{R}(-\Delta P)=\hat{R}_k(P^*_{k,tot}-\Delta P)-$

$\hat{R}_k(P^*_{k,tot} - 2\Delta P)$. We know that

$$\begin{aligned} &\hat{R}(P^*_{k,tot})P^*_{k,tot} \\ >&(\hat{R}(P^*_{k,tot}) - \Delta R(-\Delta P))/(P^*_{k,tot} - \Delta P). \end{aligned} \tag{B.7}$$

Because $\frac{a}{b} > \frac{a-c}{b-d}$ leads to $\frac{a}{b} < \frac{c}{d}$, for $a, b, c, d \geq 0$, and $\frac{\hat{R}(P^*_{k,tot})}{P^*_{k,tot}} > \frac{\hat{R}_k(P^*_{k,tot}) - \Delta R(-\Delta P)}{P^*_{k,tot} - \Delta P}$, we have $\hat{R}(P^*_{k,tot} - \Delta P)/(P^*_{k,tot} - \Delta P) < \Delta R(-\Delta P)/\Delta P$.

The same procedure can be conducted as in *(a)* to show $\Delta R(-\Delta P) \leq \Delta\hat{R}(-\Delta P)$. With mathematical manipulations, we can obtain $\hat{R}(P^*_{k,tot} - \Delta P)/(P^*_{k,tot} - \Delta P) > \hat{R}(P^*_{k,tot} - 2\Delta P)/(P^*_{k,tot} - 2\Delta P)$. Therefore, ϵ_k is increasing when $P_{k,tot} < P^*_{k,tot}$.

Combining *(a)* and *(b)*, we complete the proof.

B.5 Proof of Proposition 4.2.5

The energy efficiency of user k in D2D mode and cellular mode can be expressed as $\epsilon_k^{(1)} = \frac{R_k^{(1)}}{P_{c,k}^{(1)}}$ and $\epsilon_k^{(2)} = \frac{R_k^{(2)}}{P_{c,k}^{(2)}}$, respectively. It is obvious that $2P_{con,k}^{(2)}$ is strictly larger than $P_{con,k}^{(1)}$. Therefore, it is necessary to have $2R_k^{(2)} > R_k^{(1)}$ for $\epsilon_k^{(2)} > \epsilon_k^{(1)}$. In this case, when user k uses all N subcarriers and adopts equal power allocation to every subcarrier, we have

$$B_0 \sum_{n=1}^{N} \log_2(1 + \frac{P_{k,tot}}{N\sigma^2}\hat{g}_{k,n}) > B_0 \sum_{n=1}^{N} \log_2(1 + \frac{P_{k,tot}}{N\sigma^2} g_{k,n}),$$

i.e.,

$$\prod_{n=1}^{N}(1 + \frac{P_{k,tot}}{N\sigma^2}\hat{g}_{k,n}) > \prod_{n=1}^{N}(1 + \frac{P_{k,tot}}{N\sigma^2} g_{k,n}),$$

which completes the proof.

Appendix C. Proofs for Chapter 5

C.1 Proof of Proposition 5.2.1

According to (5.4)-(5.9), the energy efficiency with the i-th relay is equivalent to

$$\varepsilon_i^{DF} = \frac{\frac{1}{2}\log_2(1+\zeta_i P_s)}{P_s + P_c},$$

where ζ_i is the equivalent CNR with the i-th relay, which is

$$\zeta_i = \min\{\frac{(1-\rho_i)|\bar{g}_{sr_i}|^2}{\sigma^2}, \frac{\alpha\eta\rho_i|\bar{g}_{sr_i}|^2|\bar{g}_{r_id}|^2}{\sigma^2}\}.$$

Note that different relays have the same transmit power source P_s due to the SWIPT capability.

Considering the i-th relay with equivalent CNR ζ_i and j-th relay with equivalent CNR ζ_j, where $\zeta_i > \zeta_j$, we denote ε_i^{DF*} and ε_j^{DF*} as the best energy efficiency with the i-th and j-th relays, respectively. Additionally, the corresponding optimal transmit powers of the i-th and j-th relays are $P_{s,i}^*$ and $P_{s,j}^*$, respectively. Accordingly, we have

$$\varepsilon_i^{DF*} = \varepsilon_i^{DF}(P_{s,i}^*) = \frac{\frac{1}{2}\log_2(1+\zeta_i P_{s,i}^*)}{P_{s,i}^* + P_c}$$

and

$$\varepsilon_j^{DF*} = \varepsilon_j^{DF}(P_{s,j}^*) = \frac{\frac{1}{2}\log_2(1+\zeta_j P_{s,j}^*)}{P_{s,j}^* + P_c}.$$

Since $P_{s,i}^*$ is the optimal power for the i-th relay, we have

$$\varepsilon_i^{DF}(P_{s,i}^*) \geqslant \varepsilon_i^{DF}(P_{s,j}^*). \tag{C.1}$$

With $\zeta_i > \zeta_j$, we have

$$\varepsilon_i^{DF}(P_{s,j}^*) > \varepsilon_j^{DF}(P_{s,j}^*). \tag{C.2}$$

According to (C.1) and (C.2), we have

$$\varepsilon_i^{DF}(P_{s,i}^*) > \varepsilon_j^{DF}(P_{s,j}^*) \text{ when } \zeta_i > \zeta_j.$$

That is, the DF relay with higher equivalent CNR always achieves higher energy efficiency. Therefore, the relay selection can be decoupled from the power allocation without loss of optimality and the DF relay with the highest equivalent CNR will render the maximum energy efficiency, which completes the proof.

C.2 Proof of Proposition 5.2.2

Since the DF relay selection scheme is decided by $\min\{\zeta_{r_i}^{DF}, \zeta_{d_i}^{DF}\}$, there are two cases: $\zeta_{r_i}^{DF} \geq \zeta_{d_i}^{DF}$ and $\zeta_{r_i}^{DF} < \zeta_{d_i}^{DF}$.

$\zeta_{r_i}^{DF} \geq \zeta_{d_i}^{DF}$

To achieve the best CRN, $\zeta_{d_i}^{DF} = \frac{\alpha\eta\rho_i|\bar{g}_{sr_i}|^2|\bar{g}_{r_id}|^2}{\sigma^2}$ should be maximized. It is obvious that $\zeta_{d_i}^{DF}$ increases as ρ_i increases and $\zeta_{r_i}^{DF}$ increases as ρ_i decreases. Therefore, in this case, we increase ρ_i until

$$\zeta_{d_i}^{DF} = \zeta_{r_i}^{DF},$$

i.e.,

$$\frac{\alpha\eta\rho_i^*|\bar{g}_{sr_i}|^2|\bar{g}_{r_id}|^2}{\sigma^2} = \frac{(1-\rho_i^*)|\bar{g}_{sr_i}|^2}{\sigma^2},$$

which results in the optimal splitting ratio $\rho_i^* = \frac{1}{1+\alpha\eta|\bar{g}_{r_id}|^2}$.

$\zeta_{r_i}^{DF} < \zeta_{d_i}^{DF}$

In this case, $\zeta_{r_i}^{DF} = \frac{(1-\rho_i)|\bar{g}_{sr_i}|^2}{\sigma^2}$ should be maximized. Since $\zeta_{r_i}^{DF}$ increases as ρ_i decreases and $\zeta_{d_i}^{DF}$ increases as ρ_i increase, we decrease ρ_i until $\zeta_{d_i}^{DF} = \zeta_{r_i}^{DF}$ and obtain the same optimal splitting ratio $\rho_i^* = \frac{1}{1+\alpha\eta|\bar{g}_{r_id}|^2}$.

Combining both cases, we complete the proof.

C.3 Proof of Proposition 5.2.3

According to Taylor expansion, we have the following approximation

$$\mathbb{E}[\frac{X}{Y}] \approx \frac{\mathbb{E}[X]}{\mathbb{E}[Y]} - \frac{\text{cov}[X,Y]}{\mathbb{E}[Y]^2} + \frac{\mathbb{E}[X]}{\mathbb{E}[Y]^3}\text{var}[Y], \tag{C.3}$$

where X and Y are two random variables, var$[\cdot]$ is the variance operator, and cov$[\cdot]$ is the covariance operator. Let $X = |\bar{g}_{sr_i}|^2|\bar{g}_{r_id}|^2$ and $Y = 1 + \alpha\eta|\bar{g}_{r_id}|^2$, $\mathbb{E}[\frac{|\bar{g}_{sr_i}|^2|\bar{g}_{r_id}|^2}{1+\alpha\eta|\bar{g}_{r_id}|^2}]$ is approximately expressed as

$$\mathbb{E}[\frac{|\bar{g}_{sr_i}|^2|\bar{g}_{r_id}|^2}{1+\alpha\eta|\bar{g}_{r_id}|^2}] = \frac{\lambda_1|\bar{g}_{sr_i}|^2}{(\lambda_1+\alpha\eta)^2} + \frac{\alpha^2\eta^2|\bar{g}_{sr_i}|^2}{(\lambda_1+\alpha\eta)^3}, \tag{C.4}$$

which completes the proof.

C.4 Proof of Proposition 5.2.4

The function of ε^{DF} w.r.t. P_s is

$$\varepsilon^{DF} = \frac{\frac{B}{2}\log_2\left(1+\zeta_{r_i}^{DF}P_s\right)}{P_s+P_c}. \tag{C.5}$$

It is obvious that $\varepsilon^{DF} \geq 0$ when $P_s \geq 0$. And $\varepsilon^{DF} = 0$ only when $P_s = 0$. Let $P_s \to \infty$, we have

$$\lim_{P_s\to\infty} \varepsilon^{DF} = \lim_{P_s\to\infty} \frac{\frac{B}{2}\log_2(1+\zeta_{r_i}^{DF}P_s)}{P_s+P_c} = \quad 0 \tag{C.6}$$

according to *L'Hôpital's rule*.

Then $\varepsilon^{DF}(0) = 0$, $\varepsilon^{DF}(\infty) = 0$, and $\varepsilon^{DF} > 0$ for $0 < P_s < \infty$. Meanwhile, when $0 < P_s < \infty$, ε^{DF} is continuous and derivable. Hence, there exists a global maximizer $\widehat{P}_s^{DF}$, which must be one of the critical points of ε^{DF}.

To determine the critical points, let $\frac{\partial \varepsilon^{DF}}{\partial P_s} = 0$ and we obtain

$$\frac{\zeta_{r_i}^{DF}(P_s + P_c)}{1 + \zeta_{r_i}^{DF} P_s} = \ln(1 + \zeta_{r_i}^{DF} P_s). \tag{C.7}$$

Define

$$f(P_s) = \frac{\zeta_{r_i}^{DF}(P_s + P_c)}{1 + \zeta_{r_i}^{DF} P_s} \tag{C.8}$$

and

$$g(P_s) = \ln(1 + \zeta_{r_i}^{DF} P_s). \tag{C.9}$$

Obviously, $g(P_s)$ is monotonically increasing. The value of $g(P_s)$ increases from 0 to $+\infty$ when $P_s \geq 0$. For $f(P_s)$, we have

$$\frac{\partial f(P_s)}{\partial P_s} = \frac{\zeta_{r_i}^{DF}(1 - \zeta_{r_i}^{DF} P_c)}{(\zeta_{r_i}^{DF} P_s + 1)^2}. \tag{C.10}$$

If $\zeta_{r_i}^{DF} P_c < 1$, $f(P_s)$ is monotonically increasing. The value of $f(P_s)$ increases from $\zeta_{r_i}^{DF} P_c$ to 1. If $\zeta_{r_i}^{DF} P_c > 1$, $f(P_s)$ is monotonically decreasing. The value of $f(P_s)$ decreases from $\zeta_{r_i}^{DF} P_c$ to 1. If $\zeta_{r_i}^{DF} P_c = 1$, $f(P_s)$ is equal to 1. In any case, there exists one and only one intersection point for $f(P_s)$ and $g(P_s)$, which is the only critical point satisfying (C.7). Therefore, ε^{DF} is a unimodal function and $\hat{P}_s^{\,DF}$ is the unique global maximizer that can be solved by

$$\frac{\zeta_{r_i}^{DF}(P_c + \hat{P}_s^{\,DF})}{1 + \zeta_{r_i}^{DF} \hat{P}_s^{\,DF}} = \ln(1 + \zeta_{r_i}^{DF} \hat{P}_s^{\,DF}), \tag{C.11}$$

which completes the proof.

C.5 Proof of Proposition 5.2.5

Rewrite the CNR at the destination node in AF relay sensor networks, $\zeta_{d_i}^{AF}$, as a function of power splitting ratio ρ_i as

$$\begin{aligned} y(\rho_i) =& \zeta_{d_i}^{AF} = \frac{\alpha\eta\rho_i(1-\rho_i)|\bar{g}_{sr_i}|^2|\bar{g}_{r_id}|^2}{\alpha\eta\rho_i|\bar{g}_{r_id}|^2\sigma^2 + (1-\rho_i)\sigma^2} \\ =& \frac{a\rho_i(1-\rho_i)}{b\rho_i + c(1-\rho_i)}, \end{aligned} \tag{C.12}$$

where

$$\begin{aligned} a =& \alpha\eta|\bar{g}_{sr_i}|^2|\bar{g}_{r_id}|^2, \\ b =& \alpha\eta|\bar{g}_{r_id}|^2\sigma^2, \\ c =& \sigma^2. \end{aligned}$$

Taking the derivative of (C.12) w.r.t. ρ_i, we have

$$\frac{\partial y}{\partial \rho_i} = \frac{-a(b-c)\rho_i^2 - 2ac\rho_i + ac}{[(b-c)\rho_i + c]^2}. \tag{C.13}$$

Define a function $\Theta(\rho_i)$ representing the numerator of (C.13), i.e., $\Theta(\rho_i) \triangleq -a(b-c)\rho_i^2 - 2ac\rho_i + ac$. Since $[(b-c)\rho_i + c]^2 > 0$, the sign of (C.13) only depends on $\Theta(\rho_i)$. It is clear that $\Theta(0) = ac > 0$, $\Theta(1) = -ab < 0$, and $\Theta(\rho_i)$ is a quadratic function. Therefore, there exists an optimal ρ_i^* satisfying $\Theta(\rho_i^*) = 0$, which maximizes $y(\rho_i)$. According to the property of the quadratic function, there are two possible cases: $b > c$ and $b < c$.

(a) $b > c$

In this case, the greater root should be chosen. Therefore, the optimal splitting ratio

is

$$\begin{aligned}\rho_i^* =& \frac{2ac - \sqrt{4a^2c^2 + 4a(b-c)ac}}{-2a(b-c)} \\ =& \frac{1}{1+\sqrt{\alpha\eta}|\bar{g}_{r_i d}|}.\end{aligned}$$

(b) $b < c$

In this case, the smaller root should be chosen. Since $-(b-c) > 0$, the smaller root actually is the same as the greater root in case *a*. Therefore, the expression for the optimal splitting ratio is the same.

Combining *(a)* and *(b)*, we complete the proof.

Vita

Shengjie Guo was born in Hebei, China. He completed his undergraduate studies at the University of Electronic Science and Technology of China, July, 2012. From June 2013 to August 2015, he studied in Southern Illinois University for his graduate degree. From August 2015, he was transferred to Louisiana State University to pursue graduate studies in electrical and computer engineering. He is currently a candidate for the degree of Doctor of Philosophy in electrical and computer engineering, which will be awarded December 2018.